Characterization of the mitotic localization and function of the novel DREAM target GAS2L3.

and

Mitotic kinesins are regulated by the DREAM complex, often up-regulated in cancer cells, and are potential targets for anti-cancer therapy.

Charakterisierung der mitotischen Lokalisation und Funktion von GAS2L3, eines kürzlich gefundenen Zielgens des DREAM Komplexes.

und

Mitotische Kinesine werden vom DREAM Komplex reguliert, sind in Krebszellen häufig hochreguliert und sind potentielle Ziele für die Krebstherapie.

Doctoral thesis for a doctoral degree
at the Graduate School of Life Sciences,
Julius-Maximilians-Universität Würzburg,
Section Biomedicine
submitted by

Patrick Wolter

from

Bad Mergentheim

Würzburg, 2015

Submitted on:

Office stamp

Members of the *Promotionskomitee*:

Chairperson:	**Prof. Dr. Alexander Buchberger**
Primary Supervisor:	**Prof. Dr. Stefan Gaubatz**
Supervisor (Second):	**Prof. Dr. Georg Krohne**
Supervisor (Third):	**Prof. Dr. Antje Gohla**

Date of Public Defence:

Date of Receipt of Certificates:

Substantial parts of the thesis were first published in the following articles:

Wolter, P., Schmitt, K., Fackler, M., Kremling, H., Probst, L., Hauser, S., Gruss, O.J., and Gaubatz, S. (2012). **GAS2L3, a target gene of the DREAM complex, is required for proper cytokinesis and genomic stability**. J. Cell Sci. *125*, 2393–2406.

and

Fackler, M., Wolter, P., and Gaubatz, S. (2014). **The GAR domain of GAS2L3 mediates binding to the chromosomal passenger complex and is required for localization of GAS2L3 to the constriction zone during abscission**. FEBS J. *281*, 2123–2135.

Table of Contents

1 SUMMARY

The recently discovered human DREAM complex (for DP, RB-like, E2F and MuvB complex) is a chromatin-associated pocket protein complex involved in cell cycle-dependent gene expression. DREAM consists of five core subunits and forms a complex either with the pocket protein p130 and the transcription factor E2F4 to repress gene expression or with the transcription factors B-MYB and FOXM1 to promote gene expression.

Gas2l3 was recently identified by our group as a novel DREAM target gene. Subsequent characterization in human cell lines revealed that GAS2L3 is a microtubule and F-actin cross-linking protein, expressed in G2/M, plays a role in cytokinesis, and is important for chromosomal stability.

The aim of the first part of the study was to analyze how expression of *GAS2L3* is regulated by DREAM and to provide a better understanding of the function of GAS2L3 in mitosis and cytokinesis.

ChIP assays revealed that the repressive and the activating form of DREAM bind to the *GAS2L3* promoter. RNA interference (RNAi) mediated GAS2L3 depletion demonstrated the requirement of GAS2L3 for proper cleavage furrow ingression in cytokinesis. Immunofluorescence-based localization studies showed a localization of GAS2L3 at the mitotic spindle in mitosis and at the midbody in cytokinesis. Additional experiments demonstrated that the GAS2L3 GAR domain, a putative microtubule-binding domain, is responsible for GAS2L3 localization to the constriction zones in cytokinesis suggesting a function for GAS2L3 in the abscission process.

DREAM is known to promote G2/M gene expression. DREAM target genes include several mitotic kinesins and mitotic microtubule-associated proteins (mitotic MAPs). However, it is not clear to what extent DREAM regulates mitotic kinesins and MAPs, so far. Furthermore, a comprehensive study of mitotic kinesin expression in cancer cell lines is still missing.

Therefore, the second major aim of the thesis was to characterize the regulation of mitotic kinesins and MAPs by DREAM, to investigate the expression of mitotic kinesins in cancer cell line panels and to evaluate them as possible anti-cancer targets. ChIP assays together with RNAi mediated DREAM subunit depletion

experiments demonstrated that DREAM is a master regulator of mitotic kinesins. Furthermore, expression analyses in a panel of breast and lung cancer cell lines revealed that mitotic kinesins are up-regulated in the majority of cancer cell lines in contrast to non-transformed controls. Finally, an inducible lentiviral-based shRNA system was developed to effectively deplete mitotic kinesins. Depletion of selected mitotic kinesins resulted in cytokinesis failures and strong anti-proliferative effects in several human cancer cell lines.

Thus, this system will provide a robust tool for future investigation of mitotic kinesin function in cancer cells.

2 ZUSAMMENFASSUNG

Der vor kurzem entdeckte humane DREAM Komplex (für DP,RB ähnlich, E2F und MuvB Komplex) ist ein Chromatin bindender Pocket-Protein-Komplex involviert in Zellzyklusphase abhängiger Genregulation. DREAM besteht aus fünf Kernproteinen, die entweder zusammen mit dem Pocket-Protein p130 und dem Transkriptionsfaktor E2F4 die Genexpression reprimieren oder zusammen mit den Transkriptionsfaktoren B-MYB und FOXM1 die Genexpression fördern.

GAS2L3 wurde vor kurzem als neues Zielgen des DREAM Komplexes identifiziert. Eine anschließende Charakterisierung in humanen Zelllinien offenbarte, dass GAS2L3 in der Lage ist, das F-Aktin und das Mikrotubuli Cytoskelett zu binden und zu vernetzen. Außerdem ist GAS2L3 speziell während der G2/M Phase exprimiert, spielt eine Rolle in der Cytokinese und ist wichtig für die genomische Integrität.

Der erste Teil der Arbeit hatte zum Ziel zu ergründen in welcher Art und Weise DREAM *GAS2L3* reguliert. Außerdem sollte das Verständnis der Rolle von GAS2L3 in der Cytokinese erweitert werden.

Hierzu durchgeführte ChIP Analysen zeigten, dass sowohl der reprimierende als auch der aktivierende DREAM Komplex an den Promoter von GAS2L3 bindet. Experimente, in denen GAS2L3 durch RNA-Interferenz (RNAi) depletiert wurde, demonstrierten, dass GAS2L3 in der Cytokinese am Prozess der Einschnürung der Teilungsfurche beteiligt ist. Anschließende auf Immunfluoreszenzmikroskopie basierende Lokalisationsstudien zeigten, dass GAS2L3 an der mitotischen Spindel in der Mitose und am Midbody in der Cytokinese lokalisiert ist. Weiterführende Studien zeigten, dass die GAR Domäne von GAS2L3, eine mutmaßliche Mikrotubuli-Bindedomäne, für die Lokalisierung von GAS2L3 in der für die Abszission wichtigen Konstriktionszone verantwortlich ist. Dieses Ergebnis lässt vermuten, dass GAS2L3 eine Rolle in diesem Prozess spielt.

Der DREAM Komplex ist bekannt dafür G2/M Genexpression zu fördern. G2/M Zielgene des Komplexes sind unter anderem mehrere mitotische Kinesine und mitotische Mikrotubuli-Bindeproteine. Bisher ist die Art und Weise und das Ausmaß der Regulierung dieser Proteingruppen durch DREAM aber nur ungenügend

untersucht worden. Des Weiteren fehlt bisher eine umfassende Charakterisierung der Expression von mitotischen Kinesinen in Krebszellen.

Deswegen befasste sich der zweite Teil der Arbeit mit der Charakterisierung der Regulation von mitotischen Kinesinen und Mikrotubuli-Bindeproteinen durch DREAM, untersuchte die Expression dieser beiden Proteingruppen in Krebszelllinien und evaluierte diese anschließend als potentielle Ziele für die Krebstherapie.

Eine Kombination aus ChIP Analysen und RNAi Experimenten zeigte, dass DREAM eine zentrale Rolle in der Regulierung von mitotischen Kinesinen spielt. Expressionsanalysen deckten auf, dass mitotische Kinesine in der Mehrheit der Krebszelllinien hochreguliert sind im Gegensatz zu den nicht entarteten Kontrollzelllinien. Schließlich wurde ein auf Lentiviren basierendes induzierbares shRNA System etabliert, welches mitotische Kinesine effektiv herunterregulieren konnte. Depletion ausgewählter mitotischer Kinesine führte zu Fehlern in der Cytokinese und hatte starke Auswirkungen auf das Wachstumsverhalten von mehreren Krebszelllinien.

Aufgrund dieser Erkenntnisse wird das lentivirale System eine solide Ausgangsbasis für zukünftige Untersuchungen von mitotischen Kinesinen in Krebszellen bilden.

3 INTRODUCTION

3.1 The eukaryotic cell cycle

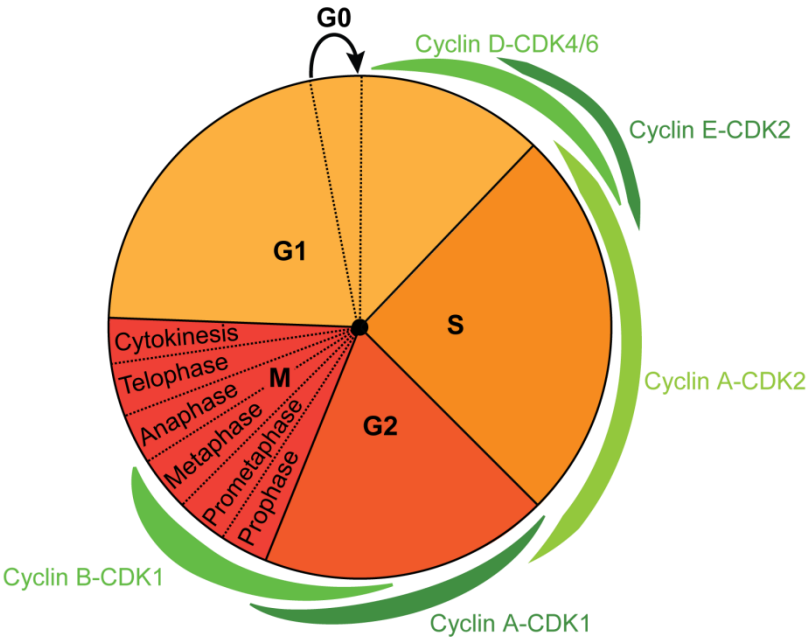

Figure 1: The mammalian cell cycle.
The mammalian cell cycle is a clockwork machinery which guides the cell through its reproductive process. The cell cycle coordinates genome duplication, genome distribution and cell division which produce in the end two daughter cells. The cell cycle is divided in 4 different phases. **G1** is the phase in which the cell is highly metabolic active awaiting external mitogenic signals. These signals stimulate the proliferative activity of the cell. The cell starts to replicate its DNA in **S** phase and subsequently prepares for cell division and monitors for DNA damage in **G2** phase. In **M** phase, the cell organizes the distribution of the DNA and the physical separation into two daughter cells. This phase can be subdivided into six phases (red). The daughter cells reenter G1 phase until external stimuli initiate a new cell cycle round and grow to their usual size. Different cyclin-dependent kinases (CDKs, green) guide the cell through the cell cycle phases ensuring a coordinated progress. Differentiated cells, e.g., neurons, can enter **G0**, a non-proliferative, quiescent state, for an undefined period of time. All events between two M phases are described as Interphase.

All proliferating eukaryotic cells use the cell cycle for their genome duplication and distribution to two daughter cells (David O Morgan, 2007).The cell cycle consists of several distinct phases which organize these events (Figure 1).

Interphase consists of all phases between two cell divisions and prepares the cell for its next division. Starting with Gap1 phase (G1), also called growth phase, which describes all events between the last cell division until the cell starts with DNA synthesis. G1 is used for cell growth and high metabolic activity. S phase (S) is the subsequent phase reserved for genome replication. In S phase, DNA is synthesized

until two identical copies are present for each chromosome. Gap2 phase (G2) is the phase in which the cell grows even more and produces all proteins necessary for cell division. Additionally, G2 is the important phase for DNA damage repair which can occur during DNA-replication.

Mitotic (M) phase is the phase of cell division (see 3.3). M phase includes mitosis, the separation and segregation of sister-chromatids and cytokinesis, the physical separation of the mother cell into two daughter cells. After these events the daughter cells reenter the next G1 phase starting the next cell cycle or enter G0 phase (G0) a non-proliferative, quiescent state. Differentiated cells, e.g., neurons, or cells lacking extracellular mitogenic signals, e.g., growth factors, enter G0 and stop cell cycling for an indefinite period.

To assure coordinated progression through the cell cycle, eukaryotic cells have developed a sophisticated regulatory mechanism (David O Morgan, 2007).This task is mainly guided by cyclin-dependent kinases (CDK) and their respective regulatory subunits, the cyclins (Figure 1).

Remarkably, this regulatory system is well conserved in the eukaryotic kingdom and varies only in its complexity. The following paragraph refers to the mammalian control system.

After receiving extracellular mitogenic signals, mammalian cells start to produce cyclin D which forms a complex with CDK4 and CDK6. Active cyclin D-CDK4/6 complexes guide the cell through G1. The successive accumulation of cyclin E leads to the formation of a cyclin E-CDK2 complex thereby promoting G1/S transition. A cyclin A-CDK2 complex guides the cell through S phase. To pass through G2 phase and to enter M phase, the cell needs cyclin A-CDK1 and a cyclin B-CDK1 activity. The subsequent M phase is solely guided by the cyclin B-CDK1 complex. The oscillating production and degradation of cyclins is the major driving force to ensure the unidirectional progress through the cell cycle.

The most important task of the cell cycle is the correct duplication and segregation of the DNA thereby ensuring genome integrity. To guarantee this, three major checkpoints developed in different phases of the cell cycle (David O Morgan, 2007). The first one is the G1/S checkpoint in late G1 phase which monitors whether the cell has everything prepared for DNA synthesis. After passing this checkpoint, the cell is committed to pass through S phase and is independent on extracellular signals. The second checkpoint is the G2/M DNA damage checkpoint in late G2 phase. This

checkpoint monitors the replication process, controls DNA damage repair, and subsequently allows the cell to enter M phase. The third checkpoint is the spindle assembly checkpoint in M phase (Musacchio, 2011; Musacchio and Salmon, 2007). This checkpoint monitors the correct spindle microtubule-chromosome attachment and bi-orientation of the chromosomes at the equatorial plate in metaphase to ensure proper separation and segregation of the sister-chromatids to the opposite cell poles.

De-regulation of the regulatory cell cycle machinery occurs very frequently in tumours allowing uncontrolled proliferation. This circumstance is often exploited in anti-cancer therapy (Asghar et al., 2015).

The pocket protein family members retinoblastoma-associated protein (RB), p107 and p130 act downstream of cyclin D-CDK4/6 together with the E2F transcription factor family to control G1/S transition (Figure 2) (Bertoli et al., 2013). The E2F family members E2F1-3 associate with RB in early G1 to form complexes which repress G1/S gene expression. After phosphorylation by cyclin D-CDK4/6, RB dissociates from E2F1-3 subsequently allowing E2F1-3 to promote G1/S gene expression. Similarly, E2F4 and E2F5 associate with p107 and p130 in G1 to repress G1/S gene expression. Phosphorylation of p107 and p130 by cyclin D-CDK4/6 leads to the dissociation of these pocket proteins from the promoters together with E2F4 and E2F5 to promote G1/S gene expression. E2F6-8 transcription factors do not associate with pocket proteins and inactivate genes in S phase. The pocket proteins are de-phosphorylated after cell division and rejoin with the E2F transcription factors in early G1 of the next cell cycle.

The retinoblastoma (Rb) pathway is frequently altered and inactivated in tumours, promoting tumourigenesis in a tissue-specific context (Di Fiore et al., 2013).

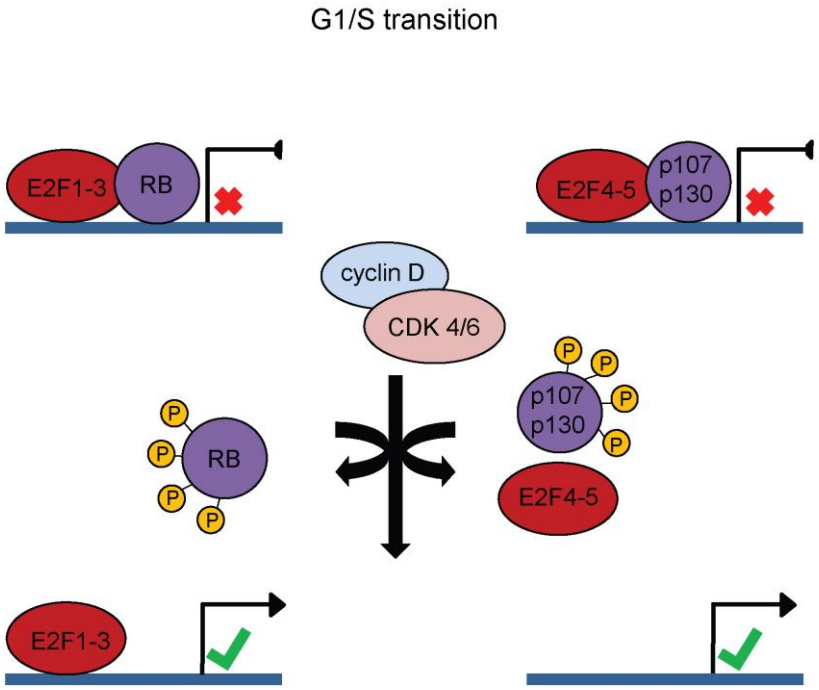

Figure 2: The Pocket protein family regulates G1/S transition together with the E2F transcription factor family.
The pocket protein family members RB, p107, and p130 repress genes important for transition from G1 to S phase together with the E2F transcription family members E2F1-5. Mitogenic signals stimulate the formation of cyclin D-CDK4/6 complexes which promote G1/S transition. Subsequent phosphorylation of the pocket proteins leads to their dissociation from the promoters. This enables the "activating" E2F transcription factors E2F1-3 to promote gene expression whereas the "repressive" E2F transcription factors E2F4-5 dissociate from the promoters to allow gene expression. The conserved regulatory mechanism governs the coordinated G1/S transition.

3.2 The DREAM complex

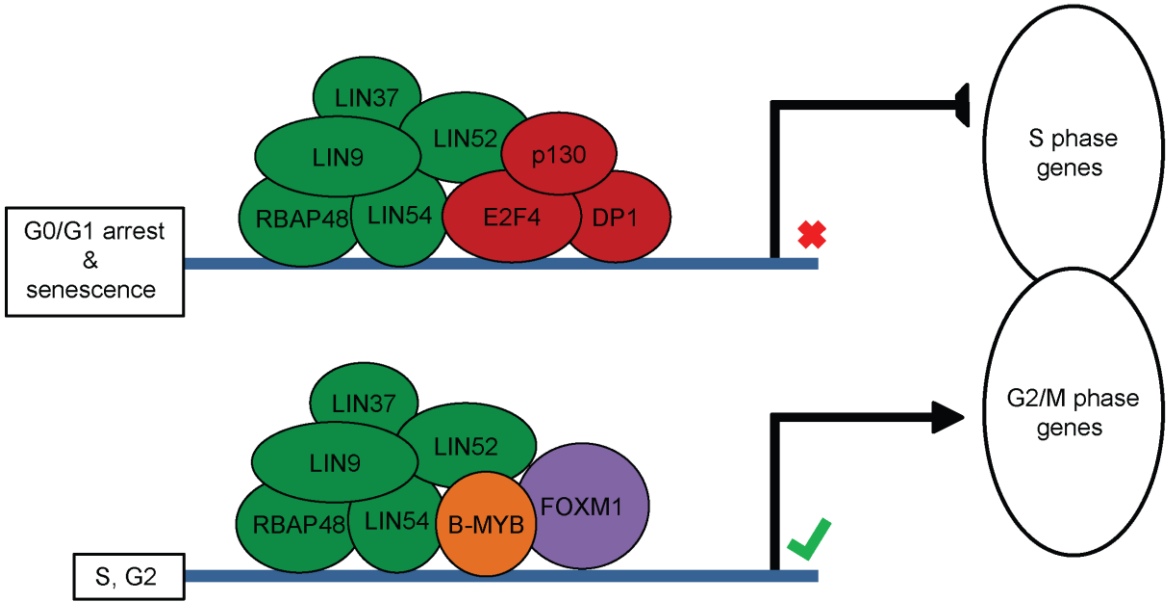

Figure 3: The mammalian DREAM complex.
DREAM is a regulator of cell cycle-dependent gene expression which consists of five permanent subunits (green). In G0, G1 arrested, and senescent cells, DREAM associates with the pocket protein p130 (red) and the transcription factor E2F4 (red) to repress gene expression. After G1/S transition (Figure 2) the core complex (green) associates with the transcription factors B-MYB (orange) and FOXM1 (purple) to promote gene expression.

The DREAM complex, a chromatin-associated pocket protein complex regulating cell cycle-dependent gene expression, is an evolutionary conserved complex existing in invertebrates and vertebrates (Sadasivam and DeCaprio, 2013) and possibly also in plants (Fischer and Decaprio, 2015; Kobayashi et al., 2015).

In mammals, the designated name for the repressive complex is DREAM (for DP, RB-like, E2F and MuvB complex) and for the activating complex B-MYB-MuvB. For simplicity, in this study the mammalian complex is referred to as repressive or activating DREAM complex.

First evidence of the complex was provided by biochemical analyses in the fly *Drosophila melanogaster* (Korenjak et al., 2004; Lewis et al., 2004). The complex was named dREAM (*Drosophila* Rbf, E2f2 and Mip complex) because purification of the complex revealed an interaction of the RB family proteins Rbf1 andRbf2 with E2f2 and the dimerization partner (Dp), Myb and Myb-interacting proteins (Mip40, Mip120 and Mip130), dLin52, and the chromatin assembly factor 1 Caf1. A highly related

complex purified by the Botchan laboratory was named Myb-MuvB (MMB) because of the shared homology of *Drosophila* Mip proteins with the nematode synMuvB genes (Lewis et al., 2004). Although originally implicated in gene repression, more recent data revealed that *Drosophila* dREAM is involved in both, gene repression and activation (Georlette et al., 2007).

A short time later, a similar complex was purified in the nematode *Caenorhabditis elegans* (Harrison et al., 2006). This complex was named DRM complex (Dp, Rb and MuvB complex). Multivuval (Muv) class B genes encode genes responsible for vulva differentiation in *C. elegans.* Synthetic mutations of several genes in this gene class lead to the emergence of a multi vulva phenotype and the terminology as synMuvB genes.

More recently, the mammalian homologue of the complex was identified by several groups (Litovchick et al., 2007; Pilkinton et al., 2007; Schmit et al., 2007). In contrast to the fly and worm complex, the mammalian complex can switch between at least two forms in a cell cycle-dependent manner. The core-module of the complex consists of 5 permanent subunits (LIN9, LIN37, LIN52, LIN54, and RBAP48), homologues of the nematode synMuvB genes. In G0, the DREAM core associates with E2F4, DP1 and p130 whereas in S phase and G2/M phase the complex associates with the transcription factors Myb-related protein B (B-MYB) and forkhead box protein M1 (FOXM1) (Figure 3) (Sadasivam et al., 2012). In G0, the complex represses transcription of E2F target genes (Litovchick et al., 2007). The kinase DYRK1A promotes the assembly of the repressive DREAM complex by phosphorylation of LIN52 to sustain quiescence and RAS induced senescence (Litovchick et al., 2011). Upon DNA damage, the activating complex can also switch to the repressive complex to repress gene expression in a p53-dependent manner (Mannefeld et al., 2009).

In contrast, in S phase and G2 phase the B-MYB/FOXM1/DREAM complex promotes expression of genes important to pass these phases (Esterlechner et al., 2013; Knight et al., 2009; Osterloh et al., 2007; Reichert et al., 2010; Sadasivam et al., 2012; Schmit et al., 2007).

In vivo, loss of the DREAM subunit Lin9 in mice interferes with embryonal development leading to embryonal lethality (Reichert et al., 2010). In conditional Lin9-knockout mice, adult mice lose the proliferative capability of intestinal epithelial cells

and die (Reichert et al., 2010). In addition, mitotic defects, misshaped nuclei, and bi-nucleated cells were observed in these mice together with reduced G2/M gene expression. It is likely that the developmental phenotype of the Lin9 k.o. mice is a consequence of the reduced expression of genes whose products are involved in mitosis and cytokinesis. Consistent with this notion, Lin9 depletion by RNAi in mouse embryonic stem cells (ESC) leads to reduced proliferation and reduced G2/M expression (Esterlechner et al., 2013).

Despite being part of the RB-E2F pathway (see 3.1), a role of DREAM in tumourigenesis and in developed tumours remains elusive (Sadasivam and DeCaprio, 2013). Interestingly, the DREAM-associated transcription factors B-MYB and FOXM1 are frequently up-regulated in tumours (Koo et al., 2012; Mannefeld et al., 2009; Parikh et al., 2014; Ramsay and Gonda, 2008; Raschellà et al., 1999; Tao et al., 2014). Up-regulation of these transcription factors correlate with aggressiveness, surviva,l and recurrence in a variety of tumours. This also applies for a variety of DREAM target genes such as *PRC1*, *KIF20A*, *TOP2α*, UBE2C, and *CCNB2* which are found, e.g., in the CIN70 signature of genes which correlate with chromosomal instability (CIN) and tumour malignancy (Carter et al., 2006).

3.3 M phase (mitosis and cytokinesis)

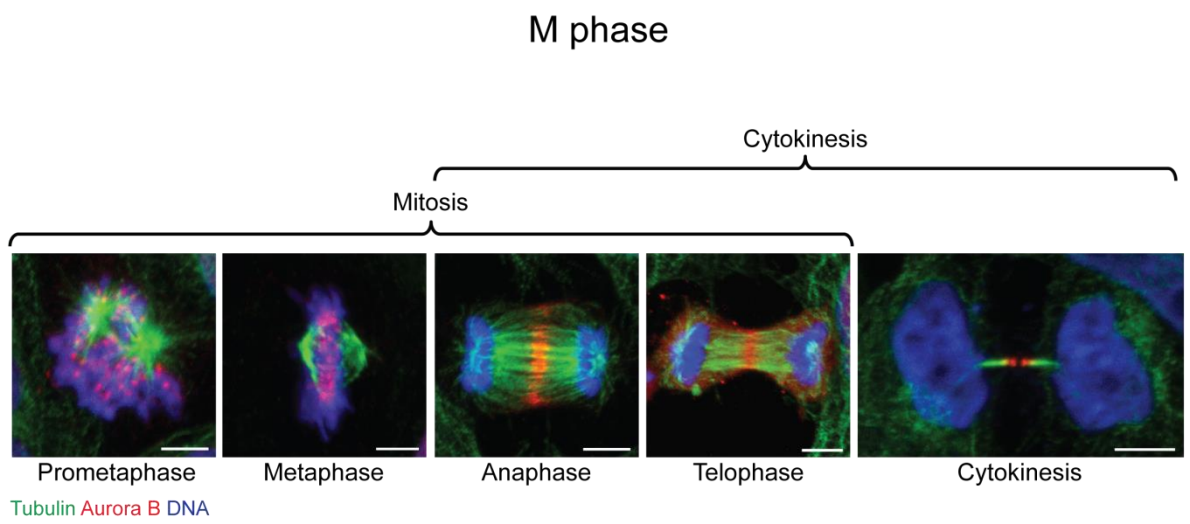

Figure 4: M phase comprises of the two events mitosis and cytokinesis.
M phase is the final phase in the cell cycle which organizes the cell division of the mother cell into two daughter cells by coupling the two events mitosis and cytokinesis. Mitosis mainly describes the separation and segregation of the sister-chromatids (blue). This process can be subdivided into five phases (prophase, prometaphase, metaphase, anaphase, and telophase). Each phase is defined by characteristic events and can be distinguished by the mitotic spindle morphology (green) and the status of DNA segregation (blue). Cytokinesis describes the physical separation of the mother cell into two daughter cells. This process is timed with mitosis and starts slightly delayed in anaphase. In the end, the daughter cells are only connected by a thin intercellular bridge which consists of microtubules (green). Abscission, the last step in cytokinesis, mediates the disintegration of intercellular bridge microtubules and membrane scission at these places which irreversibly separates the two daughter cells. The dynamic process of M phase implicates not only dramatic changes in the mitotic spindle but also in the localization of M phase-organizing factors. For example the mitotic master kinase Aurora B (red) localizes to chromosomes in the beginning of mitosis, re-locates to the mitotic spindle in anaphase, and localizes to the center of the intercellular bridge in cytokinesis. White bars: 5 µM.

M phase is a critical phase in the cell cycle of the eukaryotic cell which is responsible for cell division by coupling the two events mitosis and cytokinesis (Figure 4) (Alberts et al., 2008; David O Morgan, 2007). Mitosis mainly describes all events concerning karyokinesis, the process of nuclear division. In other terms, karyokinesis comprises the separation and segregation of sister-chromatids to produce daughter cells with an identical set of chromosomes. Cytokinesis describes all events concerning the physical division of the mother cell into two daughter cells.

Mitosis can be subdivided into five principle phases, each phase describes a sequence of characteristic events whose completion leads to the next phase. The phases are termed prophase, prometaphase, metaphase, anaphase and telophase (David O Morgan, 2007).

In prophase, chromatin condensation occurs to form the tightly packed, characteristic chromosomes which consist of two connected sister-chromatids. The two centrosomes, the major microtubule organizing centers (MTOC), separate and the initiation of mitotic spindle assembly occurs.

In prometaphase, the nuclear envelope breaks down (NEB). Mitotic spindle microtubules invade the chromosomes and connect to the kinetochores of the chromosomes. The two centrosomes orient opposite of each other and the chromosomes migrate to the central region between the centrosomes.

In metaphase, chromosomes align at the equatorial plate and center of the mitotic spindle. Kinetochore microtubules attach sister-chromatids to the opposite poles of the mitotic spindle. After proper attachment, sister-chromatids await the signal for their separation.

In anaphase, sister-chromatids lose their cohesion and separate. This allows their segregation to the opposite spindle poles. The spindle poles move farther apart from each other, the central spindle evolves and the cell cortex elongates to enable sister-chromatid segregation.

In telophase, two identical nuclei reassemble at the cell poles around the segregated chromatids while they are starting the decondensation process.

Cytokinesis starts slightly delayed to the events of mitosis with in anaphase (Figure 4) (David O Morgan, 2007).The initiating event is the reorganization of the mitotic spindle to establish the spindle midzone. During elongation of the cell cortex, the anaphase spindle is involved in the signaling to the equatorial cortex for cleavage plane specification. Accumulation and activation of cleavage plane associated factors lead to the formation and activation of the contractile/actomyosin ring. Contraction of the contractile ring leads to cleavage furrow ingression. Thereby the cell begins to divide into two compartments. In addition, the contractions cause the compaction of the midzone spindle. Termination of the process leads to the establishment of the intercellular bridge containing a midbody in its center. The final abscission occurs next to the midbody at the constriction zones. First, constriction zone microtubules disassemble and then membrane scission finalizes the division into two daughter cells.

The stages of cytokinesis are tightly timed to the stages and completion of mitosis. Eukaryotic cells have a checkpoint in mitosis integrated which can arrest the cell in metaphase thereby preventing the transition to anaphase. The spindle assembly

checkpoint (SAC) serves as control system to monitor that correct chromosome alignment in metaphase takes place before cytokinesis is initiated to prevent chromosome mis-segregation (Figure 5) (Musacchio, 2011; Musacchio and Salmon, 2007). Correct attachment of microtubules to kinetochores is monitored by two mechanisms. Mitotic checkpoint complex (MCC) proteins (MAD2, Bub3, BubR1) ensure that all chromosomes are attached to microtubules. The kinase Aurora B, as part of the chromosomal passenger complex (CPC), however, monitors the bi-orientation of chromosomes to ensure their amphitelic attachment to kinetochore microtubules.

MCC proteins bind Cdc20, the regulatory subunit of the E3 ubiquitin ligase anaphase-promoting complex (APC/C), at kinetochores to inhibit APC/C activity. After correct chromosome alignment, the SAC is rapidly turned off, Cdc20 is released, and the APC/C starts to target its substrates for degradation by the 26S proteasome. Two APC/C key substrates are cyclin B and securin. Cyclin B-CDK1 activity is important for entry and maintenance of mitosis. Cyclin B degradation leads to inactivation of CDK1. Subsequent dephosphorylation of its substrates allows metaphase to anaphase transition and initiation of cytokinesis. Securin is an inhibitor of the protease separase. Destruction of securin allows separase to cleave cohesin which ends sister-chromatid cohesion allowing their segregation in anaphase.

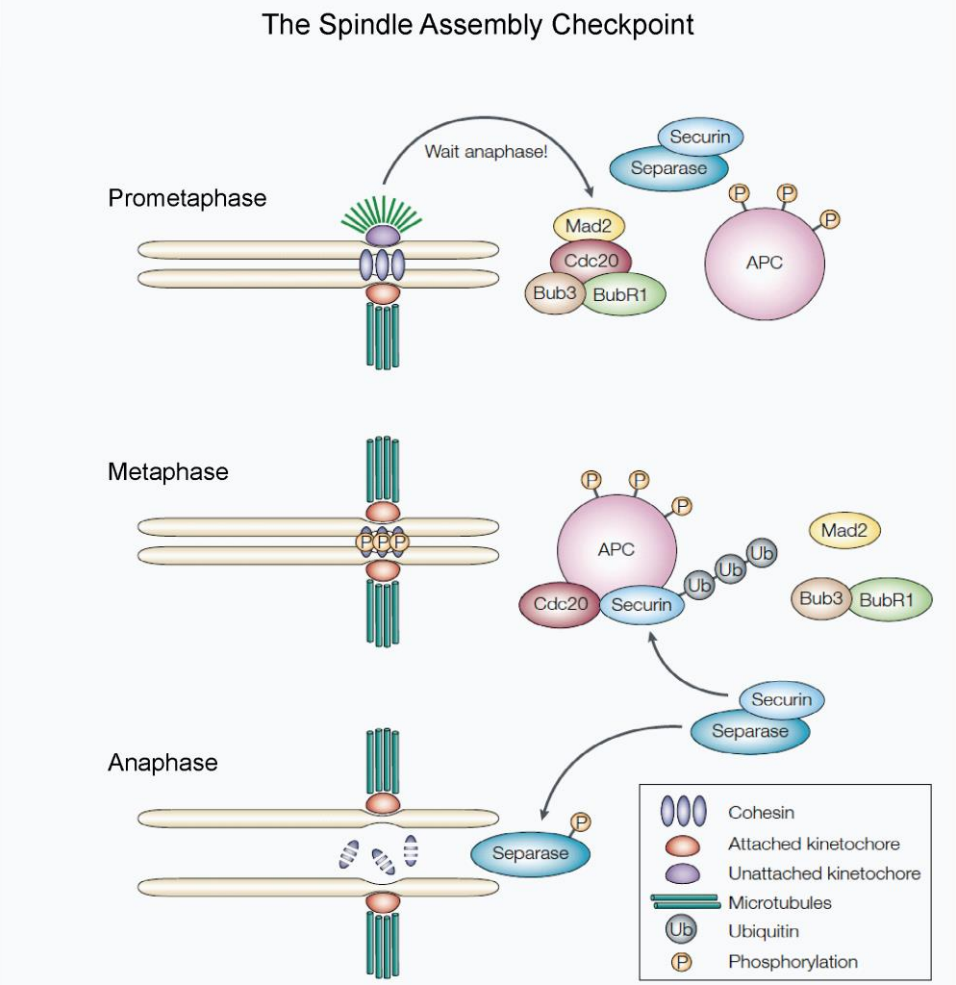

Figure 5: The spindle assembly checkpoint (SAC) controls chromosome alignment in metaphase and metaphase to anaphase transition.
The main task of the SAC is to inhibit the activity of the E3 ubiquitin ligase anaphase promoting complex (APC). The mitotic checkpoint proteins (MCC) Mad2, Bub3 and BubR1 inhibit the catalytic subunit cdc20 until all kinetochore microtubules are correct attached to the kinetochores in metaphase. Release of cdc20 leads to the activation of the APC/C which targets the inhibitor securin for degradation. The protease separase subsequently cleaves cohesin which ends sister-chromatid cohesion allowing their separation to the opposite cell poles in anaphase.
The APC/C also targets cyclin B for degradation which inactivates the cyclin-dependent kinase 1 (CDK1) leading to the removal of inhibitory phosphorylations of proteins regulating metaphase to anaphase transition.
Figure adapted from Musacchio and Hardwick, (2002)

3.4 The central spindle: Assembly, cleavage furrow ingression, and abscission

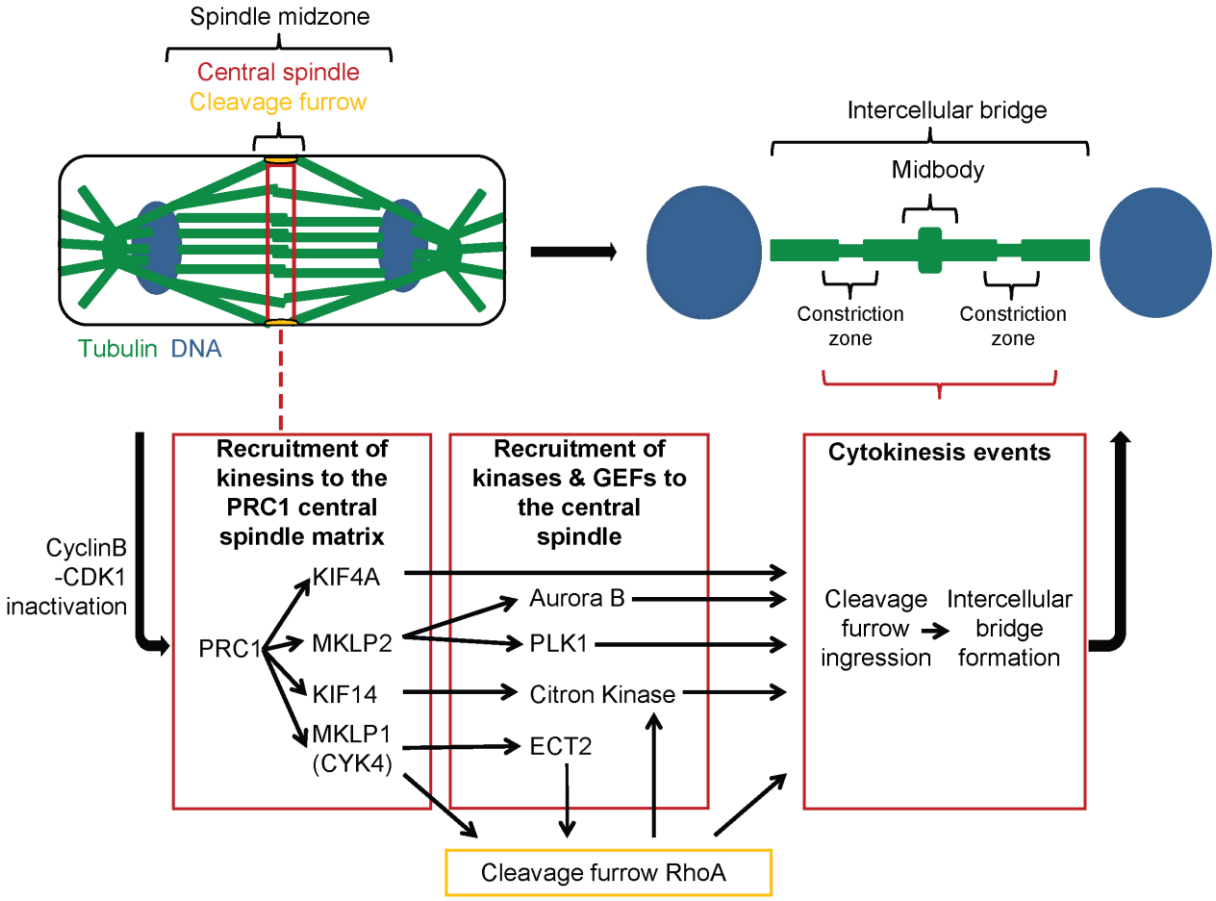

Figure 6: Central spindle organization and re-organization of the midzone spindle into the intercellular bridge in cytokinesis.
Upon metaphase to anaphase transition, initiated by CDK1 inactivation, the sister-chromatids (blue) move to opposite cell poles. The process is accompanied by the assembly of the central spindle (red) and establishment of the cleavage furrow (yellow). The part of the mitotic spindle which is located between the dividing chromosomes is named spindle midzone. Cleavage furrow ingression leads to the compaction of midzone microtubules and termination of the process forms the intercellular bridge. In its center originates a bulk of microtubules named midbody which consists of the overlapping former central spindle microtubules. The midbody is a protein-dense structure which mediates abscission, the final step of cytokinesis. Next to the midbody originate the constriction zones, the future sites of abscission, with characteristic thin microtubule filaments.
Recruitment of microtubule-associated proteins (MAPs) and motor proteins, e.g., kinesins, forms the backbone of central spindle assembly. The properties of these factors allow the bundling, stabilization and cross-linking of overlapping plus end microtubules. The MAP protein regulator of cytokinesis 1 (PRC1) is thought to create a docking matrix at the central spindle because of its early localization to the central spindle and its interaction with the most relevant mitotic kinesins (KIF4, MKLP2, KIF14, and MKLP1) at this place. These kinesins support not only directly central spindle integrity but also target key components for cytokinesis to the central spindle, e.g., the mitotic master kinases Aurora B and PLK1 and the small GTPase RhoA GEF ECT2. This ability promotes cleavage furrow ingression and formation of the intercellular bridge. Central spindle proteins partially re-locate in the process of intercellular bridge formation to mediate the abscission event.

The mitotic spindle is a self-organizing structure (Cross and McAinsh, 2014; Glotzer, 2009; Green et al., 2012; Mierzwa and Gerlich, 2014). The characteristic metaphase spindle consists of three microtubule populations emanating from the spindle pols, the centrosomes (Glotzer, 2009). Kinetochore microtubules, named kinetochore fibers, connect the chromosomes to the mitotic spindle. Interpolar microtubules are microtubules which emanate from one spindle pole and bundle with interpolar microtubules of the other pole. Astral microtubules emanate from the spindle poles to the cell cortex.

The motor protein kinesin KSP/EG5/KIF11 is the important factor for the bundling of interpolar microtubules in metaphase (Heald et al., 1996; Kapoor et al., 2000). In constrast, astral microtubules are focused to the cell cortex by the cortical localized motor protein dynein which is important for spindle positioning (Kotak and Gönczy, 2013; Kotak et al., 2012).

Upon anaphase onset, the mitotic spindle undergoes a dramatic reorganization (Barr and Gruneberg, 2007; Glotzer, 2009; Mierzwa and Gerlich, 2014). Kinetochore fibers shorten to drive poleward movement of sister-chromatids. Astral microtubules elongate together with the cell cortex. Antiparallel microtubules from the mitotic spindle and de novo nucleated microtubules at their branches (Uehara and Goshima, 2010) get bundled at their plus ends, between the dividing sister-chromatids, to form the midzone spindle. Subsequently, spindle midzone microtubules signal to the equatorial cell cortex to specify and initiate cleavage furrow ingression thereby causing their own compaction. After termination of cleavage furrow ingression, the compacted midzone microtubules give rise to a new structure named intercellular bridge. At its center is the midbody, a protein-dense structure, which mediates the final steps of cytokinesis leading to abscission at constriction zones adjacent to the midbody.

The reorganization of the mitotic spindle and establishment of the midzone spindle in anaphase is self-organized by an interplay of multiple motor proteins, e.g., mitotic kinesins and dynein (3.5), microtubule-associated proteins (MAPs), and kinases (Figure 6) (Barr and Gruneberg, 2007; Glotzer, 2009; Green et al., 2012; Mierzwa and Gerlich, 2014).

The three mitotic master kinases CDK1, Aurora B and the Polo-like kinase (PLK1) mainly mediate the organization of these events. Starting with the removal of

inhibitory phosphorylations from central spindle components after CDK1 inactivation sets central spindle assembly in motion at anaphase onset.

A key factor in central spindle assembly is the protein regulator of cytokinesis (PRC1), a microtubule interacting and bundling protein (Mollinari et al., 2002; Walczak and Shaw, 2010; Zhu et al., 2006). PRC1 binds to antiparallel microtubules after release from inhibitory phosphorylations of CDK1 and PLK1 (Cundell et al., 2013; Gao et al., 2011; Hu et al., 2012b; Jiang et al., 1998). Targeting of cytoplasmic PRC1 to the plus end of antiparallel microtubules and restriction of PRC1 function to this narrow zone is dependent on its binding partner kinesin KIF4A (Kurasawa et al., 2004; Zhu and Jiang, 2005). In this zone, PRC1 serves as matrix and interaction partner for multiple kinesins (Figure 6), MAPs, and kinases.

A second key factor in central spindle assembly is the centralspindlin complex which consists of the mitotic kinesin-like protein 1 (MKLP1/KIF23) and the Rho-family GTPase-activating protein (CYK-4/MgcRacGAP) (Mishima et al., 2002; Pavicic-kaltenbrunner et al., 2007). Centralspindlin activation depends on the removal of CDK1 inhibitory phosphorylations of MKLP1 (Mishima et al., 2004) and on Aurora B mediated phosphorylation of MKLP1 (Guse et al., 2005). The subsequent MKLP1 release from its inhibitor 14-3-3 is followed by clustering and accumulation of centralspindlin at the central spindle which produces essential midzone microtubule filament bundling (Douglas et al., 2010; Hutterer et al., 2009).

The third essential contributor in central spindle assembly is the CPC which consists of Aurora B, Survivin, Borealin and the inner centromere protein INCENP (Van Der Horst and Lens, 2014). Until anaphase CPC localization is chromosome associated at centromeres. Upon removal of a CDK1 phosphorylation of INCENP (Hümmer and Mayer, 2009), the CPC is relocated to the midzone spindle by the mitotic kinesin-like motor protein (MKLP2/KIF20A) (Gruneberg et al., 2004). Aurora B midzone activity regulates the phosphorylation status of multiple midzone proteins (Carmena et al., 2012; Glotzer, 2009).

A similar targeting of PLK1 to the midzone is also dependent on MKLP2 whereas phosphorylation of MKLP2, to induce its microtubule bundling activity, is dependent on PLK1 (Neef et al., 2003).

In addition to the mentioned key players, multiple MAPs play a role in midzone spindle assembly, e.g., the kinsesin HSET/KIFC1 is important for midzone stability (Cai et al., 2010), the kinesins KIF4A (Bastos et al., 2014), and KIF2A (Uehara et al.,

2013) regulate midzone spindle length together with Aurora B. KIF14 localizes to the midzone spindle together with the citron kinase to promote midbody formation and cytokinesis (Bassi et al., 2013; Gruneberg et al., 2006).

In summary, CDK1 inactivation initiates central spindle assembly, and induces the translocation and activity of the regulating kinases Aurora B and PLK1. All of the three kinases activate motor proteins and MAPS to translocate, bind, bundle and cross-link microtubule filaments until the central spindle is assembled.

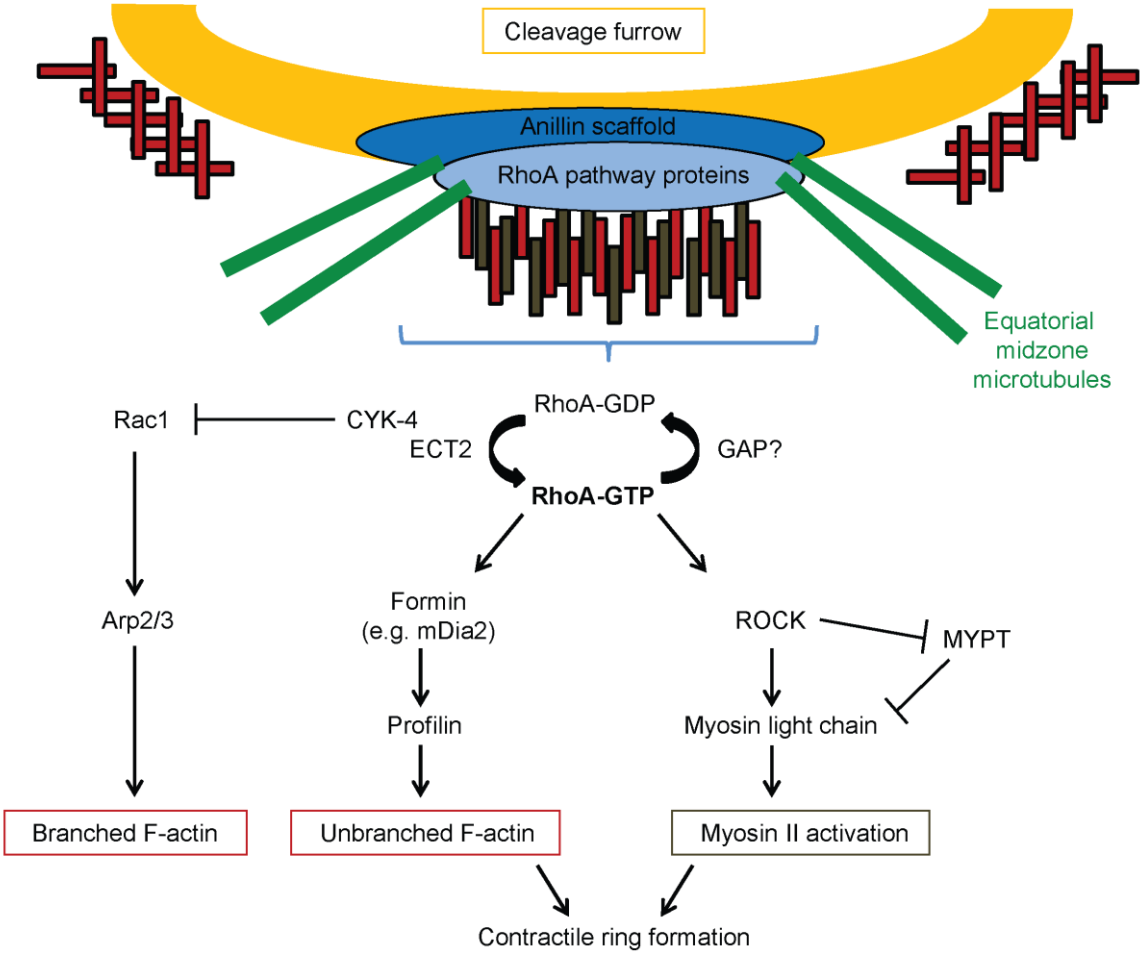

Figure 7: Cleavage furrow ingression, a task for the RhoA pathway.
Cleavage furrow specification between the dividing chromosomes in anaphase involves the signaling from equatorial midzone microtubules (green). Factors for cleavage furrow ingression accumulate in the furrow and the RhoA pathway gets subsequently activated. Central event is the activation of the small GTPase RhoA by its GEF ECT2 which is transported to the cell cortex by the centralspindlin complex (MKLP1/CYK-4) after metaphase to anaphase transition. Activation of RhoA effector proteins in the cleavage furrow lead to the activation of myosin II and nucleation of unbranched F-actin filaments which enables these factors to form the contractile ring in this narrow zone. Subsequent sliding of myosin II motor proteins against F-actin filaments creates the contractions for cleavage furrow ingression. Anillin is an important scaffold protein in the cleavage furrow which binds to myosin II, F-actin and RhoA to stabilize the contractile ring.
The RhoA pathway is adapted from Fededa and Gerlich, (2012).

Astral microtubules are important for the anchorage of the spindle to the cortex. The mitotic centromere-associated kinesin (MCAK/KIF2C) influences their stability thereby preserves spindle integrity in cytokinesis (Rankin and Wordeman, 2010).

Spindle midzone establishment leads to the stabilization of astral microtubules in the midzone center whereas polar astral microtubules stay more dynamic (Fededa and Gerlich, 2012; Mierzwa and Gerlich, 2014). This stabilization is thought to be important for cleavage plane specification by mediating the signaling from the central spindle to the cell cortex although the precise mechanism for the signaling is not well understood and other mechanism may contribute (Mierzwa and Gerlich, 2014).

In general, central spindle signaling is believed to be important to specifically activate the RhoA-pathway in a narrow zone at the cortex of the equatorial plate. The small GTPase RhoA is in the center of a pathway which controls contractile/actomyosin ring assembly and contraction (Figure 7) (Bastos et al., 2012; Fededa and Gerlich, 2012). RhoA is under control of guanine-nucleotide exchange factors (GEFs) and GTPase activating proteins (GAP). The most noticeable GEF of RhoA is the epithelial cell-transforming sequence 2 protein oncogene (ECT2). Targeting of ECT2 to the cell cortex is necessary for cleavage furrow formation (Su et al., 2011). Responsible for transportation of ECT2 is CYK-4 as part of the centralspindlin complex (Yüce et al., 2005; Zhao and Fang, 2005b). ECT2 is negatively phosphorylated by CDK1 in metaphase. Removal of the inhibition after anaphase onset together with the formation of the centralspindlin complex and subsequent PLK1 phosphorylation of CYK-4 controls the interaction of ECT2 and CYK-4 (Wolfe et al., 2009). The ability of centralspindlin to accumulate at plus ends of cross-linked midzone microtubules leads to an accumulation of a fraction of centralspindlin-ECT2 at the midzone cell cortex. ECT2 activates accumulated RhoA in this zone which in turn promotes the activation of RhoA effector proteins, e.g., the ROCK kinase and Diaphanous-related formins. The ROCK kinase promotes myosin II activation by direct phosphorylation of the myosin light chain and indirect by inhibition of the phosphatase targeting subunit MYPT (Matsumura, 2005). The activation of Formins, e.g., mDia2, and Profilin leads to the nucleation of unbranched F-actin filaments (Severson et al., 2002; Watanabe et al., 2008).

The current model proposes that both the activation of myosin II and stable linear F-actin filaments are required for the assembly and activation of the contractile ring.

The GEF ECT2, but also the GAP function of CYK-4 contributes to RhoA activation (Loria et al., 2012). The GAP domain of CYK-4 specifically inactivates the Rho-GTPase Rac1 at the cleavage furrow to support contractile ring formation (Bastos et al., 2012; Canman et al., 2008). Rac1 is active at polar sites of the cell in cytokinesis and is known to regulate spreading and adhesion by affecting the Arp2/3 complex. Arp2/3 regulates the actin cytoskeleton by nucleation and branching of F-actin filaments. Activation of the Rac1 pathway in the cleavage furrow interferes with proper ingression (Bastos et al., 2012).

Finally, the scaffold protein anillin accumulates at the cleavage furrow in anaphase and interacts with RhoA, myosin II, and actin to support contractile ring formation and function (Piekny and Glotzer, 2008).

Termination of cleavage furrow ingression leads to the disassembly of the contractile ring and anchorage of the cell membrane to the midbody at the established intercellular bridge (Mierzwa and Gerlich, 2014). Central spindle MAPs, motor proteins and kinases relocate to specific sites at the midbody (Gruneberg et al., 2004; Hu et al., 2012a). For example, PRC1 and KIF4A are associated with the midbody, CENP-E, MKLP2 and the CPC localize adjacent to the midbody and MKLP1 is part of the midbody ring which surrounds the midbody. These events initiate the last step of cytokinesis, abscission. Abscission is mainly mediated by the endosomal sorting complex required for transport-III (ESCRT-III) (Elia et al., 2011; Guizetti et al., 2011). The ESCRT-III complex forms or regulates 17 nm filaments at the constriction sites of the intercellular bridge. These filaments mediate the constriction of the membrane at the constriction zones to separate the two daughter cells. In parallel, the AAA-ATPase spastin disassembles intercellular bridge microtubules at the constriction zones to disrupt the last microtubule cytoskeleton connection between the daughter cells (Connell et al., 2009). An important regulator of abscission is the centrosome-associated protein CEP55, a microtubule bundling protein, which localizes throughout mitosis to centrosomes, to the midzone spindle in anaphase and accumulates at the midbody in late cytokinesis (Martinez-Garay et al., 2006; Zhao et al., 2006). CEP55 accumulation at the midbody is regulated by the PLK1 kinase to control abscission timing (Bastos and Barr, 2010). Upon localization to the midbody, CEP55 binds to MKLP1 (Carlton and Martin-Serrano, 2007; Lee et al., 2008; Swanton et al., 2009; Zhao et al., 2006), and serves as platform for abscission factors by mediating, e.g., the recruitment of ALIX and TSG101, components of the

ESCRT-I complex (Carlton and Martin-Serrano, 2007; Carlton et al., 2008; Morita et al., 2007). The ESCRT-I complex subsequently recruits components of the ESCRT-III complex which, in turn ,mediates the final abscission events (Elia et al., 2011; Guizetti et al., 2011).

3.5 Mitotic kinesins

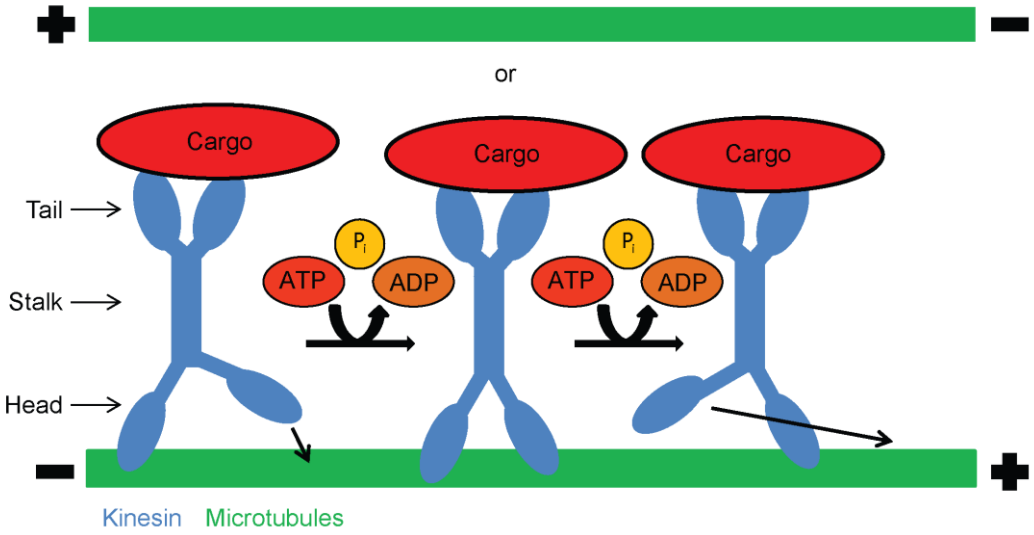

Figure 8: Kinesin motor proteins move along the microtubule cytoskeleton and are involved, e.g., in intercellular cargo transport, force generation and microtubule stability and mobility. Kinesins consist of a head, stalk and tail domain. The head comprises the motor domain which converts the energy of ATP hydrolysis into force for unidirectional movement along the microtubule cytoskeleton. The tail domain harbors recognition sequences for the interaction with the cargo (proteins, mRNAs, macromolecules, and organelles). The stalk connects the head and the tail. In humans, 45 kinesins are identified so far. Each kinesin has a unique structure and motor domain for their specialized functions. Kinesins often team up to create functional units. Anchorage of kinesins, e.g., to cell organelles and the cortex allows them to create push and pulling forces on the microtubule cytoskeleton instead of walking along these filaments.

The kinesin superfamily proteins (KIFs) are motor proteins involved in intercellular cargo transport (proteins, mRNAs, macromolecules and organelles), cell motility, ciliary function and cell division (Figure 8) (Hirokawa et al., 2009; Verhey and Hammond, 2009).

KIFs can be structured in a head domain, a stalk, and a tail part (Figure 8) (Cross and McAinsh, 2014). The head domain, also known as motor domain, contains the kinesin-specific ATP-dependent motor domain which drives unidirectional movement along microtubules, generating the necessary force via ATP hydrolysis (Figure 8) (Cross and McAinsh, 2014). The motor domain allows subcategorizing of KIFs into

14 groups, kinesin-1 to -14, according to the shared evolutionary similarity (Lawrence et al., 2004). This classification was expanded and the kinesin family (KIF) classification was introduced specifically for mammals as second naming convention which allows an even finer categorization (Hirokawa et al., 2009).

Most of the kinesins harbor a stalk structure or linker region which connects the head domain and the tail structure. The highly variable tail structure defines the individual function of kinesins harboring recognition sequences for binding partners, regulatory kinases, and cargo (Verhey and Hammond, 2009). Furthermore, KIFs can be categorized in processive, non-processive, and non-motile kinesins (Cross and McAinsh, 2014). Processive kinesins, e.g., the kinesin-7 KIF10/CENP-E, can move along microtubules as single molecules because they harbor two functional motor domains. Both are necessary for the movement without losing contact to microtubule binding sites. Non-processive kinesins, e.g., the kinesin-6 members KIF23/MKLP1 and KIF20A/MKLP2, harbor only one functional motor domain or miss the necessary neck region between two motor domains and need to team up as dimers or oligomers to be able to move along microtubules. In contrast, the non-motile kinesins, e.g., the kinesin-13 members KIF2A, KIF2B and KIF2C/MCAK, use their motor domain and the energy gained from ATP hydrolysis to depolymerize microtubules which leads to microtubule catastrophe events at plus- or minus-ends of microtubules depending on the kinesin and its localization.

In humans, there are 16 identified KIFs with known or suspected roles in mitosis and cytokinesis, so far (Table 1) (Cross and McAinsh, 2014). For example, mitotic kinesins are involved in centrosome separation, in self-organization and re-organization of the mitotic spindle, in chromosome-microtubule interaction and segregation, in midbody integrity, and in cytokinesis organization (Cross and McAinsh, 2014; Lee et al., 2012; Vicente and Wordeman, 2015). To assure spatial and temporal function, mitotic kinesins can be regulated in multiple ways (Welburn, 2013; Yount et al., 2015). The expression of mitotic KIFs is often restricted to G2/M phase. Multiple kinesins like KIFC1, KIFC2, and KIF4A harbor a destruction box (D-box) or KEN box sequences that are targeted by the APC/C together with Cdc20 (see 3.3) in M phase. The APC/C together with cdh1 performs the same task in early G1 which leads to the efficient degradation of the mitotic kinesins (Singh et al., 2014). Furthermore, in G2/M mitotic kinesin localization and function often depends on the mitotic master kinases CDK1, Aurora A, Aurora B and PLK1. They promote both,

inhibition and activation of mitotic kinesins and influence their affinity for microtubules (see 3.4). Finally, alternating binding partner or mitotic events can trigger mitotic kinesin function which allows mitotic kinesins to perform their unique tasks.

Recently, mitotic kinesins came into focus as possible targets for anti-cancer therapy (Chandrasekaran et al., 2015; Liu et al., 2013; Rath and Kozielski, 2012; Yu and Feng, 2010). The G2/M restricted expression of mitotic kinesins allows to specifically attack proliferating cells. Furthermore, multiple examples demonstrate that mitotic kinesins are deregulated in tumours, involved in tumourigenesis, responsible for drug resistance and are associated with malignancy and tumour grade in a variety of tumours (Table 1). These features provide a promising base to explore mitotic kinesins for a potential therapeutic window in anti-cancer therapy.

Table 1: Summary of mitotic kinesin function in mitosis and cytokinesis and evidence for their de-regulation in cancer.

Kinesin family classification	Kinesin family member (KIF) classification in mammals	Function in mitosis and cytokinesis	De-regulation in cancer and implication in drug resistance
Kinesin-14A	KIFC1/HSET	Spindle midzone stability (Cai et al. 2010), centrosome clustering in cancer cells (Kwon et al. 2008	Overexpression in breast cancer, correlates with progression and agressiveness (Pannu et al. 2015), overexpression mediates docetaxel resistance in breast cancer cells (De et al.2009)
Kinesin-13	KIF2A	Midzone spindle length (Uehara et al. 2013)	Overexpression in breast cancer, correlates with survival (Wang et al. 2014)
	KIF2B	Kinetochore microtubule dynamics (Bakhoum et al. 2008)	
	KIF2C/MCAK	Kinetochore microtubule dynamics (Bakhoum et al. 2008), stability of astral microtubules (Tanenbaum et al. 2011)	Overexpression in mammary carcinogenesis (Shimo et al. 2007), overexpression mediates paclitaxel resistance (Ganguly et al. 2011)
Kinesin-4	KIF4A	Chromosome condensation (Mazumdar et al. 2004), central spindle length (Bastos et al. 2013), midzone formation (kurasawa et al. 2004, Zhu et al. 2005), essential for cytokinesis (Zhu et al. 2005)	Prognostic marker for lung cancer (Taniwaki et al.2007)
	KIF4B	"	
Kinesin-7	KIF10/CENP-E	Microtubule-kinetochore capture and mitotic checkpoint silencing (Mao et al.2005)	Downregulation in hepatocellular carcinoma (Liu et al. 2009)
Kinesin-5	KIF11/KSP/EG5	Centrosome seperation and bipolar spindle formation (Kapoor et al. 2000)	Overexpression causes genomic instability and tumour formation in mice (Castillo et al. 2007)
Kinesin-3	KIF14	Regulation of cytokinesis together with the citron kinase (Gruneberg et al. 2006)	De-regulation in lung adenocarcinomas (Hung et al. 2013), prognostic marker for breast cancer (Cordon et al .2006) and lung cancer (Cordon et al. 2007)
Kinesin-12	KIF15	Bipolar spindle assembly (Heesbeen et al. 2014)	
Kinesin-8	KIF18A	Pre-anaphase chromosome oscillation (Häfner et al.2014), Chromosome alignment (Stumpff et al. 2008)	Overexpression in breast cancer, associated with tumor grade, metastasis and survival (Zhang et al. 2010)
	KIF18B	Stability of astral microtubules (Tanenbaum et al. 2011)	
Kinesin-6	KIF20A/MKLP2	Targeting of Aurora B (Gruneberg et al. 2004) and Plk1 (Neef et al. 2003) to the central spindle, essential for cytokinesis (Zhu et al.2005)	Overexpression in hepatocarcinogenesis (Gasnereau et al. 2012), overexpression in pancreatic cancer (Imai et al. 2011) and pancreatic ductual adenocarcinomas (Stangel et al. 2015)
	KIF20B/MPP1	Required for late cytokinesis (Abaza et al. 2003)	
	KIF23/MKLP1	Part of the centralspindlin complex (Glotzer et al. 2009), essential for cytokinesis and involved in multiple processes of cytokinesis (Mierzwa et al. 2014, Zhu et al. 2005)	Overexpression in non-small cell lung cancer (Välk et al. 2010), overexpression in glioma (Takahashi et al. 2012)
Kinesin-10	KIF22/KID	Chromosome arm alignment and congression (Wandke et al .2012)	Overexpression in breast and lung cancer (Oncomine data mining by Yu et al. 2014)

3.6 The Growth arrest-specific protein 2 (GAS2) family

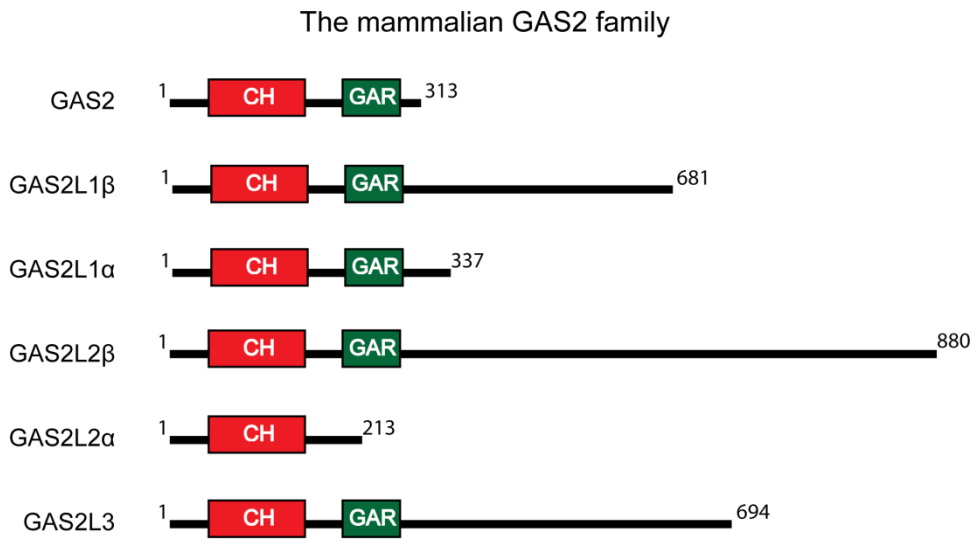

Figure 9: The mammalian Growth-arrest specific protein 2 (GAS2) family.
The GAS2 family consists of the four family members GAS2, GAS2L1, GAS2L2, and GAS2L3. The proteins harbor two conserved domains and differ in their unstructured C-terminal part. The calponin homology domain (CH) is a putative actin-binding domain and the Gas2-related (GAR) domain resembles a putative microtubule-binding domain. The GAS2 family members are differently expressed in tissues and in the cell cycle indicating a specific function for each protein (see 3.6).

The GAS2 family consists of GAS2 and its three relatives Growth arrest-specific protein 2 like 1 (GAS2L1), GAS2L2, and GAS2L3 (Figure 9). Orthologues of the protein family are evolutionary conserved in vertebrates, are not present in yeast, and one identified paralogue named Pigs (pickled eggs) is existing in *Drosophila melanogaster* (Pines et al., 2010). The protein family shares two conserved domains in the N-terminal part, a calponin homology (CH) domain and a Gas2-related (GAR) domain. The CH domain is a putative actin-binding domain and the GAR domain resembles a putative microtubule-binding domain.

A related family of cross-linking proteins are spectraplakins which also harbor CH and GAR domains (Sun et al., 2000; Suozzi et al., 2012). In spectraplakin family members, such as the microtubule-actin cross-linking factor (MACF), the CH domain acts as an actin-binding domain and the GAR domain acts as a microtubule-binding domain.

In the GAS2 family, the C-terminal part shows greater variation between family members and orthologues. The first family member *GAS2* was identified in a screen for genes specifically expressed at growth arrest, the hitherto uncharacterized genes

received their family name (Schneider et al., 1988). GAS2 is an actin filament-associated protein (Brancolini et al., 1992) for which the GAR domain is shown to localize to microtubules (Sun et al., 2000). The GAS2 family members GAS2L1 and GAS2L2 encode for two isoforms α and β, with α being the shorter isoform missing the long unstructured C-terminal part (Goriounov et al., 2003). The CH-domain of GAS2L1 and GAS2L2 is responsible for actin filament binding and the GAR domain for microtubule filament binding. Surprisingly the unstructured C-terminus is able to bind to microtubule filaments. The shorter isoforms GAS2L1α and GAS2L2α co-localize with actin filaments whereas the longer isoforms GAS2L1β and GAS2L2β localize at branching points of the two filament systems suggesting that these GAS2 family member can act as cross-linking proteins. More recently, it was confirmed that GAS2L1 and GAS2L2 act as cross-linker, mediating the filament cross-linking together with the microtubule End-binding protein 1 (EB1) (Stroud et al., 2014). Previously, we and others could show that GAS2L3 is also a cross-linking protein co-localizing with both the actin and the microtubule cytoskeleton (Stroud et al., 2011; Wolter, 2011; Wolter et al., 2012). *In vivo* and *in vitro* analyses of GAS2L3 mutants suggest that the CH domain acts as actin-binding domain, like for all members of the protein family. Surprisingly, the C-terminal part of GAS2L3 and not the GAR domain mediates the binding of GAS2L3 to microtubules. Interestingly, *in vitro* the C-terminal part of GAS2L3 co-sediments with both F-actin and microtubules revealing several binding sites for both cytoskeleton filaments as well. In contrast to other GAS2 family members, the GAS2 domain of GAS2L3 does not localize to microtubules and mediates the binding of GAS2L3 to the CPC in mitosis instead (Fackler et al., 2014).

Additionally to variations in the protein structure, GAS2 family proteins are differently expressed in tissues suggesting specialized functions for the proteins. GAS2 is ubiquitously expressed in human tissues according to the Genecards database (Safran et al., 2003) and its mRNA level are high in interphase HeLa cells (Wolter et al., 2012).

Immunoblotting of GAS2L1 for different mice tissues shows a distinct expression in the testis and to an lesser extent in the brain for the β isoform (Goriounov et al., 2003). *GAS2L1* mRNA expression can be detected by Northern blot in multiple mice and human tissues but so far this could not be validated on protein level. HeLa cells also display only basal *GAS2L1* mRNA level (Wolter et al., 2012). Interestingly,

GAS2L1 protein level can be induced after growth arrest induction but only to a rather weak extent (Goriounov et al., 2003).
In contrast, the GAS2L2 mRNA is specifically expressed in the skeletal muscle tissue in humans indicating a highly specialized function (Goriounov et al., 2003).
GAS2L3 mRNA is ubiquitously expressed in human tissues and cell lines (Stroud et al., 2011). In contrast to other GAS2 family members, GAS2L3 protein expression is restricted to G2/M phase indicating a cell division-specific role (Wolter et al., 2012).
Despite extensive characterization of the domains and the actin- and microtubule-binding ability of the GAS2 family members rather little is known about their *in vivo* function.

3.7 Aim of the project

Gas2l3 was identified by our group as DREAM target gene in conditional Lin9-knockout MEFs after comparative microarray gene expression analysis (Reichert et al., 2010). Subsequent characterization in human cell lines revealed, that GAS2L3 is an F-actin and microtubule cross-linking protein expressed in G2/M, plays a role in cytokinesis, and is important for chromosomal stability (Wolter, 2011; Wolter et al., 2012).
The aim of the first part of the study was to analyze *GAS2L3* regulation and to comprehend GAS2L3 function in mitosis and cytokinesis.
Besides *Gas2l3*, the microarray gene expression analysis identified several mitotic kinesins and MAPs as DREAM target genes. So far, it is not clear to what extent DREAM regulates mitotic kinesins and MAPs. In addition, a comprehensive analysis of mitotic kinesin expression in cancer cells is still missing.
In this regard, the aim of the second part of the study was to characterize the regulation of mitotic kinesins and cytokinesis MAPs by DREAM and to analyze their expression and therapeutic potential in cancer cell lines.

4 MATERIALS AND METHODS

4.1 Materials

4.1.1 Chemical stocks and reagents

All chemicals, if not further mentioned, were applied from the following companies in analyzing quality (p.a.):

AppliChem, Merck, Invitrogen, Sigma-Aldrich, ROTH

Chemical	**Stock concentration**
Agarose	Ready to use
Amonium persulfate (APS)	10% in H_2O
Bovine serum albumin (BSA)	3% in H_2O
Bromophenol blue	4 mg/ml in H_20
Diethylpyrocarbonate (DEPC)	Ready to use
dNTP (dATP, dCTP, GTP, TTP)	2 mM (each NTP) in H_2O
Doxorubicin	1 mM in H_2O
DMSO	Ready to use
Dithiothreitol (DTT)	1 M in H_2O
Ethidium bromide	10 mg/ml in H_2O
Hoechst 33342	10 mg/ml in H_2O
Hoechst 33258	10 mg/ml in H_2O
Luminol	250 mM in DMSO
p-Coumaric acid	90 mM in DMSO
Phenylmethylsulphonyl fluoride (PMSF)	100 mM in isopropanol
Polybrene (Hexadimethrine bromide)	4 mg/ml in H_2O
Propidium iodide (PI)	1 mg/ml in H_2O
Ponceau S solution	0.1% Ponceau S in 5% CH_3COOH
Protease Inhibitor Cocktail (PIC)(Sigma)	Ready to use
Proteinase K	10 mg/ml in 50 mM Tris pH 8.0, 1 mM $CaCl_2$
ProtoGel 30% (Biozym)	Ready to use
Random Primer (Roche)	500 µg/ml in H_2O
RNAse	10 mg/ml in 10 mM Tris pH 7.4, 150 mM NaCl
Shandon Immu-Mount (Thermo Scientific)	Ready to use
Sodium dodecyle sulfate (SDS)	20% in H_2O
TEMED (99%)	Ready to use
Trifast (Peqlab)	Ready to use
Triton X-100	Ready to use
Tween-20	Ready to use

4.1.2 Enzymes

Enzyme	Company
His-Taq DNA Polymerase (15 U/µl)	Provided by AG Prof. Gessler
Absolute QPCR SYBR Green mix	Thermo Scientific
M-MLV-RT Transcriptase (200 U/µl)	Thermo Scientific
RiboLock RNase-Inhibitor (40 U/µl)	Thermo Scientific
T4 DNA Ligase (400 U/µl)	New England Biolabs
Restriction endonucleases (10 U/µl)	Thermo Scientific (Fermentas) & New England Biolabs

4.1.3 Antibiotics

Antibiotic	Stock concentration	Final concentration	Application
Ampicillin	100 mg/ml	100 µg/ml	Selection of *E. coli* bacteria
Blasticidin	10 mg/ml	Cell line-dependent (1.1.10)	Selection of cell lines

4.1.4 Buffers and solutions

4.1.4.1 General buffers

Buffer	Ingredients
DNA Loading Buffer (5x)	15% ficoll
	0.05% bromophenol blue
	0.05% xylene cyanol
	0.05 M EDTA
	in 1 X TAE
Miniprep Solution S1	25 mM Tris/HCl, pH 8.0
	10 mM EDTA
	100 µg/ml RNAse A
Miniprep Solution S2	200 mM NaOH
	1% SDS
Miniprep Solution S3	29.44 g KCH_3COO
	11.5 ml CH_3COOH
	28.5 ml H_2O
Luria Bertani (LB) liquid Medium	25 g powder in 1 l H_2O, autoclaved
Luria Bertani (LB) Agar	40 g powder in 1 l H_2O, autoclaved
Phosphate buffered saline (PBS) (1x)	13.7 mM NaCl
	0.3 mM KCl
	0.64 mM Na_2HPO_4
	0.15 mM KH_2PO_4
	adjust pH to 7.4 with HCl
TAE buffer (1x)	40 mM Tris base
	5 mM CH3COOH
	10 mM EDTA, pH 8.0
Tris buffered saline (TBS) (1X)	50 mM Tris/HCl, pH 7.4
	150 mM NaCl
TE buffer (1x)	10 mM Tris/HCl, pH 7.5
	1 mM EDTA

4.1.4.2 Buffers for whole-cell lysates

Buffer	Ingredients
Bradford solution	50 mg Coomassie Brilliant Blue G250
	23.75 ml ethanol
	50 ml 85% (v/v) H_3PO_4
	ad 500 ml H_2O / filter twice
TNN lysis buffer	50 mM Tris/HCl, pH 7.5
	120 mM HCl
	5 mM EDTA
	0.5% NP-40
	10 mM $Na_4P_2O_7$
	2 mM Na_3VO_4
	100 mM NaF
	add to 500 ml H_2O
	Protease Inhibitor cocktail (PIC) 1:1000 (add fresh)
	1 mM DTT (add fresh)
	1 mM PMSF (add fresh)

4.1.4.3 Buffers for immunoblotting

Buffers	Ingredients
Acrylamide solution	30% (w/v) acrylamide
	0.8% (w/v) N,N´-methylenbisacrylamide
Blotting buffer (1x)	0.6 g Tris base
	2.258 g glycine
	150 ml methanol
	add to 1 l H_2O
Blocking Solution	3% milk poweder in TBS-T (w/v)
Electrophoresis sample buffer (ESB) (3x)	300 mM Tris/HCl, pH 6.8
	15 mM EDTA
	150 mM DTT
	12% (w/v) SDS
	15% (w/v) glycerol
	0.03% (w/v) bromophenol blue
Enhanced chemiluminescence (ECL) solution	10 ml 100 mM Tris/HCl, pH 8.5
	50 µl 250 mM luminol
	22 µl 90 mM p-Coumaric acid
	3 µl 30% H_2O_2
Ponceau S	0.1% Ponceau S
	5% CH_3COOH
SDS running buffer (10x)	144 g glycine
	30 g Tris
	10 g SDS
	add to 1 l H_2O
Stripping buffer	15 g glycine
	1 g SDS
	10 ml Tween-20
	add to 1 l H_2O
	adjust to pH 2.2
Separating gel buffer	1.5 M Tris/HCl, pH 8.8
Stacking gel buffer	0.8 M Tris/HCl, pH 6.8
TBS-T	0.5% Tween-20 (v/v) in TBS

4.1.4.4 Buffers for chromatin immunoprecipitation (ChIP)

Buffer	Ingredients
RIPA buffer	150 mM NaCl
	50 mM Tris, pH 8.0
	5 mM EDTA
	1 % IGEPAL
	0.5 % sodium deoxycholate
	0.1 % SDS
	Protease inhibitors (freshly added)
	PMSF (freshly added)
IP wash buffer	100 mM Tris, pH 8.5
	0.5 LiCl
	1 % IGEPAL
	1 % sodium deoxycholate
	Protease inhibitors (freshly added)
	PMSF (freshly added)
TE buffer (for ChIP)	10 mM Tris pH, 8.0
	1 mM EDTA
	Protease inhibitors (freshly added)
	PMSF (freshly added)
ChIP elution buffer	70 mM Tris, pH 8.0
	1 mM EDTA
	1.5 % SDS

4.1.4.5 Buffers for flow cytometry (FACS)

Buffer	Ingredients
Sodium citrate	38 mM in 1x PBS

4.1.4.6 Buffers for immunostaining

Buffer	Ingredients
Blocking solution	3% BSA in PBS (w/v)
Methanol	100%, store at -20°C
PBST	0.1-0.3% Triton-X in 1x PBS (v/v)
PSP	15 g paraformaldehyde
(3% paraformaldehyde,	10 g sucrose
2 % sucrose)	add to 500 ml in 1x PBS, store at -20ºC
4% PFA	4% PFA in PBS (w/v), store at -20°C
Trichloracteic acid (TCA)	10% TCA in PBS (w/v), store at 4°C

4.1.5 Transfection reagents

Tranfection reagent	Company
Metafectene® reagent	Biontex Laboratories
Lipofectamine® 2000 reagent	Life Technologies
Lipofectamine® RNAiMAX reagent	Life Technologies
HEPES buffer solution (HBS) (2x)	8.2 g NaCl
	5.95 g HEPES, acid
	0.105 g Na_2PO_4
	add to 500 ml ddH_2O
	adjust to pH 6.95, 7.00, 7.05 (with 5 M NaOH)
	Storage at 4°C
	sterile filtered
2.5 M $CaCl_2$	sterile filtered

4.1.6 Antibodies

4.1.6.1 Primary antibodies

Name	Lab ID	Origin & Clonality	Application & Dilution	Vendor	Catalog number
β-Actin	#196	Mouse monoclonal	WB 1:5000	Santa Cruz Biotechnology	sc-47778
Aurora B	#194	Rabbit polyclonal	IF 1:500	Abcam	ab2254
Aurora B pT232	#218	Rabbit polyclonal	IF 1:100	Rockland Immunochemicals	300-401-677
B-MYB (N-19)	#79	Rabbit polyclonal	ChIP 2µg	Santa Cruz Biotechnology	sc-724
B-MYB	-	Mouse monoclonal	WB 1:5	Gift from Watson laboratory (Hybridoma)	Tavner et al. 2007
CEP55	#262	Rabbit monoclonal	WB 1:20000	Abcam	ab170414
FOXM1	#165	Rabbit polyclonal	ChIP 2µg	Santa Cruz Biotechnology	sc-502
GAS2L3 (C8)	#215	Mouse monoclonal	01:50	Abnova	H00283431-M02
IgG	-	Rabbit IgG	ChIP 2µg	Sigma-Aldrich	I5006
KIFC1/HSET	#263	Rabbit polyclonal	WB 1:2000	Cell Signaling	12313
KIF2C/MCAK	#257	Sheep polyclonal	WB 1:5000	Gift from Wordeman laboratory	
KIF4A	#259	Rabbit polyclonal	WB 1:2000	Bethyl Laboratories, Inc.	A301-074A
KIF14	#261	Rabbit polyclonal	WB 1:2000	Bethyl Laboratories, Inc.	A300-912A
KIF20A/MKLP2	#260	Rabbit polyclonal	WB 1:1000	Bethyl Laboratories, Inc.	A300-879A
KIF23/MKLP1	#211	Rabbit polyclonal	IF 1:500 WB 1:5000	Santa Cruz Biotechnology	sc-867
LIN9	#163	Rabbit polyclonal	ChIP 2µg	Abcam	ab62329
Myosin IIA	#226	Rabbit polyclonal	IF1:500	Sigma-Aldrich	M8064
Phalloidin Alexa Fluor 594	#280	-	IF 1:50	Invitrogen	A12381
p21	#178	Rabbit polyclonal	WB 1:1000	Santa Cruz Biotechnology	sc-397
p130	#33	Rabbit polyclonal	ChIP 2µg	Santa Cruz Biotechnology	sc-317
PRC1	#258	Rabbit polyclonal	WB 1:2000	Santa Cruz Biotechnology	sc-8356
RhoA	#171	Mouse monoclonal	IF 1:100	Santa Cruz Biotechnology	sc-418
Spastin	#272	Mouse monoclonal	IF 1:100	Santa Cruz Biotechnology	sc-53443
α-tubulin	#158	Mouse monoclonal	IF 1:100	Sigma-Aldrich	T6074

4.1.6.2 Secondary antibodies

Name	Application & Dilution	Vendor
Anti-mouse HRP conjugated	WB 1:5000	GE Healthcare
Anti-rabbit HRP conjugated	WB 1:5000	BD Biosciences
Anti-sheep HRP conjugated	WB 1:1000	Santa Cruz Biotechnology (sc-2473)
Anti-mouse Alexa Fluor 488	IF 1:500	Invitrogen
Anti-mouse Alexa Fluor 594	IF 1:500	Invitrogen
Anti-rabbit Alexa Fluor 594	IF 1:500	Invitrogen

4.1.7 Plasmids

4.1.7.1 Plasmids for transient overexpression in mammalian cells

Plasmid	Lab ID	Description
pCDNA3-EGFP-GAS2L3	#1033	Mammalian overexpression
pCDNA3-EGFP-GAS2L3 (aa 170-310)	#1149	Mammalian overexpression
pCDNA3-EGFP-GAS2L3 (Δ170-309)	#1334	Mammalian overexpression

4.1.7.2 Plasmids for retroviral shRNA transduction

Plasmid	Lab ID	Description
pMSCV480-Blasticidin	#652	Empty control vector (Voorhoeve and Agami, 2003)
pMSCV480-shp53-Blasticidin	#679	shRNA for stable down-regulation of p53 (Voorhoeve and Agami, 2003)

4.1.7.3 Plasmids for lentiviral shRNA transduction

Plasmid	Lab ID	Description
pINDUCER10 (Blasticidin resistance)	#1369	Backbone for inducible miR30-shRNA expression (Meerbrey et al.2011), blasticidin resistance was cloned into the vector by Marc Fackler.
pCMV-VSV-G	#1348	Lentiviral packaging plasmid
psPAX2	#1386	Lentiviral packaging plasmid

4.1.8 Primer sequences

4.1.8.1 Primer for quantitative real-time PCR

housekeeping genes			
Gene	**Lab ID**	**Sequence (5' to 3')**	**Directionality**
GAPDH	SG645	GCCCAATACGACCAAATCC	fw
	SG646	AGCCACATCGCTCAGACAC	rev
RPS14	SG620	GGCAGACCGAGATGAATCCTCA	fw
	SG621	CAGGTCCAGGGGTCTTGGTCC	rev

DREAM subunit genes			
Gene	**Lab ID**	**Sequence (5' to 3')**	**Directionality**
LIN9	SG580	CCCCACCACGGTTACATTAT	fw
	SG581	CGGCGACTGTCCTAATAAAGG	rev
LIN37	SG789	CACTGGCAAAAGGCCATC	fw
	SG790	GGTCGAACAGCTTGATCACAT	rev
LIN52	SG684	GATGACATCGACATGTTGAAAGA	fw
	SG685	CCGTGTCATCTCTCTGGACTC	rev
LIN54	SG787	GCCACATCAGCCAGTAGCTC	fw
	SG788	TAACAACCACTGGCTTTGCTT	rev
MYBL2	SG630	TCCACACTGCCCAAGTCTCT	fw
	SG631	AGCAAGCTGTTGGTCTTCTTTGA	rev
FOXM1	SG1022	ACTTTAAGCACATTGCCAAGC	fw
	SG1023	CGTGCAGGGAAAGGTTGT	rev

Genes of interest			
Gene	**Lab ID**	**Sequence (5' to 3')**	**Directionality**
BIRC5	SG568	GCCCAGTGTTTCTTCTGCTT	fw
	SG569	CCGGACGAATGCTTTTTATG	rev
GAS2L3	SG1058	GCTGTCGGCATGAAGAGC	fw
	SG1059	AATCGATGAGAACAACTACAAGGA	rev
CEP55	SG1886	AAATAACACAGTTGGAATCCTTGAA	fw
	SG1887	TCAGTCTCTCCTTGGAAAGTGAC	rev
PRC1	SG1890	TTTACAAACCGAGGAGGAAATC	fw
	SG1891	TCGTGCCTTCAACTCTTCTTC	rev
KIFC1	SG1874	GAAGAACGGAGGGGACTGAT	fw
	SG1875	ACAGGGCTGCTTCTGATGTC	rev
KIF2A	SG1970	GAAAACTCTCGTACCTGCATGAT	fw
	SG1971	TGTATTAAGAGTATTTTCACAGGATGC	rev
KIF2B	SG1972	CAACCAGCGAGAGACAACCT	fw
	SG1973	TCATGCACCATAACCACATTG	rev
KIF2C	SG1870	AGGAGCATCTGGTTAACTCTGC	fw
	SG1871	TCTGCCCAGAGGTTCTGC	rev
KIF4A	SG1878	TGGTCAGACAGCCCAGATG	fw
	SG1879	TCTTCTAGCTTGGCGTTCATT	rev
KIF4B	SG1974	TTCCAAGTTAACTCGACTGCTG	fw
	SG1975	GCAGGACTCACACAGGCTATC	rev
KIF10	SG1976	AACAGGCCCAAGATACCTCA	fw
	SG1977	TCCACAAGTTAAGGGTTTATTTGA	rev
KIF11	SG1978	CATCCAGGTGGTGGTGAGAT	fw
	SG1979	TATTGAATGGGCGCTAGCTT	rev
KIF14	SG1882	CCTGTCTTTTTGCTTATGGTCAG	fw
	SG1883	TCTTCACTAAATCCCATCATCG	rev
KIF15	SG1980	GCTGCTGAAGCCTATCAGGT	fw
	SG1981	GATGTTGATGCCACACGTCTA	rev
KIF18A	SG1982	AGCATGGTGCCATCCTACA	fw
	SG1983	TCTGCAGTTAACGAACTGTTTGA	rev
KIF18B	SG1984	GTGGGTACTGCTGTCTGTGG	fw
	SG1985	CCATCACTGTGGTGACACCTT	rev
KIF20A	SG1866	CGGCGACTAGGTGTGAGTAAG	fw
	SG1867	GGATCCCTTGCGACATGA	rev
KIF20B	SG1986	AGGCTCGGAAGAGGAAGAGT	fw
	SG1987	TTCAAATTAGTTCTGGGTGTAGCA	rev
KIF22	SG1988	GCCCTGAGGAAGAGGAGATT	fw
	SG1989	GGTCCATGCTGCTTAGCTTC	rev
KIF23	SG1862	CCTAACGTCCCGCAGTCTT	fw
	SG1863	AGGTTTCCGGGGTGTCTTAG	rev

4.1.8.2 Primer for chromatin immunoprecipitation (ChIP)

ChIP Primer			
Gene	**Lab ID**	**Sequence (5' to 3')**	**Directionality**
GAPDH2	SG540	GGCAGCAAGAGTCACTCCA	fw
	SG541	TGTCTCTTGAAGCACACAGGTT	rev
BIRC5	SG612	CCATTAACCGCCAGATTTGA	fw
	SG613	GCGGTGGTCCTTGAGAAAG	rev
CEP55	SG1919	TCCTTTGTGAAATCCCGTTG	fw
	SG1920	GATTCTCCCTGTGTGAAGTGC	rev
PRC1	SG1892	GGGTGGTTGTTGCTCTCG	fw
	SG1893	CGCACCTTCTCCTCATGG	rev
GAS2L3	SG2077	CCCCGCCTTATGATTGGT	fw
	SG2078	TGGGCCTCAGGGTCAGTA	rev
KIFC1	SG1876	ACCAGGAGGCGCTAGTCC	fw
	SG1877	ACTGGCCAAGCGAAACTG	rev
KIF2A	SG1999	CCGGATCCCGTACTGTCA	fw
	SG2000	GTGGTTTCAGGGGCTTTCTA	rev
KIF2B	SG2001	GTTCTTTCTCGCCATGATCC	fw
	SG2002	AGTGAGGGTGAAGGGGTTG	rev
KIF2C	SG1896	ATCCCAGAGCCCTCATTGT	fw
	SG1897	ACCTTGTACTGCGGGGTTC	rev
KIF4A	SG1880	TGAAACTTGGCGGTTAAAGC	fw
	SG1881	CCCCGTAACTCACCAAACTAA	rev
KIF4B	SG2005	GGTGTCTCTGGGAGGGATTT	fw
	SG2006	AATGTCCCTTCCCCGTTC	rev
KIF10	SG2007	GAGGGTCCTGGCCATTTT	fw
	SG2008	CCCCCTACCTGCTGTTCA	rev
KIF11	SG2009	GCTCCAGTGAGGATACTGCAT	fw
	SG2010	CCCAGAAACTAAGCAACGACTC	rev
KIF14	SG1884	TTCAAATTGCGGCCTTCT	fw
	SG1885	ACCCCCTCGACACAGTCC	rev
KIF15	SG2011	CCCTCCAAGTAGAGGCAAAAG	fw
	SG2012	CTTCGCCAGTCGTGTTTCTT	rev
KIF18A	SG2013	ACCCAGAACCCATTAATCCA	fw
	SG2014	GCCTATGCCCTCTGCTAGG	rev
KIF18B	SG2015	CGGGGACCACAGAGACTG	fw
	SG2016	GGTTGGGCACACGAGAGTAG	rev
KIF20A	SG1868	AAATAGTGTACCGGCGTTGG	fw
	SG1869	TTTGTCTTAAGGGGAAAAACGA	rev
KIF20B	SG2017	TACTCCCAGCGTTCAGTGC	fw
	SG2018	TGCGATGTTACCGTTTTCAA	rev
KIF22	SG2019	CGGCGCGTAGTCTTGATT	fw
	SG2020	CCATTCCACTCCCTCCTTG	rev
KIF23	SG1894	CCTAACGTCCCGCAGTCTT	fw
	SG1895	GCCTCGTACTCACGCTGAC	rev

4.1.8.3 Primer for cloning

pInducer shRNA cloning primer			
Name	**Lab ID**	**Sequence (5' to 3')**	**Directionality**
SG1161-3'-miR30PCREcoRIF	SG1161	CTAAAGTAGCCCCTTGAATTCCGAGGCAGTAGGCA	fw
SG1164-amplifysmir30shRNA	SG1164	CAGAAGGCTCGAGAAGGTATATTGCTGTTGACAGTGAGCG	rev

4.1.8.4 Primer for sequencing

pInducer shRNA sequencing primer		
Name	**Lab ID**	**Sequence (5' to 3')**
SG1162-Mir5	SG1162	GCTTCGGCAGCACATATACTA

4.1.9 siRNA sequences

Gene	Lab name	siRNA Sequence (5' to 3')	Reference
Mock	siControl	UAGCGACUAAACACAUCAA	siGENOME nontargeting siRNA 1, DHARMACON
GAS2L3	siRNA Gas2l3#1	GGGAUACUCUUCAAGGAUU	Wolter P. et al, 2012
GAS2L3	siRNA Gas2l3#2	CUAUGUCAGUCCGUUCUAA	Wolter P. et al, 2012
FOXM1	siFoxM1	GGACCACUUUCCCUACUUU	Wu Qi-Fei et al. 2010
MYBL2	siRNA MYB5	GCAGAGGACAGUAUCAACATT	Mannefeld M et al, 2009
LIN9	siRNA Lin9-4	GGAAGAGAGAUCAGCAUUAUU	Osterloh et al, 2007
LIN37	siRNA Lin37-2	AGAUCCUACGAGAGAUGUA	Schmit F. et al, 2007
LIN52	siRNA Lin52-2	UACAGAACCUAGCCUAUCA	Schmit F. et al, 2007
LIN54	siRNA Lin54.3	GCA AGC AAC UCU ACC UUU AU	Schmit F. et al, 2007

4.1.10 shRNA sequences

4.1.10.1 Lentiviral shRNA sequences

A comprehensive list with all analyzed sequences can be found in Table 2. List of the 97-Oligo sequences used in the thesis:

Gene KIFC1, Plasmid lab ID: #1451, Oligo lab ID: SG1802
TGCTGTTGACAGTGAGCGatagtgctaagatgctcatgttTAGTGAAGCCACAGATGTAaacatgagcatcttagcactacTGCCTACTGCCTCGGA
Gene KIF2C, Plasmid lab ID: #1453, Oligo lab ID: SG1808
TGCTGTTGACAGTGAGCGccaggaagcagactcaagaggaTAGTGAAGCCACAGATGTAtcctcttgagtctgcttcctgaTGCCTACTGCCTCGGA
Gene : KIF4A, Plasmid lab ID: #1457, Oligo lab ID: SG1778
TGCTGTTGACAGTGAGCGcgccgagatagagacagagttaTAGTGAAGCCACAGATGTAtaactctgtctctatctcggcaTGCCTACTGCCTCGGA
Gene: KIF14, Plasmid lab ID: #1461, Oligo lab ID: SG1741
TGCTGTTGACAGTGAGCGccagagcaagttggatatcaaaTAGTGAAGCCACAGATGTAtttgatatccaacttgctctgaTGCCTACTGCCTCGGA
Gene: KIF20A, Plasmid labd ID: #1463, Oligo lab ID: SG1715
TGCTGTTGACAGTGAGCGcacgcaagaacctgctatcagaTAGTGAAGCCACAGATGTAtctgatagcaggttcttgcgtaTGCCTACTGCCTCGGA
Gene: KIF23, Plasmid lab ID: # 1469, Oligo lab ID: SG1710
TGCTGTTGACAGTGAGCGcccagagtttgcagatatgataTAGTGAAGCCACAGATGTAtatcatatctgcaaactctggaTGCCTACTGCCTCGGA
Gene: PRC1, Plasmid lab ID: #1471, Oligo lab ID: SG1728
TGCTGTTGACAGTGAGCGcgacgaccatcttgcaactagaTAGTGAAGCCACAGATGTAtctagttgcaagatggtcgtctTGCCTACTGCCTCGGA
Gene: CEP55, Plasmid lab ID: #1480, Oligo lab ID: SG1929
TGCTGTTGACAGTGAGCGccagatgcaggcatgtactttaTAGTGAAGCCACAGATGTAtaaagtacatgcctgcatctgtTGCCTACTGCCTCGGA

4.1.11 Cell lines, culture medium, and antibiotics

Medium	Ingredients
Dulbecco modified Eagle's minimal essential medium (DMEM)	10% FCS
	1% Penicillin-Streptomycin (Pen-Strep)
Roswell Park Memorial Institute medium (RPMI) 1640 + Glutamax	10% FCS
	1% (Pen-Strep)
Non-small cell lung cancer (NSCLC)- Medium	RPMI 1640 + Glutamax
	10% FCS
	1% (Pen-Strep)
	1% Sodium Pyrovate
	1% HEPES, 1M, pH 7.4
	11,25 ml D-Glucose, waterfree 20% in RPMI)
MCF 10A Medium	F12 / NutMix
	10% horse serum
	1% (Pen-Strep)
	20 ng/ml EGF
	100 ng/ml Cholera toxin
	0.01 mg/ml Insulin
	500 ng/ml Hydrocortison

Cell line	Tissue	Cell type	Disease	Medium	Antibiotic concentration
BJ-ET	Skin	Foreskin fibroblast	none	DMEM	Blasticidin 4.5 µg /ml
HeLa	Cervix	epithelial	adenocarcinoma	DMEM	
MCF 10A	Mammary gland	epithelial	fbrocystic disease	MCF 10A	
MCF-7	Mammary gland	epithelial	adenocarcinoma	DMEM	
T-47D	Mammary gland (Duct)	epithelial	ductal carcinoma	RPMI 1640	
BT-20	Mammary gland	epithelial	carcinoma	DMEM	
BT-549	Mammary gland	epithelial	ductal carcinoma	RPMI 1640	
Hs 578T	Mammary gland	epithelial	carcinoma	RPMI 1640	
MDA-MB-468	Mammary gland	epithelial	adenocarcinoma	DMEM	
MDA-MB-231	Mammary gland	epithelial	adenocarcinoma	DMEM	Blasticidin 10 µg/ml
WI-38	Lung	fibroblast	none	RMPI 1640	
H226	Lung	epithelial	squamous cell carcinoma; mesothelioma	RMPI 1640	
A549	Lung	epithelial	carcinoma	RMPI 1640	
H460	Lung	epithelial	carcinoma; large cell lung cancer	RMPI 1640	Blasticidin 5.0 µg/ml
H522	Lung	epithelial	stage 2,adenocarcinoma; non-small cell lung cancer	RMPI 1640	
HOP-62	Lung	epithelial	adenocarcinoma, carcinoma	RMPI 1640	
HOP-92	Lung	epithelial	adenocarcinoma, carcinoma	RMPI 1640	
H23	Lung	epithelial	adenocarcinoma; non-small cell lung cancer	RMPI 1640	Blasticidin 5.0 µg/ml
H358	Lung/Bronchiole	epithelial	bronchioalveolar carcinoma; non-small cell lung cancer	NSCLC	
H441	Lung	epithelial	papillary adenocarcinoma	NSCLC	

Packaging cell lines	Medium	Description
Plat-E	DMEM	Packaging cell line for retroviral infection
HEK 293T	DMEM (After transfection, medium was replaced by the medium of the target cell line at the next morning)	Packaging cell line for lentiviral infection

Cell lines for immunostaining	Medium	Description
HeLa EGFP-GAS2L3	DMEM	Created in the lab (Marc Fackler)
HeLa mCherry-α-tubulin	DMEM	Created in the lab (Stefanie Hauser)
HeLa mRFP- α-tubulin GFP-H2B	DMEM	Gift from Patrick Meraldis lab
T98G	DMEM	Brain glioblastoma multiforme cell line
U2OS	DMEM	Human osteosarcoma tumour cell line

4.1.12 Markers

Marker	Company
GeneRuler 1 kb DNA ladder	Thermo Scientific (Fermentas)
GeneRuler 100 bp DNA ladder	Thermo Scientific (Fermentas)
PageRuler Prestained Protein Ladder	Thermo Scientific (Fermentas)

4.1.13 Kits

Kit	Company
GeneJET Gel Extraction Kit	Thermo Scientific
QIAquick PCR Purification Kit	QIAGEN
PureLink HiPure Plasmid Midi-/Maxiprep kit	Life Technologies

4.1.14 Beads

Beads	Company
Dynabeads Protein G	Life Technologies

4.1.15 Devices

Device	Company
Agarose gel electrophoresis system	Peqlab
SDS-PAGE gel electrophoresis system	BIO-RAD
Trans-Blot wet transfer apparatus	BIO-RAD
FACS Cytomics FC500	Beckman Coulter
Incubators	Heraeus and Nunc
Centrifuge 5417R	Eppendorf
Centrifuge 5415D	Eppendorf
Centrifuge Megafuge 1.0R	Heraeus
Thermocycler T1	Biometra
Quantitative PCR thermocycler MX3000	Stratagene
Nanodrop 2000	Thermo Scientific
Confocal microscope Nikon Eclipse Ti C1	Nikon
Fluorescence microscope Leica DMI 6000B + camera DFC350 FX R2	Leica
Microscope time-lapse chamber	Selfmade Biocenter Würzburg
Bioruptor	Diagenode
Spectrometer Ultrospec 2100 pro	Biosciences
Multiskan Ascent	Labsystems

4.2 Methods

4.2.1 Mammalian cell culture techniques

4.2.1.1 Passaging of adherent cell lines

Materials:

- Cell culture medium, preheated to 37°C
- PBS, pH 7.4
- Trypsin/EDTA

Method:
All cell lines were cultivated in a tissue culture incubator at 37°C, 95% air and 5% carbon dioxide (CO_2). Every two to three days the cell culture medium was removed and discarded. Subsequently, the cells were briefly rinsed in PBS and incubated with Trypsin/EDTA in the incubator. Cell detachment was improved by gentle shaking and observed under the microscope. The detached cells were resuspended in fresh medium and the desired cell number was seeded into a new cell culture dish.

4.2.1.2 Freezing and thawing of cell lines

Materials:

- Cell culture medium, RT
- Freezing medium: Cell culture medium + 10% DMSO (v/v), 4°C
- PBS, pH 7.4
- Trypsin/EDTA
- Cryotubes

Method:
In order to freeze a cell line from a 10 cm cell culture dish, the cell culture medium was discarded and the cells were briefly washed in PBS. Subsequently, the cells were incubated with Trypsin/EDTA in the incubator until detachment. The cells were resuspended in 10 ml cell culture medium to inhibit Trypsin/EDTA, followed by centrifugation in a 15 ml tube at 1200 g for 3 min. After discarding the medium the

cell pellet was resuspended in 1 ml freezing medium and transferred to cryotubes. After storage on ice for a view minutes, the cryotubes were stored at -80°C for at least 24 h up to 6 months. For long-term storage the cells were stored in liquid nitrogen.

In order to thaw a cell line, the cryotubes were thawed in a 37°C water bath as fast as possible. Immediately after thawing the cells were mixed with 9 ml fresh cell culture medium in a 15 ml tube and centrifuged for 3 min at 1200 g. The cell culture medium was discarded and the cell pellet was resuspended in fresh cell culture medium. The suspension was seeded in a 10 cm cell culture dish.

4.2.1.3 Counting of cells

Materials:

- Neubauer Chamber

Method:
Trypsinized cells in medium suspension were inverted several times and 10 µl of the suspension was used for the Neubauer Chamber to calculate the number of cells per ml according to this formula:

Cells/ml = (Counted cells/Number of counted large squares (4))*10^4

4.2.1.4 Transient transfection methods

4.2.1.4.1 Calcium phosphate transfection

Materials:

- 2x HBS , pH 7.05
- 2.5 M Ca_2Cl
- ddH_2O

Method:

The retroviral packaging cell line Plat-E was used for the infection of BJ-ET cells (4.2.1.5).

On the first day, a confluent 10 cm dish with Plat-E cells was splitted 1:4 into a new 10 cm dish in the afternoon. On the second day, one hour before transfection, the medium was replaced with fresh one. The plasmids were transfected by the calcium phosphate transfection method with HBS in the afternoon. 50 µl of 2.5 M Ca_2Cl were mixed with 20 µg plasmid DNA in an Eppendorf tube. To the mix ddH_2O was added until a volume of 500 µl was reached and mixed again. 500 µl of 2x HBS was transferred to a 15 ml tube and the Ca_2Cl/DNA mix was added dropwise to the HBS under constant bubbling of the HBS. The complete mix was added drop wise to the Plat-E cells to completely cover the 10 cm dish. On the third day, in the morning, the old medium was discarded and 8 ml of fresh medium was added and incubated for 24h until infection. The infection procedure of BJ-ET cells is described in 4.2.1.5.

HEK 293T cells were used as lentiviral packaging cell line for the infection of human cell lines (4.2.1.6). On the first day, a confluent 10 cm dish of HEK 293T cells was splitted 1:4 into a new 10 cm dish in the afternoon. On the second day, one hour before transfection, the medium was replaced by fresh medium. The following steps were performed under S2 conditions. 50µl of 2.5 M Ca_2Cl were mixed with 4.5 µg of the pCMV-VSV-G plasmid, 3 µg of the psPAX2 plasmid and 6 µg pINDUCER plasmid in an Eppendorf tube. To the mix ddH_2O was added until a volume of 500 µl was reached and mixed again. 500 µl of 2x HBS was transferred to a 15 ml tube and the Ca_2Cl/DNA mix was added dropwise to the HBS under constant bubbling of the HBS. The complete mix was added to the HEK 293T cells drop wise to cover the complete 10 cm dish. On the third day, in the morning, the old medium was discarded and 8 ml of fresh medium was added to the cells. The infection procedure of human cell lines is described in 4.2.1.6.

Confluent HEK 293T cells from a 10 cm dish were splitted 1:12 into 6 cm dishes. Half of the the transfection reagents and plasmids were used to downscale the method. The next day, the HEK 293T cells were incubated in 3 ml fresh medium.

4.2.1.4.2 Liposomal transfection

Materials:

- Opti-MEM® (life technologies)
- Cell culture medium (10% FCS, without Pen-Strep!)
- Transfection reagent:
  - Metafectene® reagent (Biontex Laboratories)
  - Lipofectamine® 2000 reagent (Life Technologies)
  - Lipofectamine® RNAiMAX reagent (Life Technologies)

Method:

The liposomal transfection method was applied for transient plasmid and siRNA transfections using commercial transfection reagents. The transfections were all performed as forward transfections according to the manufacturer's protocols for the reagents. The following table shows a list of seeded cell numbers at different cell culture dish sizes:

Cell line	**35 mm dish**	**6 well plate**	**6 cm dish**
HeLa	$0.2\text{-}0.4\text{x}10^5$	$1.7\text{-}2.5\text{x}10^5$	$4.2\text{x}10^5$
H23	X	X	$4.5\text{x}10^5$
MDA-MB-231	X	X	$3.5\text{x}10^5$

In the following paragraph, the ratios used for siRNA and plasmid transfections of the reagents are summarized:

Metafectene:

Metafectene was used for siRNA transfection in a siRNA (µl) / Metafectene (µl) ratio of 1:4 and for plasmid transfection in a plasmid (µg) / Metafectene (µl) ratio of 1:3.

Lipofectamine 2000:

Lipofectamine 2000 was used for siRNA transfection in a siRNA (µl) / Lipofectamine 2000 (µl) ratio of 1.7:2.5 and for plasmid transfection in a plasmid (µg) / Lipofectamine 2000 (µl) ratio of 1:2.

RNAiMAX:
RNAiMAX was used for siRNA transfection in a siRNA (µl) / RNAiMAX (µl) ratio of 1.7:2.5.

The siRNA was always transfected in a concentration of 50 nM from a 75 µM stock. In MDA-MB-231 and H23 cells only RNAiMAX was used for siRNA transfection. All of the three reagents were used in HeLa cells for siRNA transfection. 0.2 µg of plasmid DNA was transfected into HeLa cells in 35 mm dishes and 1-2 µg of plasmid DNA was transfected into HeLa cells in 6-well dishes.

4.2.1.5 Retroviral infection of BJ-ET cells

Materials:

- Polybrene (4 mg/ml)
- Filter (0.45 µm)

Method:
One day before infection, $8x10^5$ BJ-ET cells were seeded into a 10 cm dish in the afternoon. The next morning, the medium of calcium phosphate transfected Plat-E cells was filtered (0.45 µm) and transferred into a 15 ml tube and the Plat-E cells were discarded. 14 µl of polybrene and 7 ml of fresh medium were added to ~7 ml medium to a final volume of 14 ml and the medium was mixed. The BJ-ET cells were incubated for 6 h in 7 ml of the virus containing medium. Then the medium was replaced with fresh one. On the next day, the medium was replaced one more time with fresh one and in the evening the cells were selected with the desired antibiotic (4.1.11).

4.2.1.6 Lentviral infection of pINDUCER-shRNAs

Materials:

- Polybrene (4 mg/ml)
- Filter (0.45 µm)

Methods:

One day before infection, 1-2x10^5 human cells were seeded into a 6 well chamber in the afternoon. In the next morning, the medium of calcium phosphate transfected HEK 293T cells (4.2.1.4.1) was filtered (0.45 µm) and transferred into a 15 ml tube and the HEK 293T cells were discarded. 14 µl of polybrene was added to the filtered medium (~ 7ml) and 7 ml fresh medium was added to a final volume of 14 ml. The combined medium was mixed. The cell lines were incubated for 24 h in 2 ml of the virus containing medium. Then, the medium was replaced with fresh medium in the next morning and the selection process was started in the evening (4.1.11).

When HEK 293T cells were seeded in 6 cm dishes, fresh medium was added up to a volume of 5 ml + 5 µl of polybrene and mixed after filtration of the medium. The cell lines were also incubated for 24 h in 2 ml of the virus containing medium. The rest was performed as described above.

4.2.1.7 DNA damage a ssay in BJ-ET cells

Materials:

- DMEM (10% FCS)
- PBS, pH 7.4
- Doxorubicin (1 mM)

Method:

On the first day, 7x10^5 cells of the different BJ-ET cell lines were seeded per 10 cm cell culture dish. After 24 h, 1 µM of doxorubicin was added to the cells and incubated for 1 h. Then the cells were rinsed 2x with PBS and fresh DMEM was added to the cells. The washing steps were also performed for the control cells. 24 hours later, the cells were harvested and whole-cell lysates were prepared (4.2.4.1).

4.2.1.8 Cell proliferation assay with crystal violet staining

The effect of kinesin depletion on cell proliferation was analyzed using the crystal violet assay.

Materials:

- PBS, pH 7.4
- PBS, pH 7.4 + 3.7% paraformaldehyde
- Tap water
- 20% ethanol + 0.1% crystal violet
- Doxycycline (1 mg/ml)

Method:

$1x10^4$ MDA-MB-231 cells were seed into 6 cm cell culture dishes with 4 ml medium. The cells were treated either with 4 µl doxycycline or without. The medium and doxycycline were changed every two days for ten days. Then the cells were briefly washed with PBS and fixed in 3 ml PBS + 3.7% paraformaldehyde for 10 min. After washing the cells 2x with tap water, the cells were incubated with 2.5 ml of 20% ethanol + 0.1% crystal violet for 20 min. The solution was discarded and the cells were rinsed 3x with tap water. After removing the water, the cells were air-dried for several hours and stored at 4°C.

To quantify the kinesin depletion effect on proliferation in lung cancer cell lines, $2x10^3$ NCI-H460 cells and $1X10^5$ NCI-H23 cells were seeded into 6 well chambers as -/+ 1 µg/ml doxycycline triplicates. The medium and doxycycline was changed every two days for seven days. The cells were washed with PBS, fixed in 1.5 ml PBS + 3.7% paraformaldehyde for 10 min, washed again 2x with tap water and stained with 1.5 ml 20% ethanol + 0.1% crystal violet for 20 min. After washing the cells 3x with tap water, the cells were air-dried and stored at 4°C. The results were scanned and the crystal violet staining was quantified (4.2.1.9).

4.2.1.9 Quantification of the crystal violet staining

Materials:

- 10% acetic acid

Method:

The crystal violet was resuspended in 1 ml of 10% acetic acid for 10 min on a shaker. The suspension was transferred into an Eppendorf tube for storage. The crystal violet was quantified using 96-well plates and a volume of 10 µl of the suspension with 90 µl of 10% acetic acid. The absorbance of the samples was measured with an ELIZA reader with a wavelength of 595 nm. The results were normalized to the control (100 µl acetic acid).

4.2.1.10 Determination of the cell cycle phase by flow cytometry

Materials:

- Cell culture medium, 4°C
- PBS, pH 7.4
- Trypsin/EDTA
- Cryotubes (15 ml)
- 80% ethanol, 4°C
- Sodium citrate (38 mM)
- Propidium iodide (1 mg/ml)
- RNAse (10 mg/ml)

Method:

To prepare a fluorescence-activated sorting by flow cytometry (FACS) measurement, the cells were briefly washed in PBS and trypsinized until they were detached and not clumpy. This step was enhanced with gentle shaking and observed under the microscope. Thereafter, Trypsin/EDTA was neutralized in cell culture medium in a 15 ml cryotube. Then the cryotube was placed in an ice bucket until all samples were harvested. The cells were centrifuged at 1000 g for 3 min at 4°C. The cell pellet was resuspended in 5 ml cold PBS and centrifuged under the same conditions one more time. After discarding the PBS, the cell pellet was resuspended under slow shaking in

80% ethanol and stored at -20°C. The sample was stored at least one night at -20°C, but the time could be extended up to several months.
Two hours before measurement, the sample was centrifuged at 1000 g for 5 min at 4°C. After discarding the ethanol, the cell pellet was resuspended in 5 ml cold PBS and centrifuged for 3 min at the same speed and temperature. Then the PBS was discarded and the cell pellet was resuspended in 500 µl of sodium citrate (38 mM) containing 25 µl RNAse (10 mg/ml) and placed into a 37°C water bath for 30 min. After the incubation, the suspension was placed into an ice bucket and 15 µl of propidium iodide was added to the sample shortly before measurement.

4.2.2 Molecular biology methods Part I (RNA, cDNA)

4.2.2.1 RNA isolation

Materials:

- peqGOLD TriFast (PEQLAB), 4°C
- Chloroform, 4°C
- Isopropanol, 4°C
- 75% ethanol (in DEPC-H_2O), 4°C
- RNAse free H_2O (DEPC-H_2O)

Method:
The cell culture dish was placed on ice immediately after recovery from the incubator. Then the cell culture medium was discarded and the rest medium was removed by a pipette. As fast as possible TriFast was added according to the manufacturer's protocol. For a 10 cm dish, 1 ml of TriFast was added and dispensed under gentle shaking over the complete cell culture dish. After pipetting the solution a view times over the surface of the cell culture dish, the solution was transferred into an Eppendorf tube. At this point, the RNA sample could be stored for a view weeks at -20°C or for long term storage at -80°C.
For RNA purification the Trifast solution was placed for 5 min at RT. Then 200 µl of chloroform was added to the sample and it was vortexed until a homogenous solution was visible. After 2 min at RT, the sample was centrifuged at 13800 g for 10 min at 4°C. Then the aqueous part of the solution (containing the RNA) was transferred to a

new Eppendorf tube on ice and 500 µl of cold isopropanol was added to the sample. To enhance the RNA precipitation, the sample was placed for 15 min at -20°C. Then the sample was centrifuged at 13803 g for 10 min at 4°C. The isopropanol was discarded and 1 ml of 75% cold ethanol was added to the sample. The sample was vortexed and placed for 10 min at -20°C. Then the sample was centrifuged at 9585 g for 5 min at 4°C. The ethanol was removed and the sample was washed and centrifuged one more time with 75% cold ethanol under the same conditions. The ethanol was removed again and the pellet was dried for 10 min at RT in the Eppendorf tube upside down. To solubilize the RNA, 20-40 µl of DEPC-H_2O (cell line and cell quantity-dependent) was added to the pellet and the Eppendorf tube was heated at 55°C for 10 min under slow shaking. Then the sample was placed on ice for minimum 30 min before the RNA concentration was measured with the NanoDrop spectrometer.

4.2.2.2 Reverse transcription PCR (RT-PCR)

Materials:

- DEPC-H_2O
- Random primer (0.5 mg/ml)
- dNTP's (2mM)
- Ribolock RNAse inhibitor (Fermentas, 40U/µl)
- M-MLV 5X reaction buffer (Thermo Scientific)
- M-MLV-RT (Thermo Scientific, 250 U/µl)

Method:

The isolated RNA was reverse transcribed into cDNA for further applications. Each reaction was adjusted like mix 1. Then mix 1 was placed into the thermocycler and the PCR program was started. Meanwhile, mix 2 was prepared and added to mix 1 at the 4°C step. When the program finished, the cDNA was stored at -20°C or used for quantitative real-time PCR analysis.

Mix 1(PCR-tube)	
RNA:	2.0 to 2.5 µg
Random primer:	0,5 µl
DEPC-H_2O:	add to 10 µl
Mix 2	
M-MLV 5 x Reaction buffer:	5 µl
DNTPs:	6.25 µl
RiboLock RNase Inhibitor:	0.5 µl
M-MLV Reverse Transcriptase:	0.5 µl
DEPC-H_2O:	2.75 µl
PCR program:	
70°C	5 min
4°C	2 min
37°C	60 min
70°C	15 min
4°C	∞

4.2.2.3 Quantitative real-time PCR (qRT-PCR)

Materials:

- AbsoluteTM QPCR SYBR Green Mix (Thermo Scientific).
- Primer mix (10 mM): Primer 1 (fw, 5 mM) and Primer 2 (rev, 5 mM)
- ABgene® PCR Plates (Thermo Scientific)
- ddH_2O (autoclaved)

Method:

The qPCR was used to compare the relative mRNA amount for genes of interest in siRNA experiments and in a multiple cell line mRNA expression analysis. Furthermore, the qPCR was used to compare the enrichment of specific promoter elements in ChIP experiments.

The cell line mRNA expression analysis and siRNA experiments were normalized to the expression of housekeeping genes (*GAPDH*, *RPS14*), whereas the ChIP experiments were normalized to the specific promoter elements in the input.

All qPCR reactions were performed as triplicates for the statistical analysis. For each gene, mix 1 was prepared and pipetted in triplicates into the plate wells.

Mix 1	
Standard Mix 1(x 3 for triplicate)	
SYBR Green Mix:	12.5 µl
Primer mix (fw/rev):	1 µl
ddH_2O:	10.5 µl

Then 1 µl of reverse transcribed cDNA or 1 µl of the ChIP sample was added to the wells. The plates were shortly centrifuged and placed into the quantitative PCR thermocycler MX3000 from stratagene. The PCR-reaction parameters were regulated with the MXPro software:

Selected experiment type: SYBR Green with dissociation curve
Thermal profile setup (custom):

Segment 1 (activation)
95°C 14:30 min
Segment 2 (amplification)
40 Cycles
95°C 0:30 min
60°C 1:00 min
Segment 3 (Dissociation)
95°C 1:00 min
60°C 0:30 min
95°C 0:30 min

The relative expression of a gene of interest was compared to a housekeeping gene according to this formula:

$2^{-\Delta\Delta Ct}$

$\Delta\Delta Ct = \Delta Ct$ (sample) – ΔCt (reference)

ΔCt = Ct (gene of interest) – Ct (housekeeping gene)

The standard deviation of $\Delta\Delta Ct$ was calculated according to this formula:

$$s = \sqrt{s_1{}^2 + s_2{}^2}^2$$

s_1 = standard deviation (gene of interest)

s_2 = standard deviation (housekeeping gene)

The margin of error of $2^{-\Delta\Delta Ct}$ was determined according to this formula:

$2^{-\Delta\Delta Ct+/-s}$

The error used for the error bars was calculated according to this formula:
$2^{-\Delta\Delta Ct+/-s} - 2^{-\Delta\Delta Ct}$

4.2.3 Molecular biology methods part II (shRNA design and amplification, cloning, plasmid isolation)

4.2.3.1 Design and cloning of miR30 based small hairpin RNAs into the pINDUCER vector system (Meerbrey et al., 2011)

RNA interference (RNAi) is a powerful tool for studying gene function. Small hairpin RNAs (shRNAs) can be used for inducible and reversible gene silencing in human cell lines. To stably transduce shRNAs in human cell lines, miR30-based shRNA sequences were designed and cloned into the lentiviral pINDUCER backbone. Then the pINDUCER constructs were transduced into MDA-MB-231 cells (4.2.1.6) to control the knockdown efficiency of the designed shRNAs.
The process of design and cloning into the pINDUCER vector of the shRNAs is described in the following paragraphs.

4.2.3.1.1 Design of miR30 shRNAs for the pINDUCER vector system

The design of miR30 shRNAs was based on protocol from Dow et al. (2012). To find the best shRNA sequences, the cDNA of the gene of interest was uploaded into the online software DSIR (Designer of small interfering RNA, http://biodev.extra.cea.fr/DSIR/) and the resulting list was checked for different criteria mentioned in the protocol. The ranking of the hits was improved using ranking suggestions from Filhol et al. (2012). The most compatible sequences were copied into the 97-Oligo template and the Oligo was ordered for PCR amplification with the desired restriction sites.

4.2.3.1.2 PCR for shRNA amplification

The following pipetting and PCR cycle scheme was used for the PCR:

PCR pipetting scheme	
97-Oligo	1 µl
His-Taq Polymerase (15 U/µl)	0.5 µl
10x ReproFast buffer	5 µl
dNTP	5 µl
Primer SG1161	2 µl
Primer SG1164	2 µl
ddH_2O	34.5 µl
PCR program	
95°C	3 min
29x step 2-4	
95°C	45 s
54°C	30 s
72°C	1 min
72°C	10 min
10°C	∞

4.2.3.1.3 Agarose gel electrophoresis

Materials:

- 1x TAE buffer
- DNA loading buffer (5x XB)
- 1 Kb DNA ladder (Fermentas)
- Ethidium bromide solution (10 mg/ml)

Method:

To separate the PCR product (4.2.3.1.2), a 2.5% agarose gel in 1x TAE buffer was prepared using the microwave to dissolve the agarose. Ethidium bromide (2 µl / 50 ml) was added for detection. DNA loading buffer was added to the PCR product and the complete solution was separated in an agarose gel electrophoresis chamber with 1x TAE buffer under voltage (100 V) for 45 min.

4.2.3.1.4 Isolation of the PCR product from the agarose gel

Material:

- Scalpel
- GeneJET Gel Extraction Kit (Thermo Scientific)

Method:

The agarose gel containing the separated PCR product (4.2.3.1.3) was placed under UV-light and the emerging upper band (~130 bp) was photographed and cut out with a scalpel and transferred to an Eppendorf tube. The tube could be stored at -20°C.
The DNA was extracted from the agarose gel using the GeneJET Gel Extraction Kit according to the manufacturer's protocol.

4.2.3.1.5 Restriction digestion with endonucleases

The PCR product and the pINDUCER vector were digested with the same endonucleases for 4 h at 37°C after using the following pipetting scheme:

Vector digestion		**PCR digestion**	
pINDUCER10 (#1369)	5 µg	PCR product	all
NEB4	5 µl	NEB4	5 µl
BSA	0.5 µl	BSA	0.5 µl
Xho1	3 µl	Xho1	1 µl
EcoR1 (High fidelity)	1.5 µl	EcoR1 (High fidelity)	0.5 µl
ddH_20 add to	50 µl	ddH_20 add to	50 µl

To confirm that the ligation of the PCR product and the pINDUCER vector worked, a control digestion was performed after mini preparation (4.2.3.1.10). The endonucleases BamH1 and Kpn1 were used for digestion for 1 h at 37°C using the following pipetting scheme:

Test1		**Test 2**	
Plasmid	2 µl	Plasmid	2 µl
BamH1	0.25 µl	Kpn1	0.25 µl
NEB4	2 µl	NEB1	2 µl
BSA	0.2 µl	BSA	0.2 µl
ddH_2O	15.55 µl	ddH_2O	15.55 µl

4.2.3.1.6 DNA isolation after restriction digestion

Materials:

- QIAquick PCR Purification Kit (QIAGEN)
- GeneJET Gel Extraction Kit (Thermo Scientific)

Method:

The PCR product was purified using the QIAquick PCR purification kit after digestion with endonucleases (4.2.3.1.5). The digested pINDUCER vector was separated on a 0.8% agarose gel (4.2.3.1.3) and extracted like in 4.2.3.1.6 using the GeneJET Gel Extraction Kit.

4.2.3.1.7 Quantification of the DNA concentration

The DNA concentration of the purified PCR product and the pINDUCER vector (4.2.3.1.6) was measured using the NanoDrop 2000c spectral photometer from Peqlab according to the manufacturer's protocol.

4.2.3.1.8 Ligation

Materials:

- T4-DNA-Ligase
- 10x T4-DNA-Ligase buffer

Method:

The digested PCR and the pINDUCER vector were ligated using a T4-DNA-Ligase for 1 h at RT according to the following pipetting scheme:

Ligation	
Insert	4 ng
Vector	100 ng
T4-DNA-Ligase	0.5 µl
10X T4-DNA-Ligase buffer	1 µl
ddH_2O add to	10 µl

The ligation mix was used for heat shock transformation into competent DH5α bacteria (4.2.3.1.9) or stored at -20°C.

4.2.3.1.9 Heat shock transformation

Materials:

- Chemically competent DH5α bacteria, -80°C
- LB medium
- LB agar plates (+ Ampicillin 1:1000)

Method:

The competent DH5α bacteria were thawed on ice for 10 min. Then 40 µl of the bacteria suspension was incubated with 2.5 µl of the ligation mix for further 10 min on ice. The bacteria ligation mix was placed on a heating block for 90 s at 42°C for transformation. To encourage bacterial proliferation, 400 µl of warm LB medium was added to the mix and the mix was placed on a heating block for 30 min at 37°C and 700 rpm. The mix was centrifuged at 1000 g for 2 min at RT and 400 µl of the LB medium were removed. The bacterial pellet was resuspended and distributed on a warm LB agar plate (+ Ampicillin 1:1000). The LB agar plate was placed into an incubator at 37°C overnight.

The emerging colonies were picked for mini preparation (4.2.3.1.10).

4.2.3.1.10 Mini preparation

Materials:

- LB medium (+ Ampicillin 1:1000)
- Buffer S1, 4°C
- Buffer S2
- Buffer S3
- 100% ethanol
- 70% ethanol
- TE buffer

Method:

Mini preparation was used to isolate the plasmid from the bacteria after transformation. To get enough material, the colonies were picked from the LB agar plate (4.2.3.1.9) and were added to 3 ml of LB medium (+ Ampicillin 1:1000). The medium tube was placed into a shaker at 37°C, 130 rpm for overnight. At the next day, 1.5 ml LB-medium was transferred to an Eppendorf tube and the rest was stored at 4°C.

The Eppendorf tube was centrifuged for 2 min at 13200 g, the LB medium was removed and the cell pellet was resuspended in 150 µl of buffer S1. Then 150 µl of buffer S2 was added and the solution was mixed by inverting the tube 5 times. After 5 min, buffer S3 was added to the solution and again the solution was mixed by inverting the tube 5x. The Eppendorf tube was centrifuged at 13200 g for 2 min to spin down the bacterial DNA and bacterial debris. Only the aqueous solution was carefully transferred into a new Eppendorf tube, 800 µl of 100% ethanol was added, the sample vortexed and stored for 15 min at -20°C. The sample was centrifuged for 10 min at 20817 g and 4°C, the ethanol was removed and 70% ethanol was added to the sample. Then the sample was vortexed and stored for 10 min at -20°C. After centrifugation for 10 min at 20817 g and 4°C, the 70% ethanol was removed and the Eppendorf tube was dried upside down for 10 min at RT. Then the plasmid was resuspended in 20 µl of TE buffer on a heating block at 50°C for 10 min at 550 rpm and placed on ice for another 30 min.

The plasmid was stored at -20°C or used for a control digestion to test the correct ligation of vector and insert (4.2.3.1.5).

4.2.3.1.11 Midi and Maxi preparation

Materials:

- PureLink HiPure Plasmid Midi-/Maxiprep kit (Life Technologies)
- LB medium (+ Ampicillin 1:1000)
- TE buffer

Method:

After sequencing the mini preparation (4.2.3.1.10) and clarification of RNAi efficiency, the plasmids were amplified using Midi and Maxi preparations.

The residual amount (1.5 ml) of the overnight culture was added to 100-200 ml of LB medium (+ Ampicillin 1:1000) on a rotator at 130 rpm and 37°C overnight. The LB medium was transferred to 50 ml tubes and centrifuged for 10 min at 4200 g at 4°C. The LB medium was removed and the pINDUCER plasmid was isolated from the DH5α pellet using the PureLink HiPure Plasmid Midi-/Maxiprep kit according to the manufacturer‘s protocol. The plasmid was resuspended in TE buffer and the DNA concentration was measured as in (4.2.3.1.7). The plasmid was stored at -20°C.

4.2.3.1.12 Sequencing

Materials:

- Sequencing primer (SG1162)
- QIAquick PCR Purification kit (QIAGEN)

Method:
After control digestion of the mini preparation (4.2.3.1.10), the plasmid was purified using the QIAgen PCR purification kit. Then the plasmid was sent to LGC genomics for sequencing. The results were analyzed with the freeware computer software ApE (A plasmid editor).

4.2.4 Biochemical methods

4.2.4.1 Whole-cell lysates

Material:

- Cold PBS, pH 7.4
- Plastic cell scraper
- TNN lysis buffer, 4°C
- 3x ESB protein sample buffer
- Hamilton syringe
- Protease inhibitor cocktail (PIC)
- PMSF (100 mM)

Method:

The cell culture dish was placed on ice immediately after recovery from the incubator. Then the cell culture medium was discarded and 10 ml cold PBS was added to a 10 cm cell culture dish. The cells were scraped with a plastic cell scraper and the resulting suspension was transferred to a 15 ml tube. The tube was centrifuged for 3 min at 1200 g and 4°C. The PBS was removed and the cell pellet was resuspendend in 1 ml cold PBS and transferred to an Eppendorf tube. Again, the sample was centrifuged at 1200 g for 3 min at 4°C, but this time the PBS was completely removed (Hamilton syringe). At this step, the cell pellet could be shock-frozen in liquid nitrogen for long term storage at -80°C.

The cell pellet was resuspendend in tenfold TNN lysis buffer (+ PIC 1:1000, PMSF 1 mM) for 30 min at 4°C. Then the suspension was centrifuged at 20817 g for 10 min at 4°C to get rid of the cell debris. The supernatant was transferred to a new Eppendorf tube and the protein concentration was determined via Bradford (4.2.4.2).

For SDS gel electrophoresis (4.2.4.3), the lysate was mixed with 3x ESB protein sample buffer and heated for 5 min at 95°C. Then the sample was shortly centrifuged and stored at -20°C.

4.2.4.2 Determination of protein concentration according to Bradford

Material:

- Bradford solution
- Spectrometer cuvette
- BSA (10 mg/ml)

Method:

The protein concentration was determined after the method established by Bradford (Bradford, 1976). 1 ml of Bradford solution was mixed with 1 µl of the protein lysate or a BSA dilution series for the spectrometric measurement. Then the extinction was measured at 595 nm and used for the calculation of the protein concentration of the whole cell lysates (4.2.4.1).

4.2.4.3 SDS polyacrylamide gel electrophoresis (SDS-PAGE)

Materials:

- ddH_2O
- 1.5 M Tris, pH 8.8
- 0.5 M Tris, pH 6.8
- Protogel (30% Acrylamide, 0.8% Bisacrylamide)
- 20% SDS
- 10% APS
- Protein marker
- SDS-buffer

Method:

SDS-PAGE was performed using the discontinuous method described by Laemmli (Laemmli, 1970). It was carried out using the MiniProtean III system from Biorad. The 1.5 mm gels were polymerized in the lab. First, the separating gel was polymerized in the desired concentration (8-14%), then on top of it the stacking gel (5%).

Separating gel				
Gel percentage:	**8%**	**10%**	**12%**	**14%**
ddH_2O	3.55 ml	3.05 ml	2.5 ml	2.05 ml
1.5 M Tris, pH 8.8	1.85 ml	1.85 ml	1.85 ml	1.85 ml
Protogel	2 ml	2.5 ml	3 ml	3.5 ml
20% SDS	37.5 µl	37.5 µl	37.5 µl	37.5 µl
10% APS	50 µl	50 µl	50 µl	50 µl
TEMED	5 µl	5 µl	5 µl	5 µl

Stacking gel	
Gel percentage:	5% gel
ddH_2O	3.45 ml
0.5 M Tris, pH 6.8	0.7 ml
Protogel	0.8 ml
20% SDS	25 µl
10% APS	25 µl
TEMED	5 µl

The electrophoresis was performed in SDS-buffer running with constant amperage (30 mA/gel) for ~1.5 h.

4.2.4.4 Immunoblotting

Materials:

- PVDF membrane
- Whatman filter paper
- 100% methanol
- Blotting buffer, 4°C
- Ponceau S
- TBS-T (0.05-0.1%)
- Blocking solution (TBS-T 3% milk powder or TBST 5% BSA)
- 1 M Tris, pH 8.5
- Enhanced chemiluminescence (ECL) solution

Method:

A Mini Trans-Blot wet transfer apparatus from BioRad was used to blot proteins from a polyacrylamide gel (4.2.4.3) to a PVDF membrane. The PVDF membrane was incubated in 100% methanol for 1 min and placed into cold blotting buffer. The Whatman paper, sponges, PVDF membrane and the polyacrylamide gel were also equilibrated for 5 min in cold blotting buffer. The components of the Trans-Blot wet transfer apparatus were assembled according to the manufacturer's protocol. The immunoblotting was performed in cold blotting buffer for 1.5 h at constant voltage (100 V). The protein transfer was controlled by staining of the PVDF membrane with Ponceau S. After destaining with ddH_2O, the PVDF membrane was incubated for 1h in blocking solution. Then the PVDF membrane was incubated with primary antibody (against the protein of interest) in fresh block solution at 4°C, overnight. The PVDF membrane was washed 3x with TBS-T for 10 min at RT under gentle shaking. Then the PVDF membrane was incubated with a secondary antibody coupled to HRP in TBS-T for 1 h at RT under constant agitation. Again, the PVDF membrane was washed 3x with TBS-T for 10 min at RT under gentle shaking. Then the ECL components were mixed together in 1 M Tris (pH 8.5), activated by H_2O_2. The PVDF membrane was incubated for 1 min in the solution and briefly placed on Whatman paper, wrapped in plastic foil and exposed to X-ray films in a dark room.

4.2.4.5 Chromatin immunoprecipitation (ChIP)

Materials:

- PBS, pH 7.4 + 1% paraformaldehyde at RT
- PBS, pH 7.4 at 4°C
- 15 ml cryotubes
- Plastic cell scraper
- 1 M glycine at RT
- RIPA buffer, 4°C
- PMSF, 100 mM
- Protease inhibitor cocktail (PIC)
- RNAse (10 mg/ml)
- Proteinase K (20 mg/ml)
- 5 M NaCl
- Magnetic Protein G Dynabeads
- IP wash buffer
- TE buffer, pH 8.1
- Elution buffer
- QIAgen PCR Purification Kit

Methods:

For ChIP, subconfluent cell lines in 15 cm cell culture dishes (3x MDA-MB-231, 2x H460, 4x H23) were cross-linked to DNA after 48 h of culture. The cell culture medium was replaced, as quickly as possible, by 20 ml PBS (+ 1% paraformaldehyde) for 10 min at RT under gentle shaking. To end the reaction, 2.5 ml of glycine was added to the PBS and incubated for 5 min. The PBS was removed and the cells were briefly washed 2x in cold PBS to get rid of the paraformaldehyde. Then 14 ml of cold PBS were added to the cells and the cells were scraped from the cell culture dish and transferred to a 15 ml cryotube. The cells were centrifuged for 3 min at 1200 g at 4°C, the PBS was removed and the cells were combined and lysed (20x up and down pipetting) in 900 µl of RIPA buffer (+ 1 mM PMSF, PIC 1:1000) for 15 min on ice. The chromatin was sonicated for 15 min using the Bioruptor with a 30 s on/off cycle rhythm with high intensity. The chromatin solution became clear and the fragmented DNA was transferred to an Eppendorf

tube for centrifugation at 20817 g for 10 min at 4°C to get rid of the cell debris. The chromatin solution was transferred into a new Eppendorf tube and 50 µl of the chromatin solution was transferred to a separate Eppendorf tube for DNA size check. The remaining chromatin was shock-frozen with liquid nitrogen and stored at -80°C. For DNA size check, the protein-DNA cross-linking was removed by adding 2 µl of NaCl and 1 µl of RNAse on a 65°C heating block, overnight, and 550 rpm. The next day, the solution was cooled down to RT and incubated with 4 µl of Proteinase K for 30 min at 45°C and 550 rpm on a heating block. For DNA size check, the solution was separated in a 1.2% agarose gel. The DNA fragment size was between 250 and 1000 bp.

For immunprecipiation, the shock-frozen chromatin solution was thawed and divided into different Eppendorf tubes (up to 5). Fresh RIPA buffer (+ 1mM PMSF, PIC 1:1000) was added up to a volume of 500 µl. Every ChIP sample was incubated with 2 µg of the desired antibody overnight at 4°C on a rotating wheel. Then the ChIP samples were incubated for 1 h with Magnetic Protein G Dynabeads on the same rotating wheel. The ChIP samples were washed 2x with RIPA buffer (+ 1mM PMSF, PIC 1:1000), 4x with IP wash buffer (+ 1mM PMSF, PIC 1:1000), 2x with RIPA buffer (+ 1 mM PMSF, PIC 1:1000) and 2x with TE buffer (+ 1 mM PMSF, PIC 1:1000). Every second washing step was performed on the rotating wheel for 5 min at 4°C. Then the beads were resuspended in 100 µl of TE buffer and 200 µl of elution buffer was added. Additionally, the same amount of TE and elution buffer was added to the input sample. The protein-DNA complexes were eluted at 65°C for 10 min at 1400 rpm on a heating block. To remove the crosslinking, the ChIP samples were incubated with 200 mM NaCl and 6 µl RNAse for 5 h at 65°C and 550 rpm on a heating block. After cooling down to RT, the ChIP samples were incubated with 4 µl of Proteinase K for 30 min at 45°C and 550 rpm on a heating block. The DNA was purified, using the Qiagen PCR Purification Kit (1 ml binding buffer). The DNA was eluted in 50 µl of elution buffer and 1 µl of DNA was used for every qPCR well for ChIP analysis (4.2.4.5).

4.2.5 Immunofluorescence

4.2.5.1 Standard protocol

Materials:

- PBS, pH 7.4
- PBS, pH 7.4 + 0.2% Triton-X
- Blocking solution (PBS, pH 7.4 + 3% BSA)
- Fixative, e.g., PSP (PBS, 3% paraformaldehyde, 2% sucrose)
- Humid chamber
- Hoechst 33258
- Shandon Immu-Mount (Thermo Scientific)
- Colourless nail polish

Method:

For immunostaining, HeLa cells were seeded in 6 well chambers on coverslips. The cells were washed carefully with 1x PBS and fixed for 10 min with PFA. All the variations for the fixation step are described in 4.2.5.2. The cells were washed 3x with PBS and permeabilized with PBS + 0.2% Triton-X for 5 min, washed briefly with 1x PBS and blocked with PBS + 3% BSA for 30-60 min. The coverslips were transferred to humid chambers and incubated for 1 h with the first antibody in PBS on parafilm. Then the coverslips were washed 3x with PBS for 5 min and again transferred to humid chambers and incubated for additional 30 min with the secondary antibody in PBS (1:500) and Hoechst 33258 (1:2000) for nuclear staining on fresh parafilm. The cells were washed briefly with PBS and 2x with PBS for 5 min. Glass slides were prepared with one drop of Immu-Mount and the coverslips were carefully placed on the drop. After drying in the dark at RT for 1-2 h, the slides were sealed by colourless nail polish and stored at 4°C in the dark.

4.2.5.2 Special fixation methods

For better preservation of certain cell structures and antibody epitopes, fixation methods were used which differ from the standard protocol (4.2.5.1). Other changes from the standard protocol are also mentioned here:

Methanol fixation:
For staining of EGFP-GAS2L3 (localization tubulin), GAS2L3, spastin and Aurora B (for co-localization with spastin), the cells were fixed with 100% cold methanol (-20°C) at -20°C for 3-4 min. The coverslips were washed 3x with PBS directly followed by the blocking step.

4% PFA (PBS + 4% paraformaldehyde) fixation:
For actin staining, the cells were fixed in 4% PFA for 10 min at RT.
The actin cytoskeleton was directly labeled with phalloidin Alexa Fluor 594 for 20 min.

PSP (PBS, 3% paraformaldehyde, 2% sucrose) + 0.3% Triton-X:
For staining of Aurora B, MKLP2, EGFP-GAS2L3 and mutants (for co-localization with Aurora B, MKLP2), cells were fixed with 3% PFA + 0.3% Triton-X for 10 min at RT. The usual permeabilization step was not performed.

10% Trichloracetic acid (TCA):
For RhoA and myosin IIA staining, the cells were fixed with 10% TCA (4°C) for 15 min at RT.

4.2.6 Cell biology assays

4.2.6.1 Time-lapse microscopy

To visualize GAS2L3 localization in cell division over time and to analyze the GAS2L3 siRNA phenotype, time-lapse microscopy was used under different conditions:

Materials:

- 35 mm dish chamber (8 well, Ibidi (Munich,Germany))
- Time-lapse incubator chamber for the microscope (Selfmade Physiological Chemistry I)
- Fluorescence microscope Leica DMI 6000B + camera DFC350 FX R2
- Leica Application Suite 3.7 (LAS 3.7)

Methods:

4.2.6.1.1 Plasmid overexpression

2-4x10^4 HeLa cells, stably expressing mCherry-α-tubulin, were seeded into 35 mm dish chambers. After 24 h, the cells were transiently transfected with EGFP-GAS2L3 (0.2 µg using Metafectene, 4.2.1.4.2). After additional 24 h the cells were used for time-lapse microscopy. For 16 h, every 2 min, pictures were taken with low intensity and 200x magnification (20x objective and 10x tubus) to avoid phototoxicity. The pictures were framed to movies by the microscope software LAS 3.7 and transferred for subsequent analysis into Adobe Photoshop and ImageJ. The intensity of the video channels was processed and mitotic cells were analyzed. Cells expressing both fluorescent proteins in the movie were used for single cell movie compilation. Furthermore, figures showing selected frames from the movies were compiled.

4.2.6.1.2 GAS2L3 siRNA

2-4x 10^4 HeLa cells, stably expressing EGFP-H2B and mRFP-α-tubulin, were seeded into 35 mm dish chambers. After 24 h, the cells were transfected with control siRNA or different *GAS2L3*-specific siRNA (50-100 nM, Metafectene, 4.2.1.4.2) as well as 6 well chambers (1.7 x 10^5 cells) for *GAS2L3* knockdown control. After additional 24 h hours, the cells were used for time-lapse microscopy and RNA purification (4.2.2.1). For 16 h, every 2 min, pictures were taken with low intensity and 200x magnification (20x objective and 10x tubus) to avoid phototoxicity. The mechanic microscope system allowed the recording of control siRNA and *GAS2L3*-specific siRNA treated wells in parallel. The pictures were framed to movies by the microscope software LAS 3.7 and transferred for subsequent analysis into Adobe Photoshop and ImageJ. The intensity of the movie channels was processed. The movie material was used for identification and statistical analysis of the siRNA phenotype. Cells going through mitosis were labeled and the ratio of cytokinesis failure was counted. Single cell movies and figures showing selected frames were compiled.

5 RESULTS

5.1 *GAS2L3* is a DREAM target gene that is required for cytokinesis

Gas2l3 (growth arrest-specific 2 like 3) has been identified as DREAM target gene in conditional LIN9-knockout MEFs after comparative microarray gene expression analysis (Reichert et al., 2010). In human cell lines transient RNA interference (RNAi) mediated knockdown of DREAM subunits also led to reduced mRNA expression of *GAS2L3* (Wolter et al., 2012). But so far, it has not been investigated whether DREAM is a direct regulator of *GAS2L3* gene expression and whether the repressive and/or the activating form of the DREAM complex is involved.

In order to address the question whether DREAM is a direct regulator of *GAS2L3*, I performed chromatin immunoprecipitation (ChIP) assays in the two lung cancer cell lines H460 and H23 using antibodies specific for either the core complex (LIN9), the repressive complex (p130), or the activating complex (B-MYB, FOXM1). Unspecific IgG was used as a control. The ChIP-qPCR analysis revealed *GAS2L3* promoter DNA enrichment for both, the repressive and the activating form of the DREAM complex (Figure 10 A, B). The promoter DNA enrichment was not as strong as for *BIRC5*, a known DREAM target gene, but much higher than for the *GAPDH2* promoter which served as negative control. Thus, the data support that *GAS2L3* is a DREAM target gene and that DREAM is involved in its repression and activation.

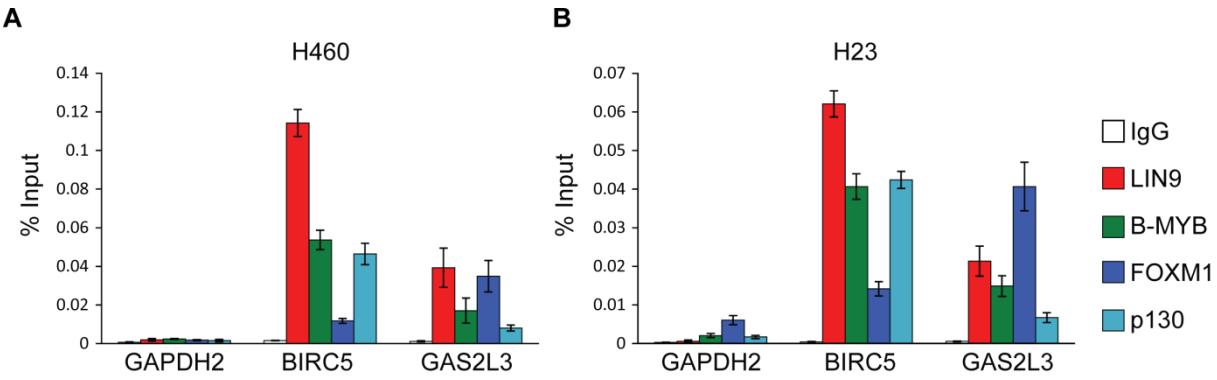

Figure 10: The repressive and the activating form of DREAM bind to the GAS2L3 promoter.
In the lung cancer cell lines H460 and H23 chromatin was immunoprecipitated using antibodies directed against LIN9, p130, B-MYB, and FOXM1. Nonspecific IgG was used as a control. ChIP-qPCR analysis was performed using *GAS2L3* promoter-specific primer with *GAPDH2* and *BIRC5* promoter-specific primer as respective negative and positive control. The ChIP-qPCR analysis shows enrichment of DREAM in H460 (**A**) and H23 (**B**) cells at the *GAS2L3* and *BIRC5* promoter normalized to 1% input. The error bars of the representative experiment were calculated of triplicates according to 4.2.2.3.

Experiments with synchronized T98G glioblastoma cells revealed that GAS2L3 mRNA expression peaks in G2/M phase (Wolter et al., 2012).These results indicate a possible role of GAS2L3 in G2/M phase.

Initial RNAi experiments using HeLa cells stably expressing EGFP-H2B and mRFP-α-tubulin in combination with time-lapse video microscopy revealed that GAS2L3 is required for cytokinesis (Kremling, 2010). In order to rule out siRNA-specific off-target effects and to gain more information about the cytokinesis phenotype, I performed time-lapse video microscopy experiments with higher spatial and temporal resolution using the same cell line and two GAS2L3-specific siRNAs. GAS2L3 depletion was verified by RT-qPCR analysis (Figure 11 D). Cells transfected with a control siRNA progressed normally through mitosis and cytokinesis (Figure 11 A). Cells transfected with either GAS2L3-siRNA #1 (Figure 11 B) or GAS2L3-siRNA #2 (Figure 11 C) were not affected in mitotic entry, in metaphase spindle organization, and in metaphase chromosome alignment. The chromosomes started to separate normally in early anaphase. In late anaphase, after beginning of cleavage furrow ingression, GAS2L3-siRNA treated cells developed oscillations of the entire mitotic spindle and chromatin from one side to the other side of the proto-daughter cells. These oscillations continued for approximately 20 min before the separated chromosomes fell back into a single chromosome mass. Finally, the cells failed to divide and entered a tetraploid interphase state with two or multiple nuclei. This phenotype was observed in 1.1% of the transfected control cells (n=93), in 17.4% of the cells transfected with GAS2L3-siRNA #1 (n=214) and in 16.8% of the cells transfected with GAS2L3-siRNA #2 (n=143) (Figure 11 E). The oscillation phenotype was accompanied by substantive membrane blebbing in early telophase (Figure 11 B, C). Example movies are published as supplementary material in Wolter et al. (2012), (movie 1-4). Measurement of the oscillation timing revealed that most of the cells displayed the phenotype approximately 8 min after anaphase onset when the cleavage furrow started to ingress (Figure 11 F).

The observed oscillation phenotype was similar to observations from reports where the cleavage furrow scaffold protein anillin was depleted or when astral microtubules were hyper-stabilized in cytokinesis (Rankin and Wordeman, 2010; Zhao and Fang, 2005a).

Cleavage furrow ingression failures are often accompanied by mis-localization and malfunction of cleavage furrow components and the actomyosin ring (Zhao and Fang, 2005a). To address this possibility, I depleted GAS2L3 in HeLa cells to analyze the localization of the two important cleavage furrow components RhoA and non-muscle myosin IIA (Figure 12 A). RhoA and myosin IIA showed a correct localization at the cleavage furrow but RhoA was also aberrantly localized at the cell cortex in large membrane blebs and myosin IIA accumulated aberrantly at the cell cortex. Cells in telophase displaying substantive membrane blebs were observed in 4.8% of the control cells (n=120) and in 26.18% of GAS2L3 depleted cells (n=119) pooled from four independent experiments (Figure 12 B).

Besides the prominent phenotype, experiments in our laboratory indicated a possible role for GAS2L3 in spindle assembly checkpoint (SAC) maintenance after prolonged spindle drug treatment (Schmitt, 2010). The question has been raised whether GAS2L3 depleted have an altered metaphase to anaphase transition in M phase which would indicate a compromised SAC in the unperturbed cell cycle. Metaphase to anaphase transition can be measured by setting the correct chromosome alignment in metaphase as starting point and the anaphase entry as end point (Figure 11 G). The time-lapse movies revealed that GAS2L3 depleted cells (Experiment 1 n=149, Experiment 2 n=132) entered anaphase 2-4 min earlier than the control cells (Experiment 1 n=158, Experiment 2 n=146) in two independent experiments with two different siRNAs against GAS2L3 ($p < 0.0001$, Mann-Whitney-U-Test, in both experiments).

Taken together, these results show that GAS2L3 is required for proper cleavage furrow ingression in cytokinesis. In this regard, GAS2L3 restricts the localization of RhoA and myosin IIA to the cleavage furrow.

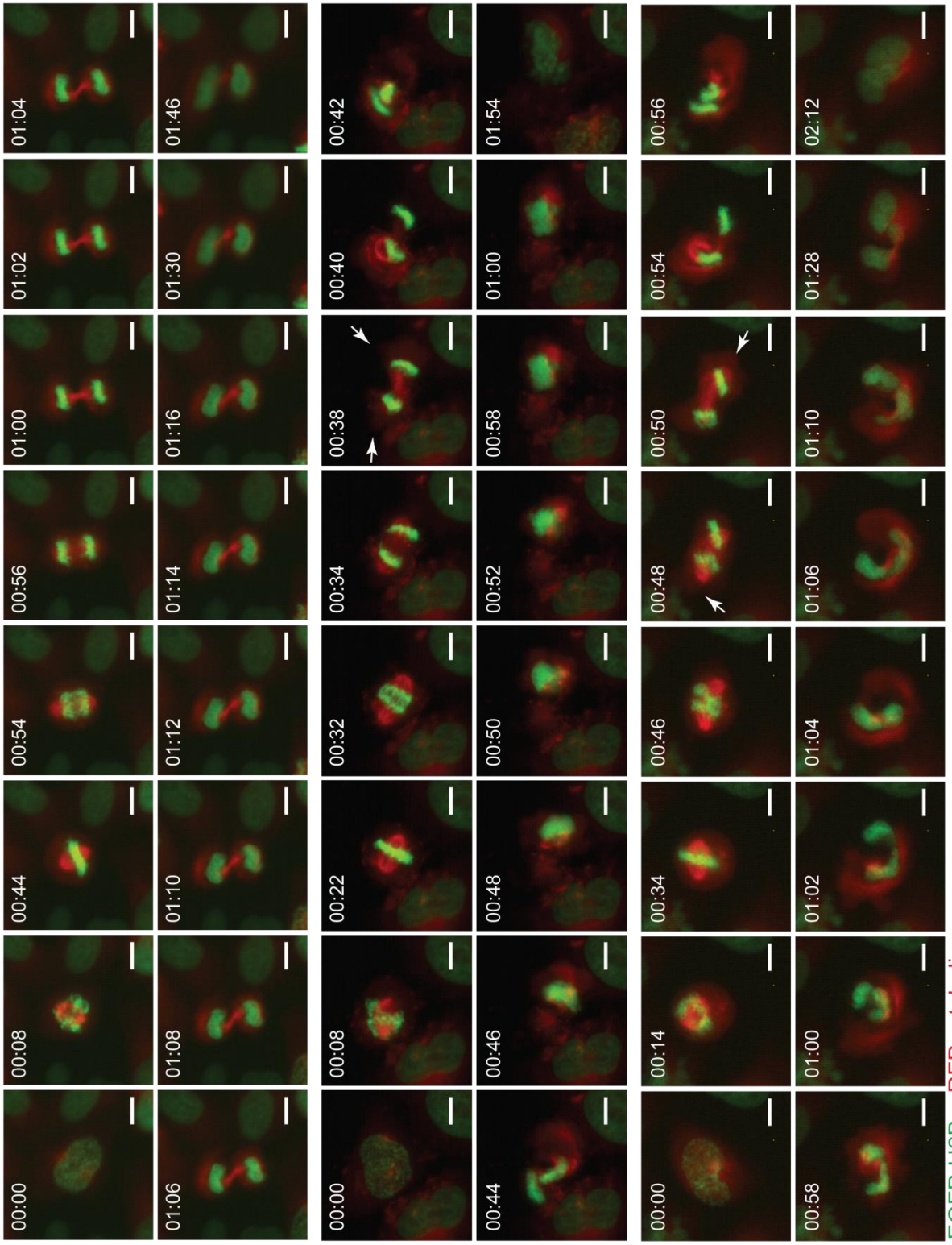
A
ctrl siRNA
B
GAS2L3 siRNA #1
C
GAS2L3 siRNA #2
EGFP-H2B mRFP-α-tubulin

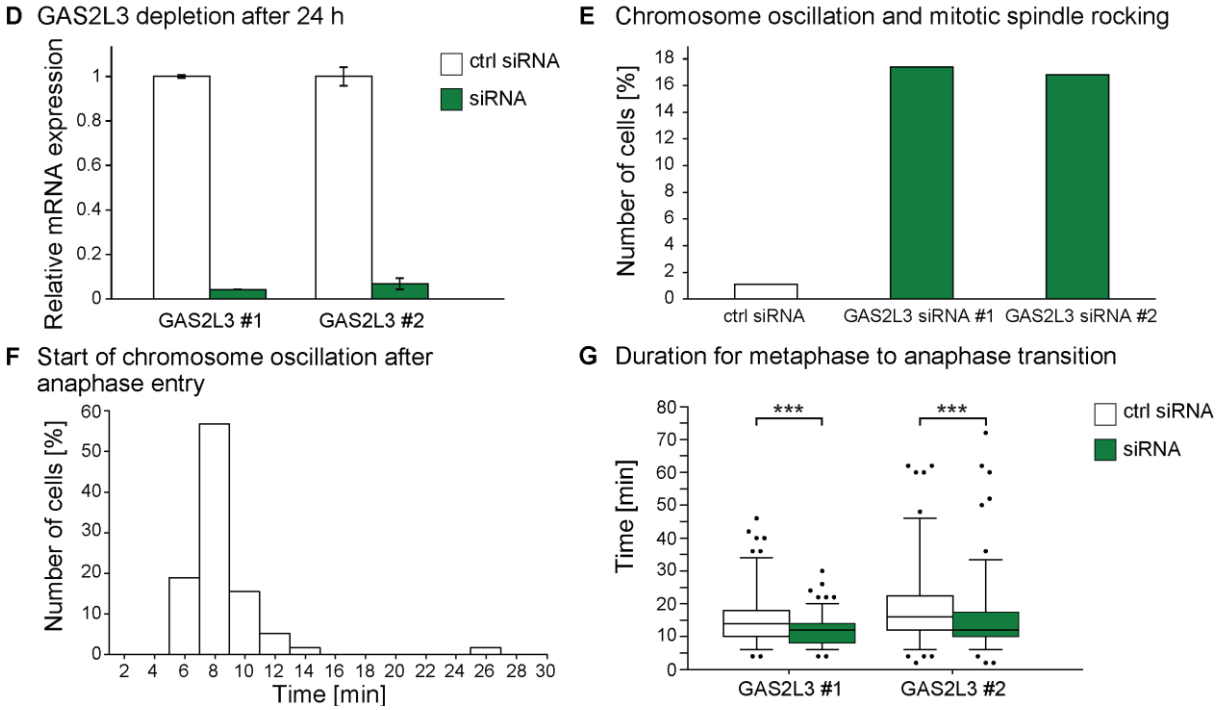

Figure 11: GAS2L3 is required for cleavage furrow ingression in cytokinesis.
(**A**-**C**) HeLa cells stably expressing EGFP-H2B and mRFP-α-tubulin were treated with either control siRNA (**A**), GAS2L3 siRNA #1, (**B**) or GAS2L3 siRNA #2. (**C**) Immunofluorescence time-lapse movies were recorded. Representative frames from the movies were selected starting with the nuclear envelope breakdown in mitosis. The time is displayed in hours:min. Scale bars: 10 µm. White arrows indicate examples for substantive membrane blebbing. (**D**) Representative GAS2L3 depletion of two independent experiments analyzed by qPCR. (**E**) The number of mitotic cells showing chromosome oscillation and mitotic spindle rocking were quantified using control (n=93), siRNA #1 (n=214) and siRNA #2 (n=143) mitotic cells from the time-lapse movies from two independent experiments. (**F**) The time when GAS2L3-siRNA treated cells (n=58) started to show chromosome oscillation was measured using anaphase entry as starting point (t=0 min). The cells were pooled from the time-lapse movies used in Figure 11 E. (**G**) Metaphase to anaphase transition was measured using the same time-lapse movies from Figure 11 E. The time was measured starting when chromosome alignment in metaphase was completed (t=0 min) and stopping when the cell entered anaphase. GAS2L3 depleted cells show a faster transition than control cells. The experiment on the left was quantified using control (n=158) and GAS2L3 siRNA #1 (n=149) mitotic cells. The experiment on the right was quantified using control (n=156) and GAS2L3 siRNA #2 (n=142) mitotic cells. The differences were statistically significant ($p < 0.0001$, Mann-Whitney-U-Test).
Figure 11 (A-C) was first published in Wolter et al. (2012).

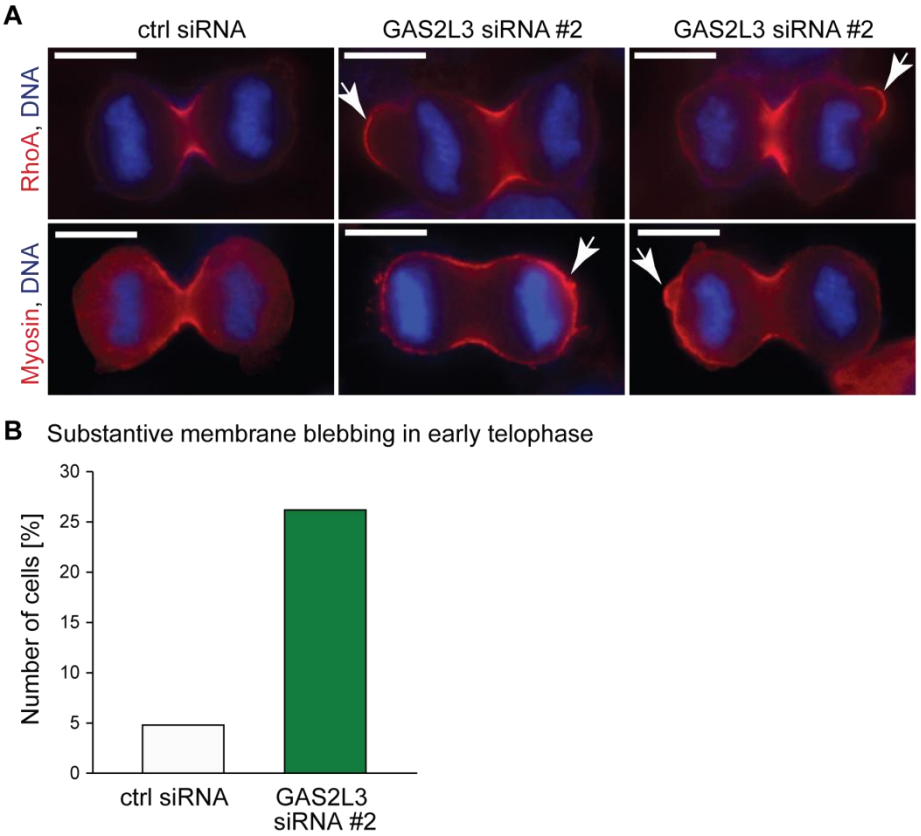

Figure 12: GAS2L3 is required for correct localization of RhoA and non-muscle myosin IIA in cytokinesis.
(**A**) Control and GAS2L3 depleted cells were fixed in TCA and stained for RhoA (red) or myosin IIA (red) and DNA (blue). Scale bars: 10 µm. Localization of RhoA and myosin IIA in the process of cleavage furrow ingression was analyzed by immunofluorescence. White arrows indicate abnormal cortical localization of RhoA and myosin IIA. (**B**) Quantification of membrane blebbing in control cells (n=120) and GAS2L3 siRNA treated cells (n=119) accompanying cleavage furrow ingression. The cells were pooled from four independent experiments.
Figure 12 A was first published in Wolter et al. (2012).

5.2 GAS2L3 localization to the mitotic spindle, to the intercellular bridge,and to the midbody

After the discovery of the prominent cytokinesis phenotype, I was interested in the localization of GAS2L3 to better understand the function of the protein.

In order to describe the subcellular localization of GAS2L3, EGFP-GAS2L3 was transiently expressed in HeLa cells and α-tubulin was used as a reference protein (Figure 13 A). In interphase cells, EGFP-GAS2L3 showed cytoplasmic localization with strong co-localization with the microtubule cytoskeleton. In mitosis, EGFP-GAS2L3 was enriched along the complete mitotic spindle from prophase until anaphase. In telophase, EGFP-GAS2L3 was accumulated at the spindle midzone

with stronger signal intensity close to the spindle midzone center. In cytokinesis, EGFP-GAS2L3 localized only to the intercellular bridge as two distinct pools close to the bridge center.

To support the localization results gained from fixed EGFP-GAS2L3 and to rule out fixation artefacts and missing localization patterns, I transiently expressed EGFP-GAS2L3 in HeLa cells stably expressing mCherry-α-tubulin and performed time-lapse video microscopy (Figure 13 B). Transiently expressed EGFP-GAS2L3 in living HeLa cells displayed an identical localization pattern as in fixed cells, confirming that EGFP-GAS2L3 localizes to the complete mitotic spindle, is enriched at the spindle midzone and accumulates at the intercellular bridge. Beside this, no further localization of GAS2L3 could be revealed.

To get additional information about the timing of EGFP-GAS2L3 accumulation to the spindle midzone and the intercellular bridge, I compared EGFP-GAS2L3 localization with the process of cleavage furrow ingression visualized by the ingression of the cell membrane (Figure 14 A). EGFP-GAS2L3 accumulated at the spindle midzone and at the intercellular bridge in parallel to the progress of cleavage furrow ingression.

Interestingly, GAS2L3 is shown to bind actin filaments *in vitro* (Stroud et al., 2011; Wolter et al., 2012). However, no co-localization with the actin-rich cell cortex or cytoplasm in mitotic cells could be detected so far. The process of cleavage furrow ingression is heavily dependent on the actin cytoskeleton and the necessary force is generated by the contractile ring also called actomyosin which can be visualized by actin staining (Glotzer, 2005). To compare the localization of the actomyosin ring and EGFP-GAS2L3 after cleavage furrow ingression, HeLa cells stably expressing EGFP-GAS2L3 were analyzed for co-localization with actin by immunostaining (Figure 14 B). The staining revealed no co-localization of EGFP-GAS2L3 and the actomyosin ring.

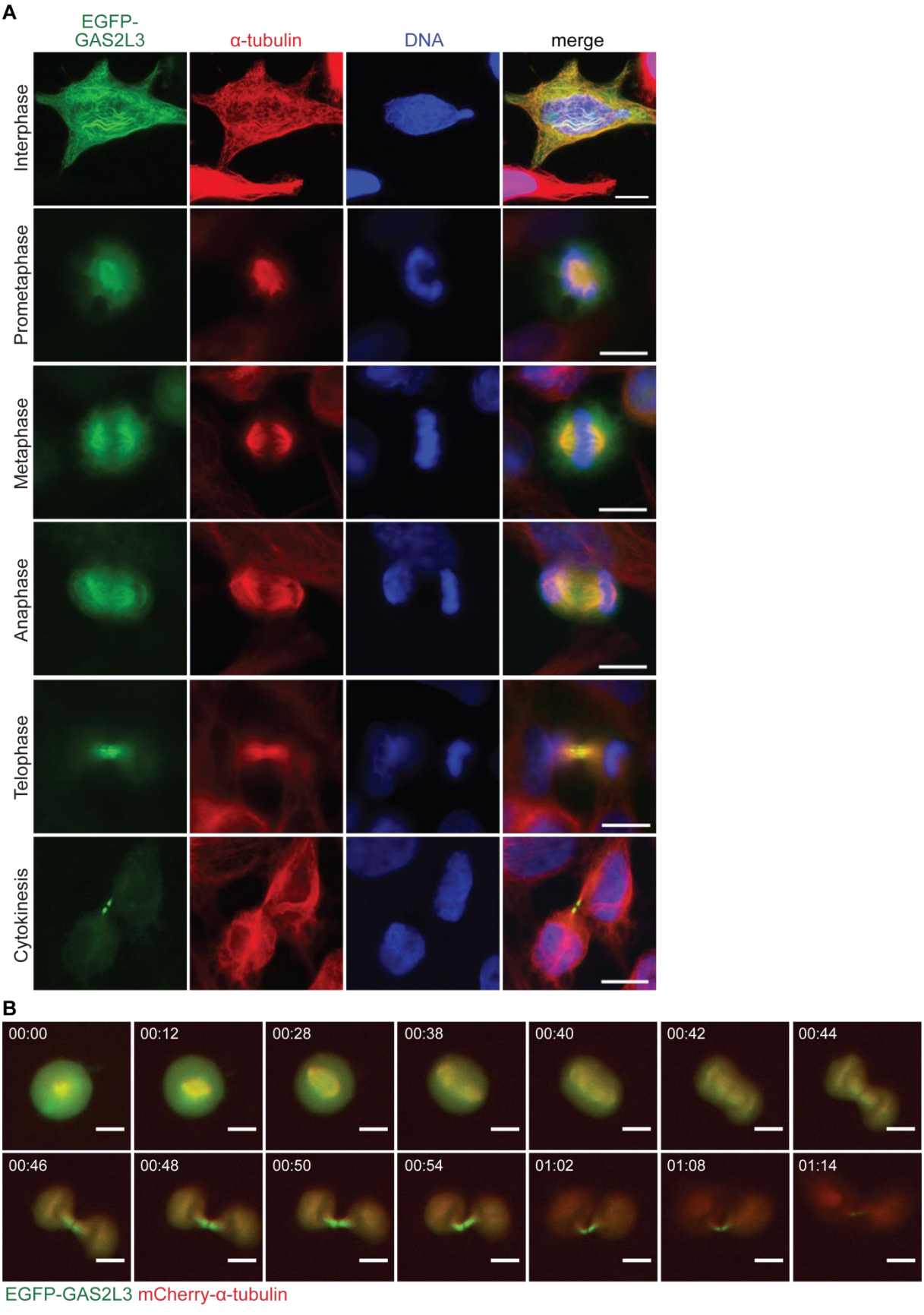
A
EGFP-GAS2L3
α-tubulin
DNA
merge
Interphase
Prometaphase
Metaphase
Anaphase
Telophase
Cytokinesis
B
00:00
00:12
00:28
00:38
00:40
00:42
00:44
00:46
00:48
00:50
00:54
01:02
01:08
01:14
EGFP-GAS2L3 mCherry-α-tubulin

Figure 13: Localization of EGFP-GAS2L3 to the mitotic spindle and to the intercellular bridge.
(**A**) HeLa cells transfected with EGFP-GAS2L3 were fixed in methanol and stained for α-tubulin (red) and DNA (blue). EGFP-GAS2L3 localization in different mitotic stages was analyzed by immunofluorescence. (**B**) HeLa cells stably expressing mCherry-α-tubulin were transiently transfected with EGFP-GAS2L3 and time-lapse movies were recorded. GAS2L3 localization in different mitotic stages was analyzed by immunofluorescence. Selected frames from the channel merge are presented here. The separated channels are provided in Figure 39 in the Appendix. Scale bars: 10 µm. Time is displayed in hours:min. Figure 13 A was first published in Wolter (2011), Wolter et al. (2012). Figure 13 B was first published in Wolter et al. (2012).

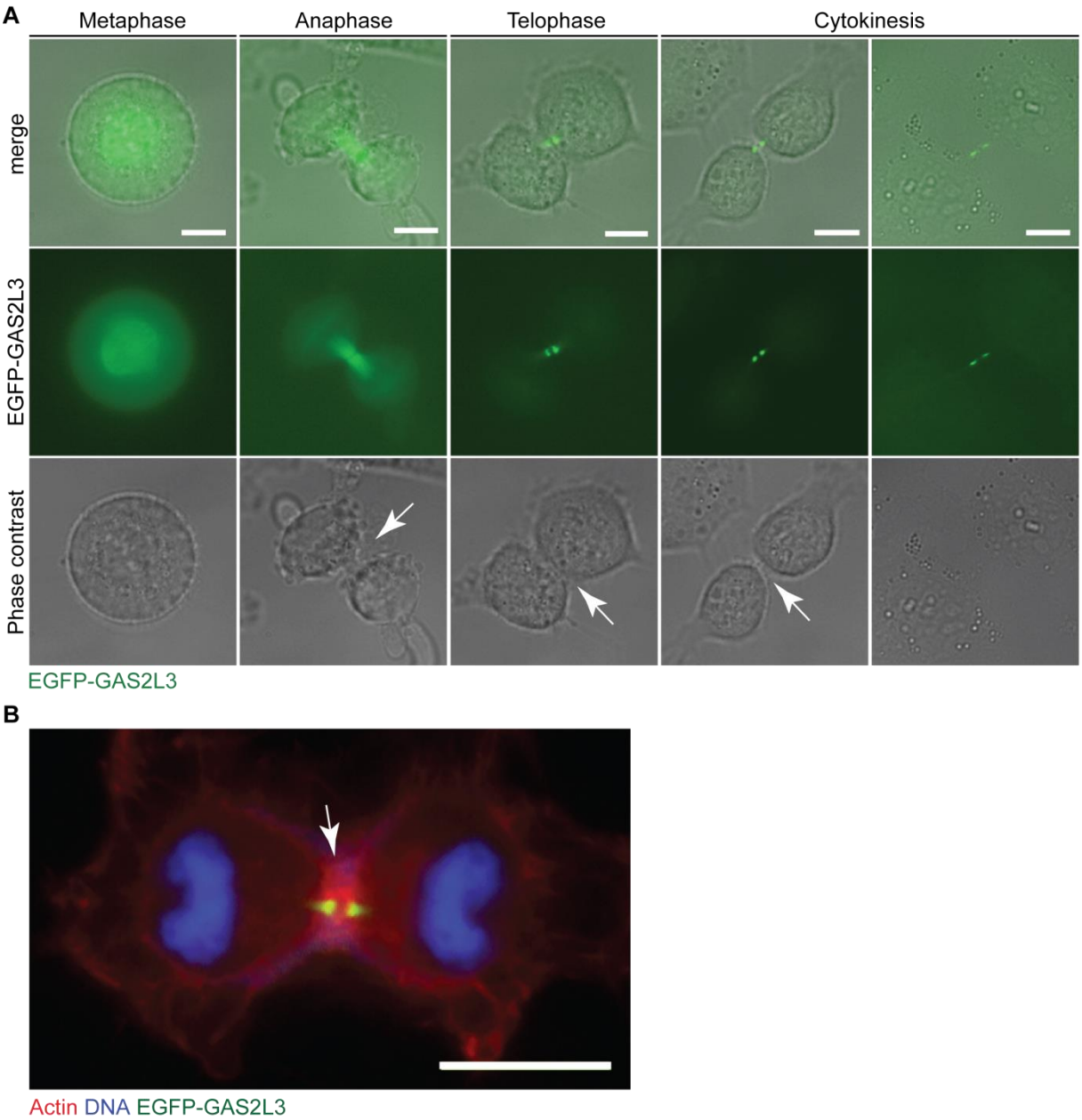

Figure 14: EGFP-GAS2L3 accumulates at the spindle midzone with progression of cleavage furrow ingression.
(**A**) Live cell imaging was performed in HeLa cells stably expressing EGFP-GAS2L3. Phase contrast microscopy was used to visualize the cell membrane. The localization pattern of GAS2L3 in the process of cleavage furrow ingression was analyzed by phase contrast and immunofluorescence. (**B**) HeLa cells stably expressing EGFP-GAS2L3 were fixed in PFA and stained for actin (red) and DNA (blue) and analyzed by immunofluorescence. The strong red staining represents the actin part of the actomyosin ring after cleavage furrow ingression. White arrows highlight the cleavage furrow. Scale bars: 10 µm. Figure 14 A was published in Wolter (2011). Figure 14 B was published in Wolter et al. (2012).

Next, I wanted to know whether the results of the EGFP-GAS2L3 localization studies resemble the localization of endogenous GAS2L3. HeLa cells stably expressing mCherry-α-tubulin were fixed in methanol and stained with a monoclonal antibody against GAS2L3 (Figure 15). Endogenous GAS2L3 localized along the entire mitotic spindle in prophase until anaphase. In telophase, endogenous GAS2L3 accumulated at the spindle midzone, apparent by stronger antibody intensity close to the spindle midzone center. In cytokinesis, endogenous GAS2L3 specifically localized as two pools to the intercellular bridge close to the center of the bridge.

In order to confirm that the localization pattern of endogenous GAS2L3 is not a fixation artefact, endogenous GAS2L3 was depleted by RNAi in HeLa cells stably expressing mCherry-α-tubulin (Figure 16). As expected, the signal of endogenous GAS2L3 at the mitotic spindle and the intercellular bridge was lost after depletion of GAS2L3, confirming the specificity of the signal.

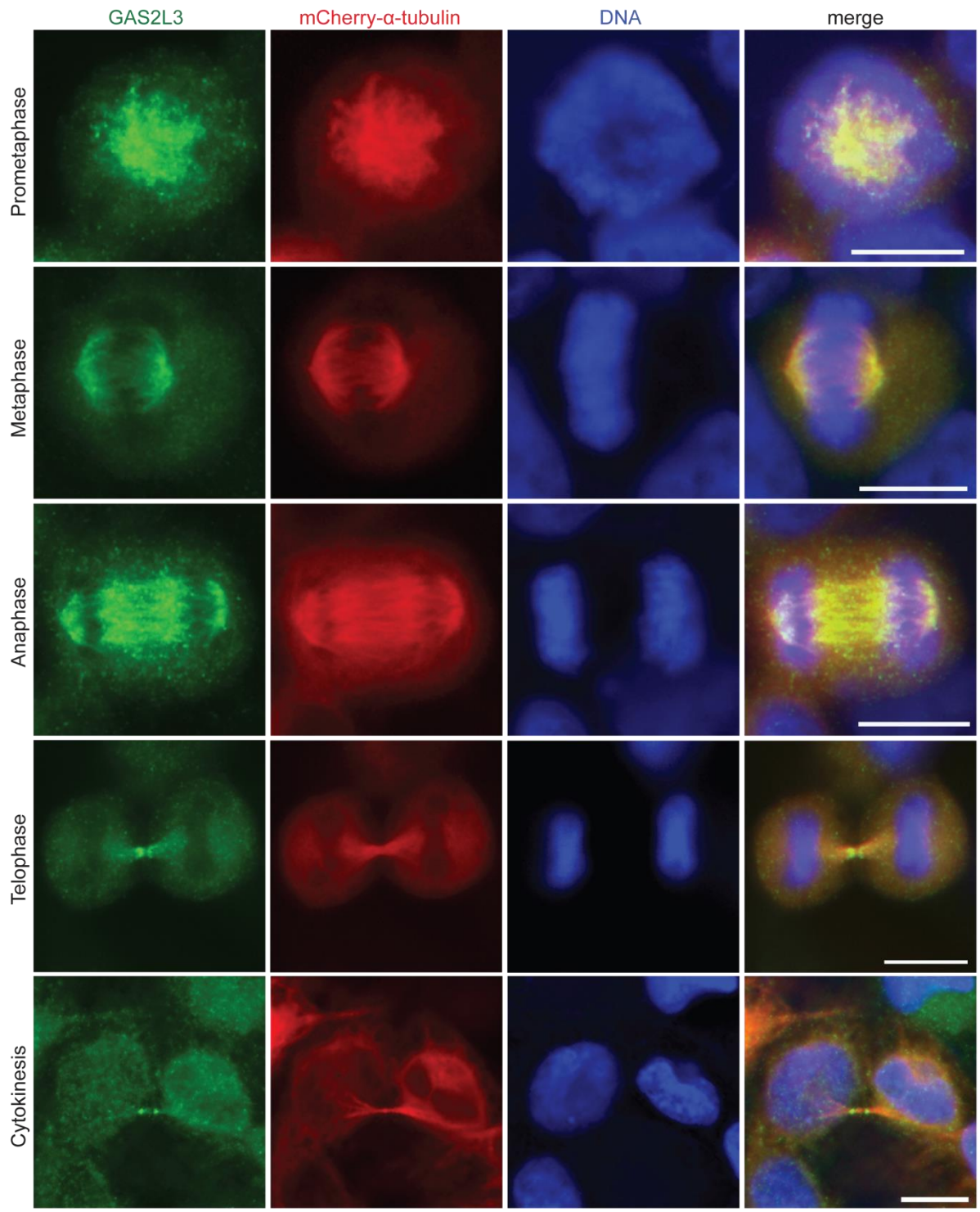

Figure 15: Localization of endogenous GAS2L3 to the mitotic spindle and to the intercellular bridge.
HeLa cells stably expressing mCherry-α-tubulin were fixed in methanol and stained for GAS2L3 (green) and DNA (blue). GAS2L3 localization in different mitotic stages was determined by immunofluorescence. Scale bars: 10 µm.

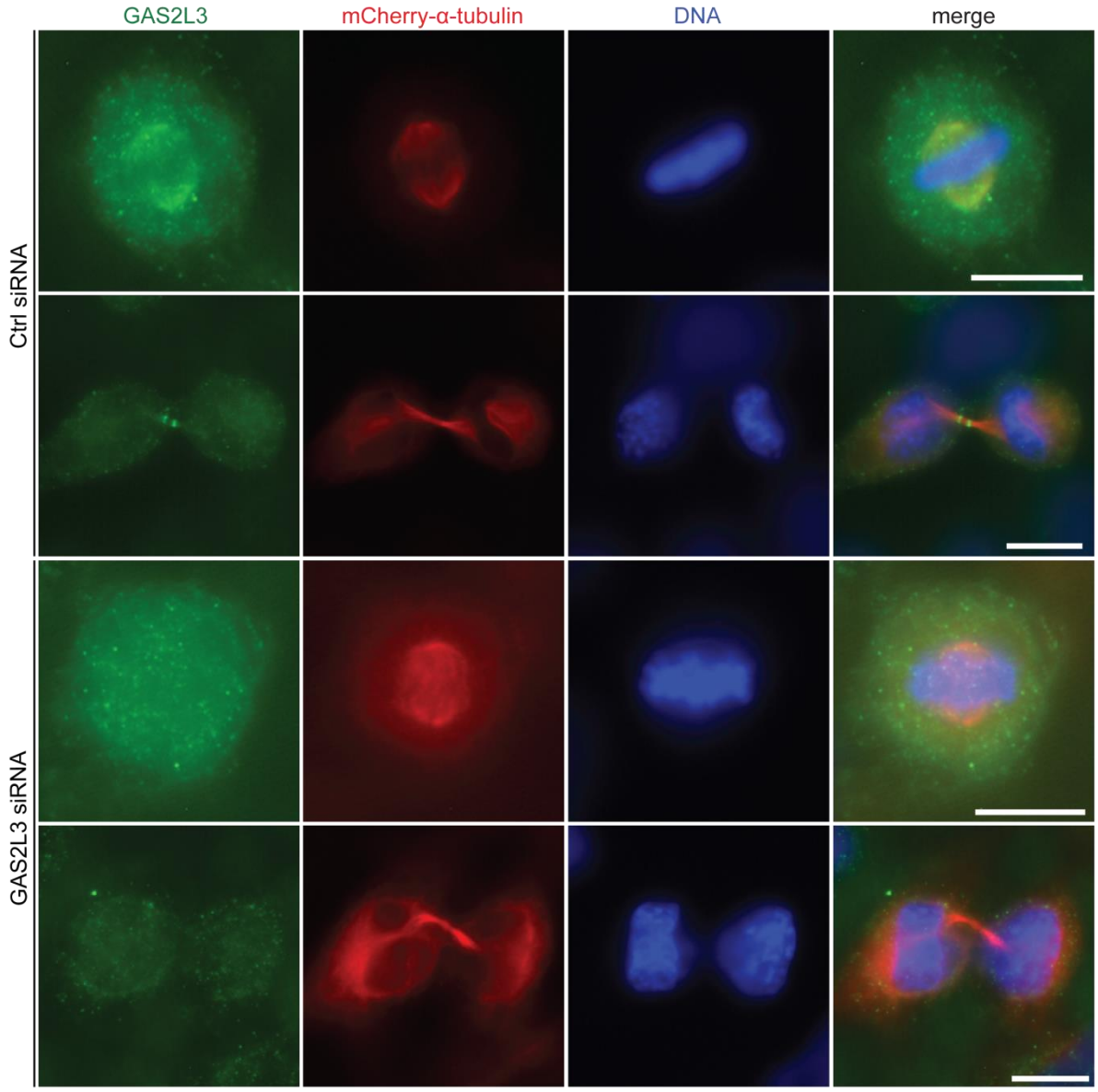

Figure 16: GAS2L3 depleted cells show no GAS2L3 antibody signal at the mitotic spindle and at the intercellular bridge.
HeLa cells stably expressing mCherry-α-tubulin were treated with GAS2L3 siRNA and fixed in methanol. The cells were stained for GAS2L3 (green) and DNA (blue). Localization of GAS2L3 to the mitotic spindle and the intercellular bridge in cytokinesis was determined by immunofluorescence. Scale bars: 10 µm.

After establishing a reliable staining method, I was interested in GAS2L3 localization during cytokinesis at the intercellular bridge in comparison to the midbody marker MKLP1, a subunit of the centralspindlin complex (Matuliene and Kuriyama, 2002; Mishima et al., 2002). Moreover, I wanted to know whether the prominent intercellular bridge localization is specific to HeLa cells. To answer these questions, HeLa, U2OS, T98G, and MCF7 cells were fixed in methanol and stained for endogenous GAS2L3 and MKLP1(Figure 17). In the final stages of cytokinesis, MKLP1 localizes to the

center of the mibody, a prominent protein-dense structure, as part of a structure called fleming body or midbody ring (Makyio et al., 2012).

The staining of different cell lines showed that endogenous GAS2L3 flanked the midbody when MKLP1 formed a ring-like structure. It further demonstrated that this localization pattern is not specific to HeLa cells.

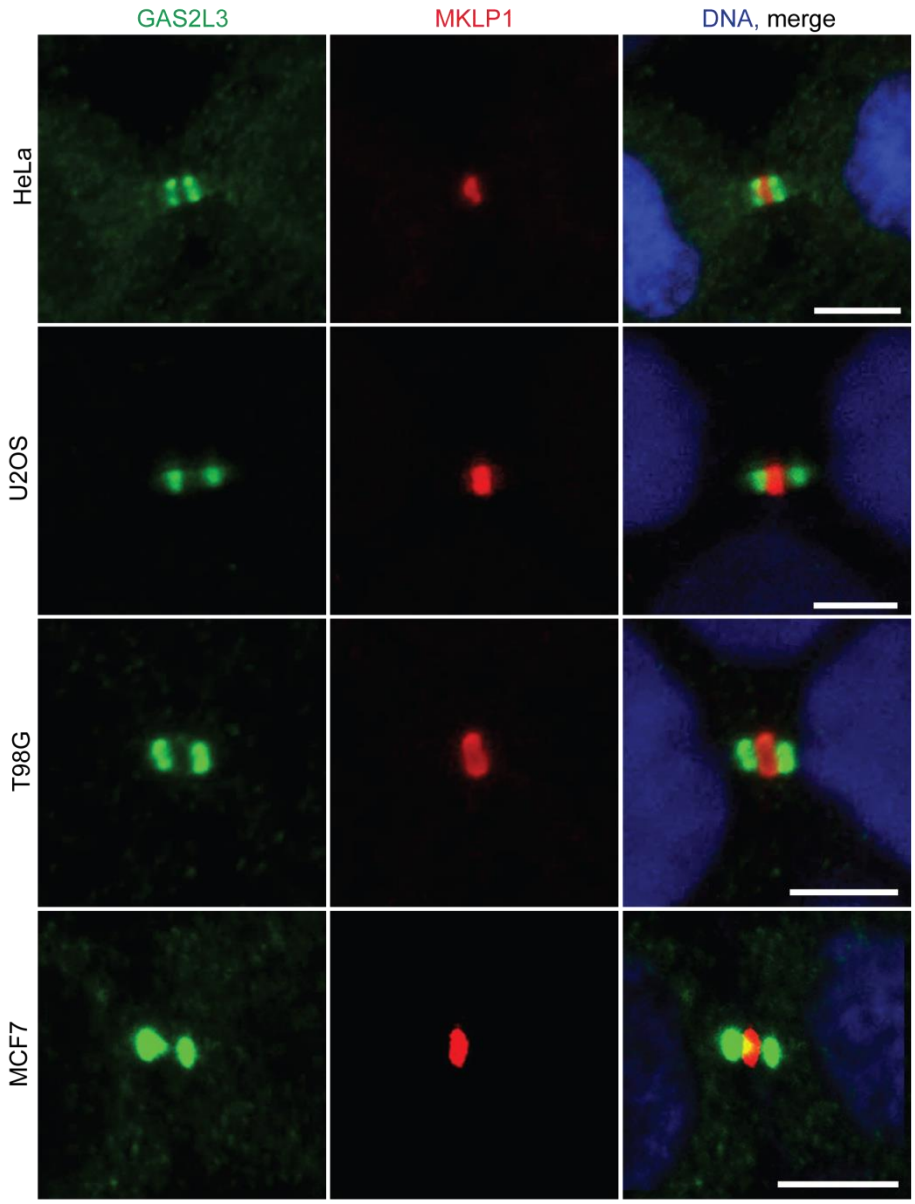

Figure 17: Localization of GAS2L3 close to the midbody ring in different cancer cell lines.
The cancer cell lines HeLa, U2OS, T98G, and MCF7 were fixed in methanol and stained for GAS2L3 (green) and the midbody marker MKLP1 (red). GAS2L3 localization in cytokinesis was analyzed by confocal laser scanning microscopy. The pictures represent maximum projections of z-stacks (step size: 0.5 µm). Scale bars: 5 µm.

5.3 A small pool of GAS2L3 localizes to the midbody center in cytokinesis and to midbody remnants in interphase cells

During the localization studies of endogenous GAS2L3 a minor concentration of GAS2L3 in the center of the intercellular bridge flanked by the two prominent pools close to the midbody was observed in a few cytokinesis cells (Figure 18 A-C). The monoclonal GAS2L3 antibody recognized in a fraction of HeLa and U2OS cells a small pool of GAS2L3 which partially co-localized with MKLP1 (Figure 18 A). The staining of GAS2L3 at the midbody center was less intense compared to the intensity of the prominent pools of GAS2L3 flanking MKLP1. This specific pool of GAS2L3 at the midbody was also observed in HeLa cells stably expressing mCherry-α-tubulin, confirming that the observed localization is not due to antibody cross-reactivity between GAS2L3 and MKLP1 (Figure 18 B). Moreover, I observed a fraction of cells in cytokinesis displaying this type of localization in T98G cells (Figure 18 C).

Thus, at least three different cell lines showed this localization pattern, suggesting that the localization pattern is not restricted to HeLa cells.

GAS2L3 was not always visible at the midbody center. One possible explanation is that the midbody pool of GAS2L3 was less accessible for the antibody because of the midbody's protein-dense environment (Otegui et al., 2005; Steigemann and Gerlich, 2009). Another explanation is, that cytokinesis is a highly dynamic process in which GAS2L3 is only visible at the midbody in a certain step of cytokinesis (Steigemann and Gerlich, 2009). The co-localization of GAS2L3 with MKLP1 when MKLP1 formed a ring-like structure (Figure 18 A, C) indicated that the co-localization takes place in cytokinesis after cleavage furrow ingression but does not clarify the duration of the co-localization.

To investigate this, I focused on post abscission daughter cells which harbor the midbody remnant. Midbody remnants are tubulin-rich structures of the midbody which survive the abscission process together with the attached midbody ring, including MKLP1 (Hu et al., 2012a; Pohl and Jentsch, 2008). Using tubulin and MKLP1 as marker, endogenous GAS2L3 and EGFP-GAS2L3 were detected at midbody remnants in interphase cells forming ring-like structures (Figure 19 A). This observation was further confirmed in U2OS and T98G cells (Figure 19 B, C).

Thus, GAS2L3 starts to localize to the midbody in late cytokinesis after cleavage furrow ingression and stays attached with post-abscission midbody remants.

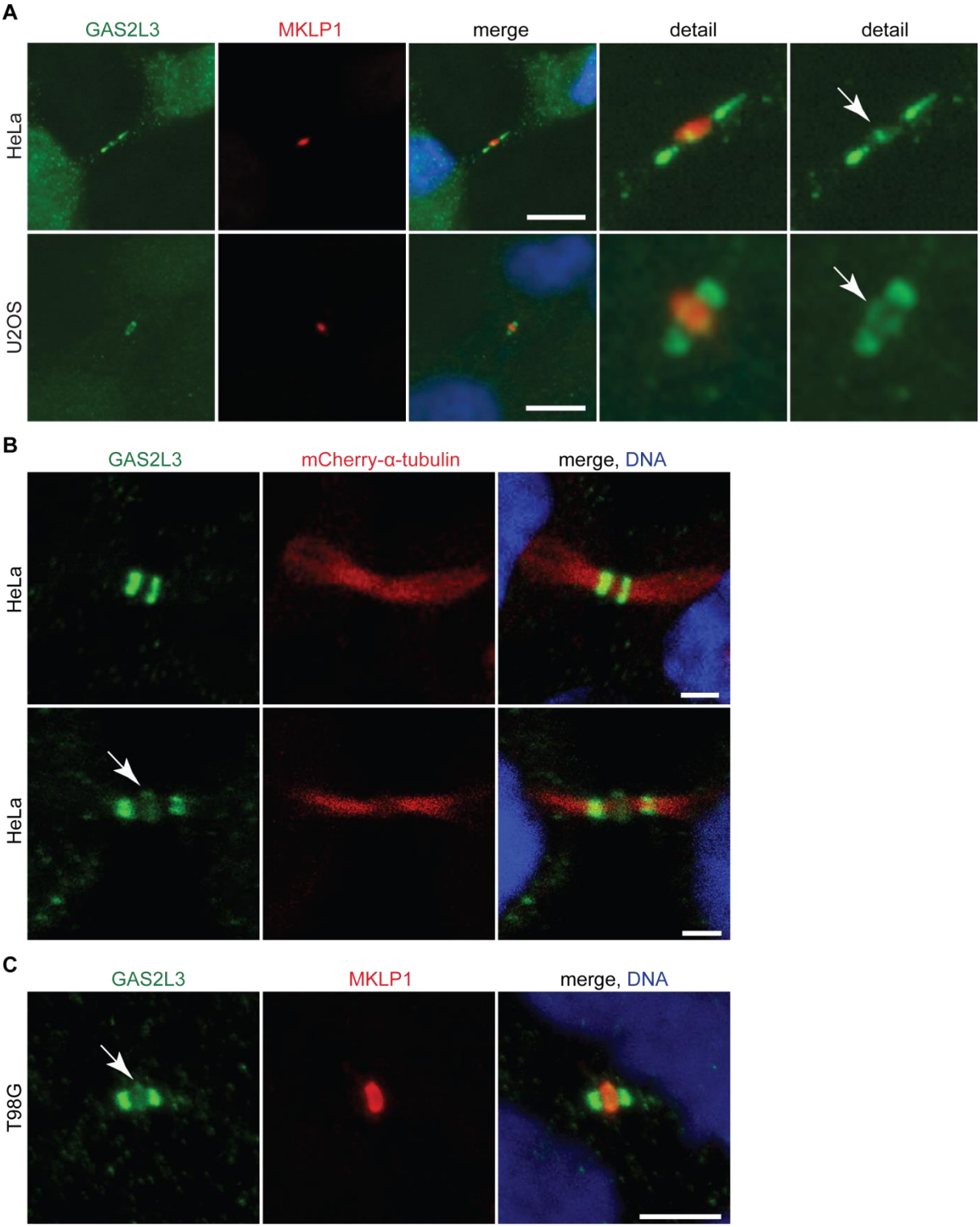

Figure 18: Localization of a small pool of GAS2L3 to the midbody center and the midbody ring. (**A**-**C**) All cell lines were fixed in methanol and stained for GAS2L3 (green) and different markers (red). White arrows indicate the small pool of GAS2L3 at the midbody center and midbody ring (**A**) HeLa and U2OS cells were stained for MKLP1 (red) as marker and analyzed for GAS2L3 localization to the midbody center and the midbody ring by immunofluorescence. Scale bars: 10 µm. (**B**) HeLa cells stably expressing mCherry-α-tubulin were analyzed for the GAS2L3 expression pattern in cytokinesis by confocal laser scanning microscopy. The pictures represent maximum projections of z-stacks (step size: 0.5 µm). Scale bars: 5 µm. (**C**) T98G cells were stained for MKLP1 (red) as marker and analyzed for GAS2L3 (geen) localization to the midbody center and the midbody ring by confocal laser scanning microscopy. The pictures represent maximum projections of z-stacks (step size: 0.5 µm). Scale bars: 5 µm. Figure 18 A was published in Wolter et al. (2012).

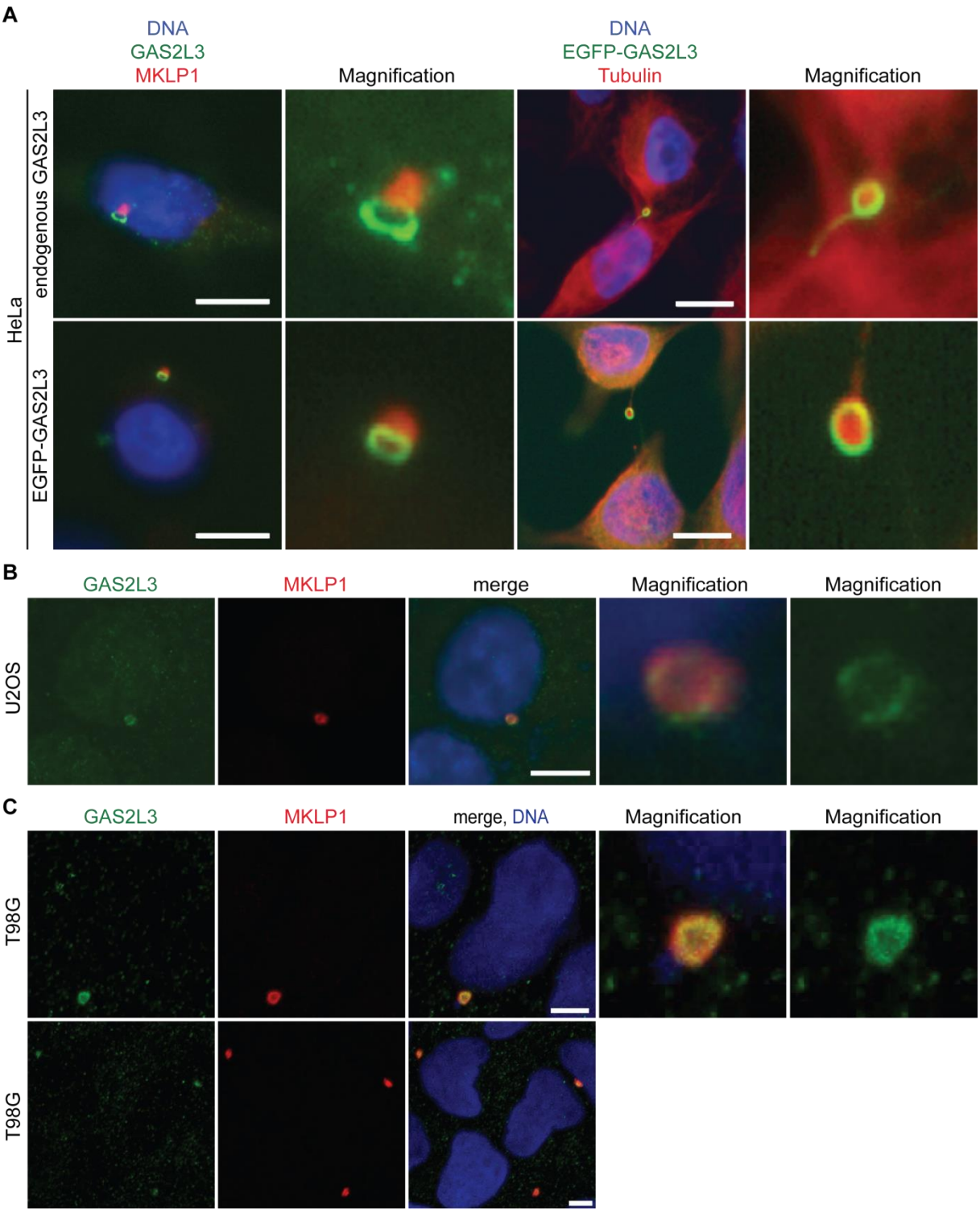

Figure 19: Localization of GAS2L3 to midbody remnants in interphase cells.
(A-C) All cell lines were fixed with methanol and stained for GAS2L3 (green) and different markers in (red). (**A**) HeLa cells stained for GAS2L3 or transiently expressing EGFP-GAS2L3 were stained with MKLP1 or α-tubulin and analyzed for localization of GAS2L3 to midbody remnants by immunofluorescence. Scale bars: 10 µm (**B**) U2OS cells were stained with MKLP1 as marker and analyzed for GAS2L3 localization to midbody remnants by immunofluorescence. Scale bars: 10 µm. **C**) T98G cells were stained with MKLP1 as marker and analyzed for localization to midbody remnants by confocal laser scanning microscopy. The pictures represent maximum projections of z-stacks (step size: 0.5 µm). Scale bars: 5 µm.
Figure 19 A was published in Wolter (2011) and Wolter et al. (2012) and Figure 19 B was published in Wolter et al. (2012).

5.4 The GAR domain is responsible for GAS2L3 localization to the constriction zone and to the midbody ring

GAS2L3 consists of two conserved domains, a calponin homology domain (CH) and a Gas2-related (GAR) domain, and an unstructured C-terminal part (Figure 20). Biochemical studies of GAS2L3 demonstrated that the CH domain can bind to actin filaments and that the C-terminal part can simultaneously bind to actin and microtubule filaments (Stroud et al., 2011; Wolter et al., 2012).

The GAR domain has been proposed to function as a microtubule-binding domain, but previous studies from our laboratory revealed that not the GAR domain but rather the C-terminal part of GAS2L3 mediates the microtubule-binding *in vivo* and *in vitro* (Wolter et al., 2012). Therefore, the function for the GAR domain of GAS2L3 still remains elusive.

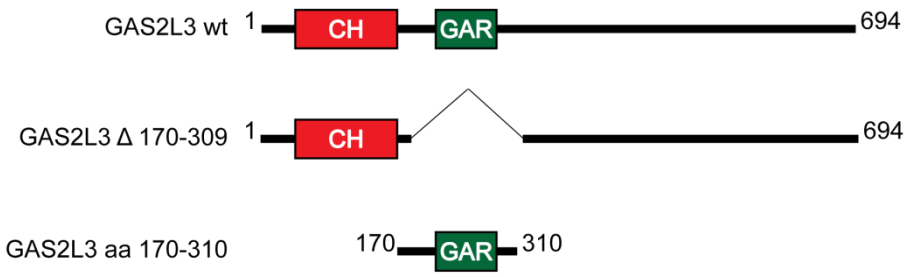

Figure 20: Schematic overview of EGFP-GAS2L3 constructs for the investigation of the GAR domain.
GAS2L3 consists of two conserved domains, a calponin homology (CH) domain and a Gas2-related (GAR) domain, and an unstructured C-terminal part. The three different constructs were fused to EGFP for localization analysis of the GAR domain in HeLa cells.

In order to determine the role of the GAR domain for GAS2L3 localization, I performed structure-function analysis of the GAS2L3 GAR domain for its localization in mitosis using three EGFP-GAS2L3 constructs from our laboratory consisting of GAS2L3 wild type (wt), an internal deletion mutant for the GAR domain (Δ170-309) and the GAR domain (aa 170-310) only (Figure 20). EGFP-GAS2L3 wt, EGFP-GAS2L3 Δ170-309 and EGFP-GAS2L3 aa 170-310 were expressed in HeLa cells. Their localization in interphase, mitosis, and cytokinesis was investigated using Aurora B as marker (Figure 21). In interphase, EGFP-GAS2L3 wt and the Δ170-309 mutant localized to the microtubule cytoskeleton comparable to the result from the EGFP-GAS2L3 localization experiment in Figure 13 A. The aa 170-310 mutant displayed a cytoplasmic and a nuclear fraction but lost its localization to microtubules.

In mitosis, EGFP-GAS2L3 wt and Δ170-309 localized to the mitotic spindle whereas the aa 170-310 mutant showed no preferential localization. Furthermore, no co-localization of the three constructs with Aurora B could be detected in the first mitotic stages. Interestingly, while EGFP-GAS2L3 co-localized with Aurora B at the intercellular bridge in cytokinesis, the Δ170-309 mutant failed to co-localize with Aurora B and rather localized close to Aurora B at the outer part of the intercellular bridge. The aa 170-310 mutant localized only to the midbody center. Thus, the mutants shared no co-localization with Aurora B in contrast to GAS2L3 wt.

Interestingly, higher resolution imaging revealed that EGFP-GAS2L3 did not only co-localize with Aurora B but also localized to the constriction zone. The constriction zone indicates the region at the intercellular bridge where abscission, the final stage of cytokinesis, will occur. This zone is ~1-2 µm away from the midbody center with a characteristic thin microtubule cytoskeleton (Elia et al., 2011; Guizetti et al., 2011). Abscission is regulated by an Aurora B-dependent mechanism in which the constriction zone can be identified by less intense Aurora B staining intensity at the constriction zone (Figure 21, Figure 22 and Figure 23 A) (Mierzwa and Gerlich, 2014; Pe'er et al., 2013).

To confirm that GAS2L3 localizes to the constriction zone and that this localization is not specific in HeLa cells, I stained U2OS and T98G cells for endogenous GAS2L3 and Aurora B (Figure 22). As expected, GAS2L3 co-localized with Aurora B whereby the Aurora B staining was less intense. In addition, I used the mitotic kinesin-like protein 2 (MKLP2) to verify the localization pattern of GAS2L3 wt and GAS2L3 Δ170-309 with Aurora B in cytokinesis (Figure 23 B). MKLP2 is part of the chromosomal passenger complex in cytokinesis and important for re-localization of Aurora B from centromers to the spindle midzone and intercellular bridge in cytokinesis (Gruneberg et al., 2004). As expected, GAS2L3 wt co-localized with MKLP2 in cytokinesis where MKLP2 staining was less intense, while the GAS2L3 Δ170-309 mutant failed again to co-localize. Its localization was rather limited next to MKLP2 at the outer region of the intercellular bridge.

To further proof that EGFP-GAS2L3 wt localizes to the constriction zone and that EGFP-GAS2L3 Δ170-309 failed to localize there, fluorescence intensity profiles of the performed co-staining's with Aurora B and MKLP2 were created (Figure 23 A, B). For cells in cytokinesis, the EGFP signal peaked for GAS2L3 wt in a region, where Aurora B and MKLP2 staining was less intense. This region was ~1-2 µm away from

the midbody center. In contrast, the intensity profiles for GAS2L3 Δ170-309 showed that the strongest EGFP intensity was ~3-4 µm away from the midbody. Furthermore GAS2L3 Δ170-309 displayed no overlap with the constriction zone and only a marginal one with Aurora B and MKLP2 more distal from the midbody center.

To demonstrate that GAS2L3 localizes to the constriction zone together with other abscission factors, I tested the possibility that GAS2L3 co-localizes with the microtubule-severing enzyme spastin. Spastin is recruited by the ESCRT-III complex to facilitate the disintegration of the microtubule cytoskeleton at the constriction zone in the abscission event (Connell et al., 2009; Guizetti et al., 2011; Neto and Gould, 2011; Yang et al., 2008). First, I co-stained Aurora B and spastin (Figure 24 A). In cytokinesis, spastin co-localized with Aurora B where Aurora B antibody staining was less intense. This observation was confirmed by immunofluorescence intensity profiles which showed a signal peak for spastin ~1-2 µm away from the midbody center where the Aurora B signal was less intense. Second, I expressed either EGFP-GAS2L3 wt or EGFP-GAS2L3 Δ170-309 and stained for spastin (Figure 24 B). In cytokinesis, GAS2L3 wt co-localized with spastin whereas GAS2L3 Δ170-309 did not show a co-localization. Immunofluorescence intensity profiles confirmed that EGFP-GAS2L3 wt and spastin shared intensity peaks 1-2 µm away from the midbody center. In contrast, the EGFP intensity peak for GAS2L3 Δ170-309 was more distal from the midbody center and separated from the spastin-peak. Quantification of intensity profiles for GAS2L3 wt (n=12) and GAS2L3 Δ170-309 (n=12) demonstrated that the constructs localized significantly different in comparison to spastin ($p < 0.0001$, Student's t test) (Figure 24).

Taken together, the results suggest that the GAR domain is required for proper GAS2L3 localization to the constriction zone and indicate a role for GAS2L3 in abscission. This idea is in line with RNAi rescue experiments where siRNA resistant GAS2L3 wt and GAS2L3 Δ170-309 was used to demonstrate that only GAS2L3 wt is able to rescue the cytokinesis phenotype (Fackler et al., 2014).

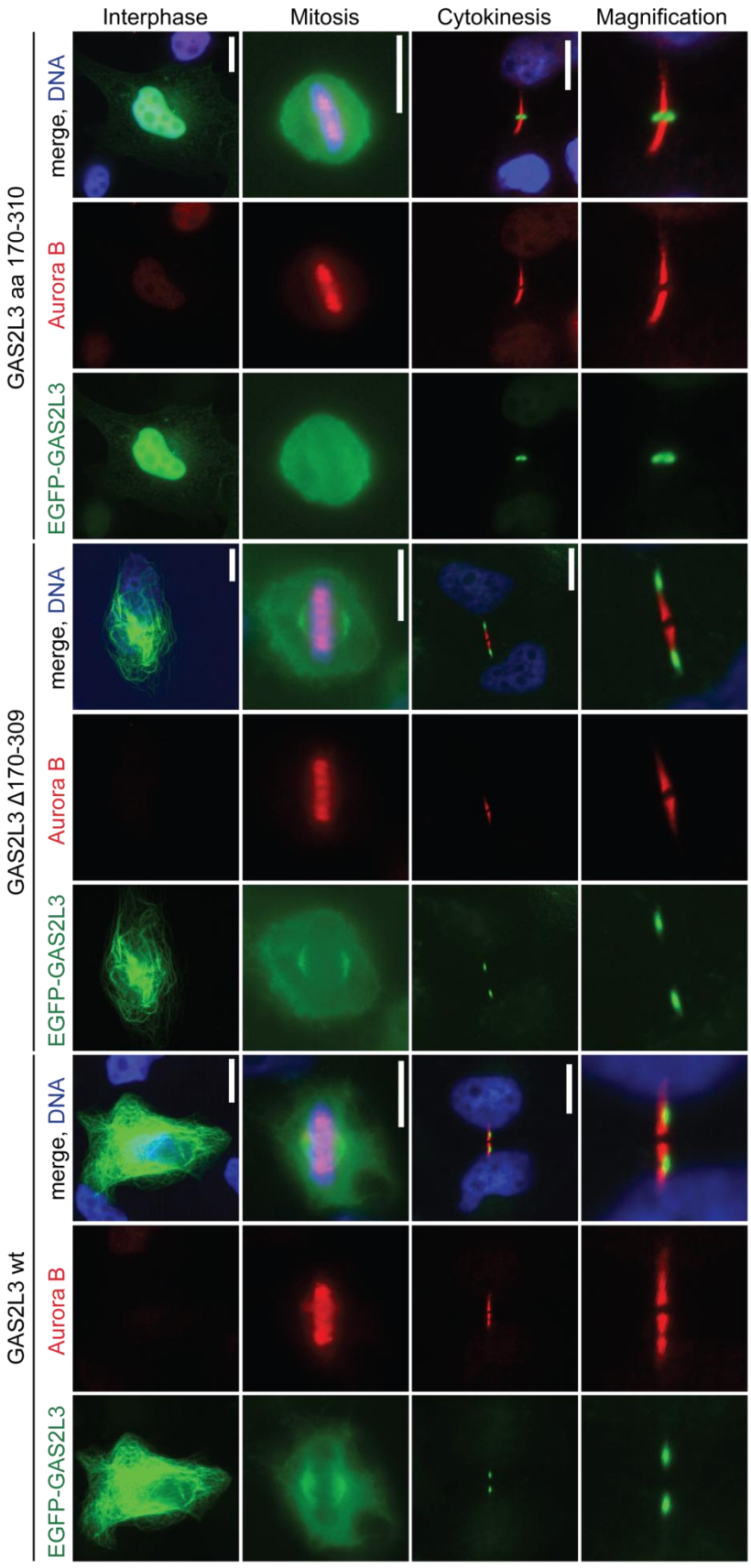
Interphase
Mitosis
Cytokinesis
Magnification
GAS2L3 wt
GAS2L3 Δ170-309
GAS2L3 aa 170-310
EGFP-GAS2L3
Aurora B
merge, DNA

Figure 21: Localization of EGFP-GAS2L3, EGFP-GAS2L3 Δ170-309, and EGFP–GAS2L3 aa 170-310 in interphase, mitosis and cytokinesis.
HeLa cells transiently expressing EGFP-GAS2L3, EGFP-GAS2L3 Δ170-309 or EGFP GAS2L3 aa 170-310 were fixed in PFA + Triton-X and stained for Aurora B (red) and DNA (blue). EGFP localization in interphase, mitosis, and cytokinesis was determined by immunofluorescence. Scale bars: 10 µm.

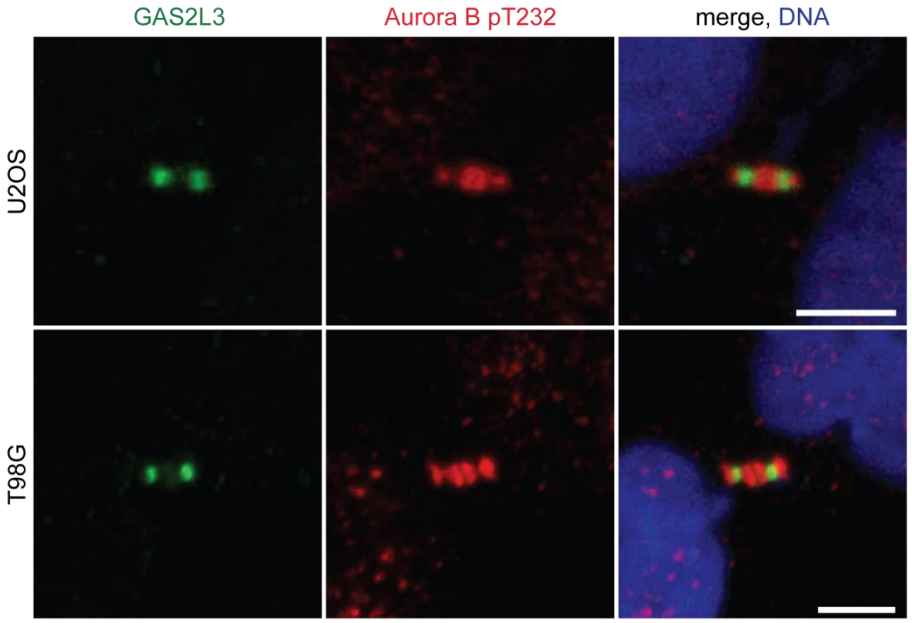

Figure 22: Co-localization of GAS2L3 with Aurora B in U2OS and T98G cells in cytokinesis.
U2OS and T98G cells were fixed in methanol and stained for GAS2L3 (green), Aurora B pT232 (red), and DNA (blue). The localization of Aurora B and GAS2L3 in cytokinesis was analyzed by confocal laser scanning microscopy. The pictures present maximum projections of z-stacks (step size: 0.5 µm). Scale bars: 5 µm.

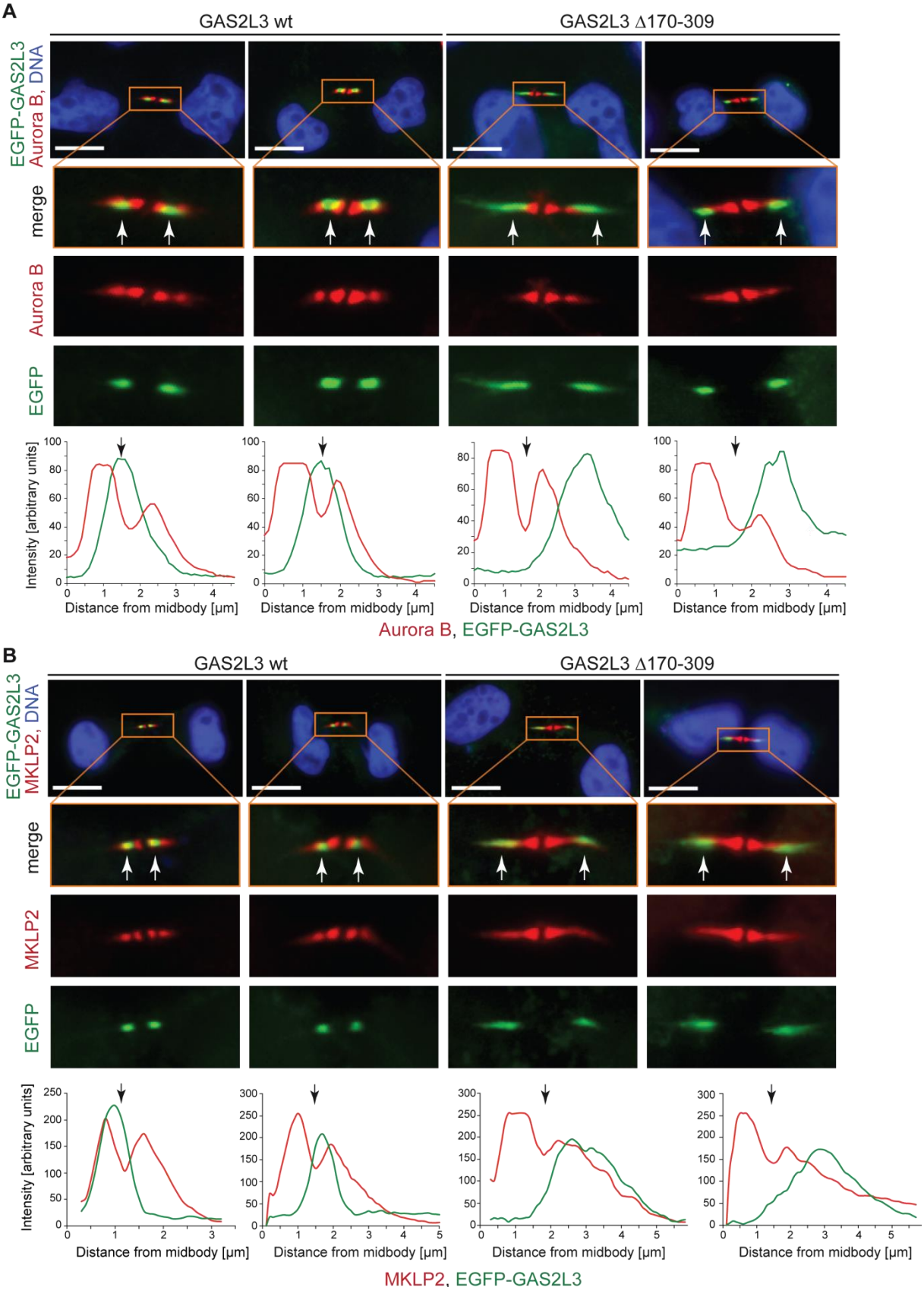
A
GAS2L3 wt
GAS2L3 Δ170-309
EGFP-GAS2L3
Aurora B, DNA
merge
Aurora B
EGFP
Intensity [arbitrary units]
Distance from midbody [μm]
Aurora B, EGFP-GAS2L3
B
GAS2L3 wt
GAS2L3 Δ170-309
EGFP-GAS2L3
MKLP2, DNA
merge
MKLP2
EGFP
Intensity [arbitrary units]
Distance from midbody [μm]
MKLP2, EGFP-GAS2L3

Figure 23: Co-localization of GAS2L3 with Aurora B and MKLP2 during cytokinesis.
(**A**) HeLa cells transiently expressing EGFP-GAS2L3 or EGFP-GAS2L3 Δ170-309 were fixed in PFA + Triton-X and stained for Aurora B (red) and DNA (blue). Detailed magnifications of the EGFP constructs to the constriction zone at the intercellular bridge are provided. The localization pattern was analyzed by immunofluorescence microscopy combined with subsequent fluorescence intensity profiles of the proteins created in ImageJ using a line along the intercellular bridge beginning at the midbody center. The staining intensities of the different antibodies above that line were quantified using ImageJ. (**B**) HeLa cells transiently expressing EGFP-GAS2L3 or EGFP-GAS2L3 Δ170-309 were fixed in PFA + Triton-X and stained for MKLP2 (red) and DNA (blue). Detailed magnifications and intensity profiles are provided. Scale bars: 10 µm.
Figure 23 was first published in Fackler et al. (2014). The intensity profiles were created by Prof. Dr. Gaubatz.

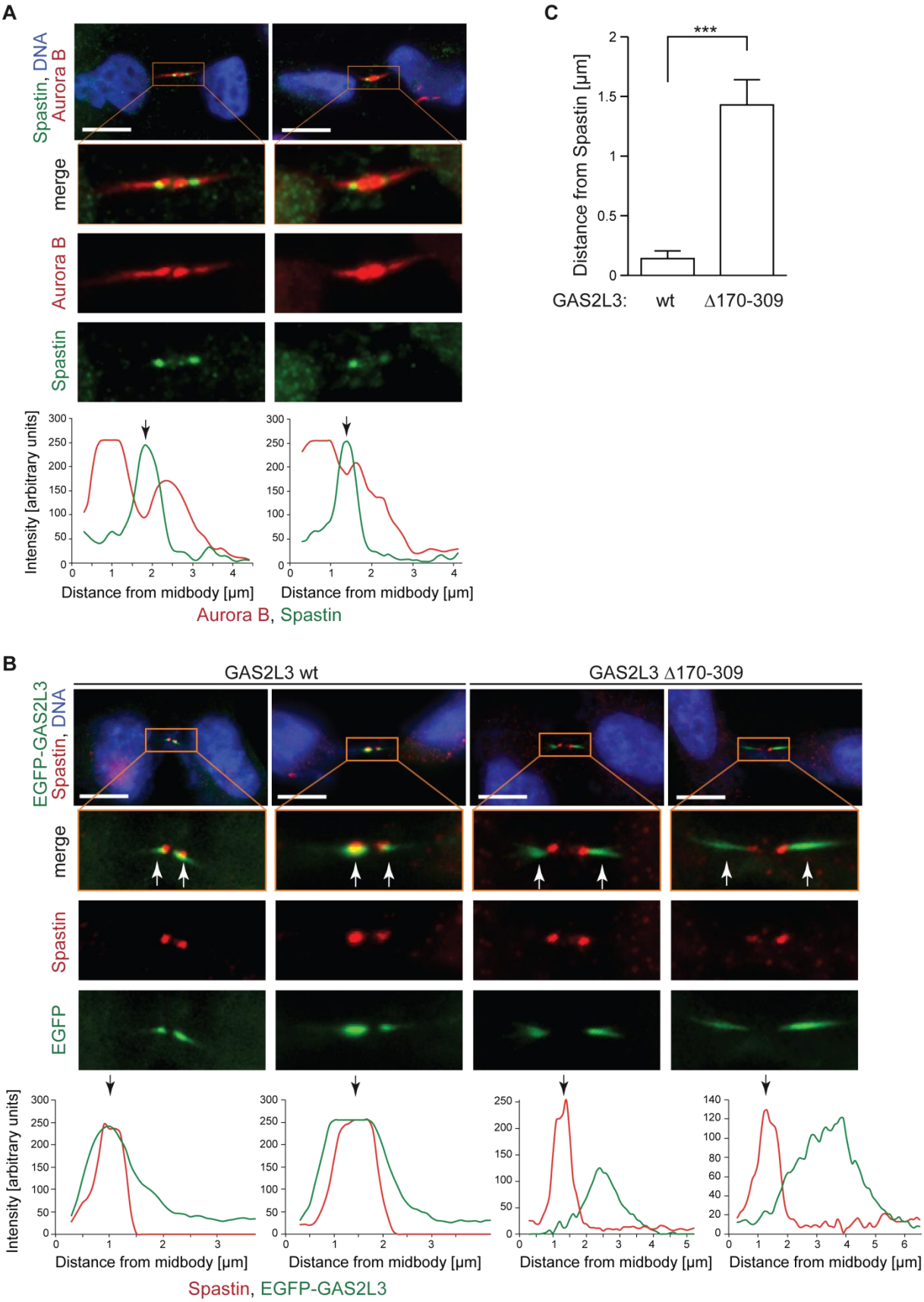
A
Spastin, DNA
Aurora B
merge
Aurora B
Spastin
Intensity [arbitrary units]
Distance from midbody [µm]
Distance from midbody [µm]
Aurora B, Spastin
C
***
Distance from Spastin [µm]
GAS2L3: wt Δ170-309
B
GAS2L3 wt
GAS2L3 Δ170-309
EGFP-GAS2L3
Spastin, DNA
merge
Spastin
EGFP
Intensity [arbitrary units]
Distance from midbody [µm]
Distance from midbody [µm]
Distance from midbody [µm]
Distance from midbody [µm]
Spastin, EGFP-GAS2L3

Figure 24: The GAR domain is required for localization of GAS2L3 to the constriction zone during cytokinesis.
(**A**) HeLa cells were fixed in methanol and stained for Aurora B (red), spastin (green), and DNA (blue). Detailed magnifications of the constriction zone at the intercellular bridge are provided. The localization pattern was analyzed by immunofluorescence microscopy combined with subsequent fluorescence intensity profiles of the proteins created in ImageJ using a line along the intercellular bridge beginning at the midbody center. The staining intensities of the different antibodies above that line were quantified using ImageJ. (**B**) HeLa cells transiently expressing EGFP-GAS2L3 or EGFP-GAS2L3 Δ170-309 were fixed in PFA + Triton-X and stained for spastin (red) and DNA (blue). Detailed magnifications of the constriction zone at the intercellular bridge are provided. The intensity profiles were created as in (A). Scale bar: 10 µm. (**C**) Fluorescence intensities of the EGFP constructs and spastin were quantified as described in (B) and the distances between the spastin and EGFP-GAS2L3 peaks (n=12) and between the spastin and EGFP-GAS2L3 Δ170-309 peaks (n=12) were calculated. The differences between the means were statistically significant ($P < 0.0001$; Student´s t test).
Figure 24 was first published in Fackler et al. (2014). The intensity profiles were created by Prof. Dr. Gaubatz.

After characterization of the EGFP-GAS2L3 wt and EGFP-GAS2L3 Δ170-309 localization in cytokinesis, I was interested in a better understanding of the midbody localization of EGFP-GAS2L3 aa 170-310 (Figure 21).Therefore, I expressed EGFP-GAS2L3 aa 170-310 in HeLa cells and used different midbody localization marker in the immunostainings (Figure 25 A-C). In cytokinesis, GAS2L3 aa 170-310 localized in some cells as perfect ring-like structure to the center of the intercellular bridge and to tubulin-dense structures after abscission (Figure 25 A). Co-staining of GAS2L3 aa 170-310 with MKLP1 in post abscission interphase cells revealed that both proteins perfectly co-localized as ring-like structures to the midbody remnant in some interphase cells (Figure 25 B).
Aurora B controls an abscission checkpoint in mammalian cells (Steigemann et al., 2009). The kinase perceives chromosome bridges in cytokinesis and subsequently initiates an abscission delay until the bridges are resolved. When the bridges are resolved Aurora B gets inactivated and localizes to the midbody center. To address the possibility whether GAS2L3 aa 170-310 co-localizes with Aurora B in this context, I expressed the GAS2L3 aa 170-310 mutant in HeLa cells and stained for Aurora B (Figure 25 C). Aurora B and GAS2L3 aa 170-310 did not co-localize. They rather localized in close proximity to the midbody. In summary, the EGFP-GAR domain mutant (aa 170-310) localization in cytokinesis is similar to the small pool of endogenous GAS2L3 which localizes to the midbody and midbody remnants (Figure 18).

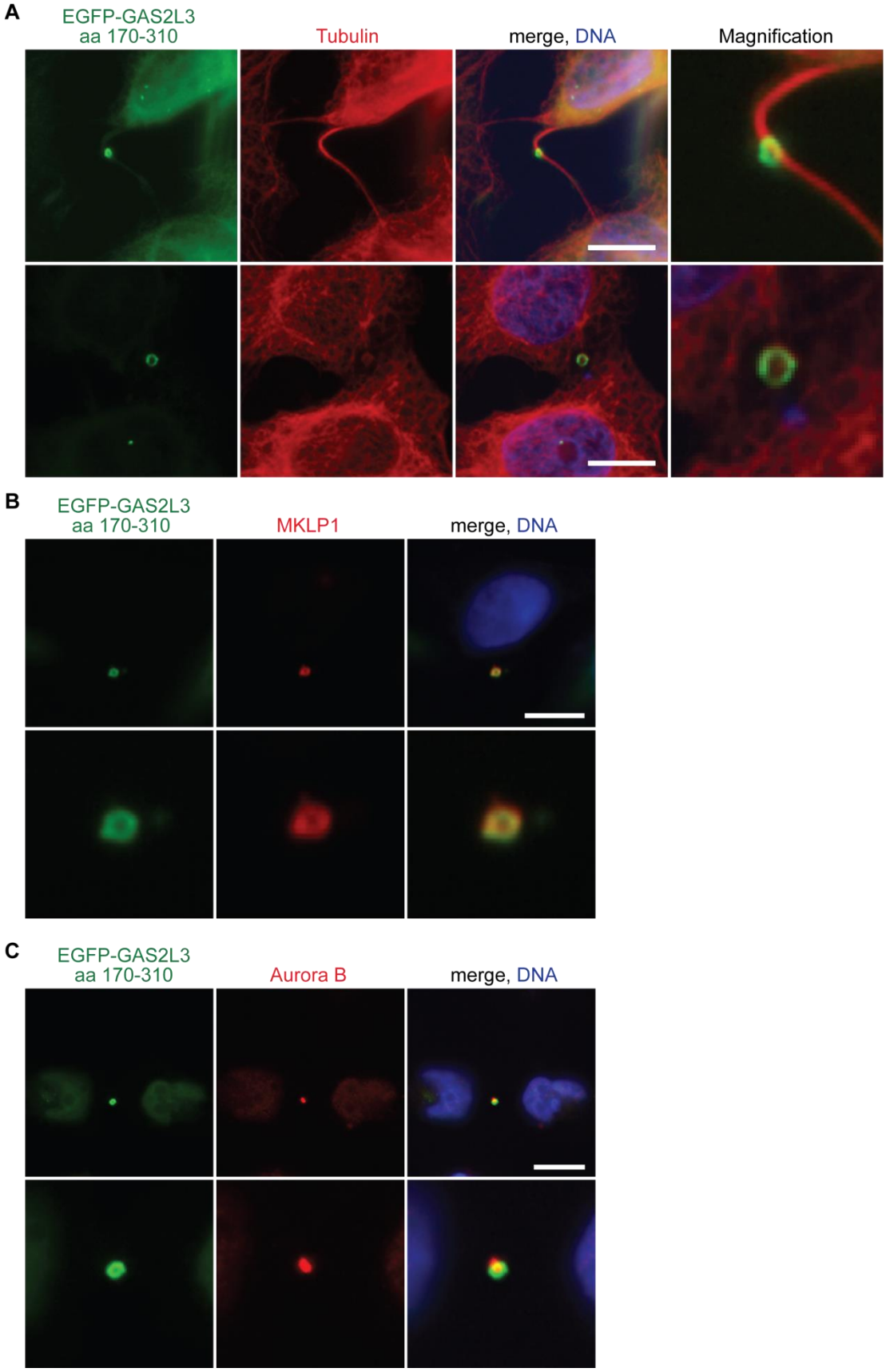

Figure 25: Localization of the GAR domain to the midbody ring and midbody remnants.
HeLa cells transiently overexpressing EGFP-GAS2L3 aa 170-310 were fixed in methanol (**A**-**B**) or PFA + Triton-X (**C**). The cells were stained for tubulin (red) (**A**), for MKLP1 (red) (**B**), and Aurora B (red) (**C**).Localization of EGFP-GAS2L3 aa 170-310 to the midbody and midbody remnants was analyzed by immunofluorescence. Scale bars:10 µm. Figure 25 A was first published in Wolter (2011).

5.5 DREAM is a master regulator of mitotic kinesins and cytokinesis genes

Recently, different approaches were performed to identify and characterize DREAM target genes by genome-wide promoter analysis, gene expression analysis, and genome-scale RNAi profiling using a variety of mouse and human cell lines as model systems (Chen et al., 2012; Esterlechner et al., 2013; Kittler et al., 2007; Litovchick et al., 2007; Reichert et al., 2010; Sadasivam et al., 2012) . Thereby, not only *GAS2L3* but also mitotic kinesins and cytokinesis genes were identified as DREAM target genes. Mitotic kinesins belong to a superfamily of microtubule-associated proteins (MAPs) with an ATP-dependent motor domain (Cross and McAinsh, 2014; Hirokawa et al., 2009). Previously, the mitotic kinesin *KIF23* was extensively studied and became the first example for the regulation of a mitotic kinesin by DREAM (Fischer et al., 2013). How DREAM regulates mitotic kinesins and microtubule-associated proteins (MAPs) involved in cytokinesis has not been investigated in detail. That raises the question whether DREAM regulates only individual mitotic kinesins or rather a larger set of mitotic kinesins and MAPs in a coordinated fashion during the cell cycle.

In order to address this question, I performed chromatin immunoprecipitation (ChIP) assays in MDA-MB-231 breast cancer cells using antibodies specific for either the core complex (LIN9) or for the activating complex (B-MYB, FOXM1). Unspecific IgG was used as control. The ChIP-qPCR analysis revealed that all tested DREAM subunits were enriched at the promoters of 11 mitotic kinesins (*KIF23*, *KIF22*, *KIF20A*, *KIF20B*, *KIF15*, *KIF14*, *KIF11*, *KIF10*, *KIF4A*, *KIF2C,* and *KIFC1*) and at the promoters of *PRC1* and *CEP55,* two example cytokinesis MAPs (Figure 26 A, B). DREAM was strongly enriched at the *BIRC5* promoter, which served as positive control. The *GAPDH2* promoter was used as negative control and displayed only a basal enrichment. DREAM did not bind to the promoters of *KIF18A*, *KIF4B*, *KIF2B* and *KIF2A*.The promoter of the mitotic kinesin *KIF18B* was not included because of difficulties with the primer design.

To confirm these results in different cell lines, I performed ChIP assays in the lung cancer cell lines H460 and H23, including an antibody specific for the repressive complex (p130) (Figure 27 A, B). The ChIP-qPCR analysis revealed that all DREAM subunits were enriched at the promoter of 6 selected mitotic kinesins (*KIF23*, *KIF20A*,

KIF14, *KIF4A*, *KIF2C*, and *KIFC1*), *PRC1*, *CEP55*, *GAS2L3,* and *BIRC5* in contrast to the *GAPDH2* promoter. The result for *GAS2L3* is presented in Figure 10.

To further proof that the DREAM complex is actively involved in mitotic kinesin regulation, DREAM subunits were depleted by RNAi in MDA-MB-231 breast cancer cells for 48 h. Changes in the gene expression of 14 human mitotic kinesins, *PRC1* and *CEP55* were analyzed by RT-qPCR (Figure 28 A, B). Depletion of LIN37, LIN52, LIN54, LIN9, B-MYB, and FOXM1 was confirmed by RT-qPCR (Figure 28 A1, B1). The subsequent gene expression analysis by RT-qPCR revealed that all mitotic kinesins, *PRC1* and *CEP55* were down-regulated after depletion of DREAM subunits in comparison to the non-specific siRNA treated control (Figure 28 A2, B2). The mitotic kinesins *KIF18A* and *KIF2A* showed a lower down-regulation and no enrichment of DREAM at their promoters (Figure 26 B). *KIF4B* and *KIF2B* were not included in the results, because they were not expressed in MDA-MB-231 cells. *KIF18B*, however, showed a strong down-regulation after RNAi depletion of all DREAM subunits.

The RNAi experiment was repeated in H23 cells. The mRNA expression of 6 selected mitotic kinesins (*KIF23*, *KIF20A*, *KIF14*, *KIF4A*, *KIF2C,* and *KIFC1*), *PRC1,* and *CEP55* was analyzed after LIN9 and B-MYB depletion (Figure 27 C). After 48 h, the mRNA of LIN9 and B-MYB was efficiently down-regulated (Figure 27 C1). All selected mitotic kinesins as well as *PRC1* and *CEP55* were drastically down-regulated in contrast to the non-specific siRNA treated control (Figure 27 C2).

Comparison of the ChIP and RNAi experiments suggests that the DREAM complex is involved in the coordinated regulation of 12 out of 16 mitotic kinesins in G2/M. Similarly, MAPs involved in cytokinesis are also regulated by DREAM.

For *KIF23* it was previously shown, that p53 represses the expression of the mitotic kinesin in a p53-p21-DREAM/p130-dependent manner (Fischer et al., 2013). Moreover, work from our group demonstrated that the DREAM complex cannot switch from the active to the repressive form in p53-negative cancer cells after induction of DNA damage (Mannefeld et al., 2009). Therefore, I addressed the question whether the repressive DREAM complex can be found at the promoters of mitotic kinesins, *PRC1*, *CEP55*, and *GAS2L3* in p53-mutated cancer cells by re-analyzing the ChIP results shown in Figure 27 A, B. Interestingly, the ratio of the promoter enrichment between the activating and the repressive subunits of DREAM was comparable in H460 (wt p53) and H23 (mutated p53) cells, suggesting no

influence of p53 on the formation of the repressive form of the DREAM complex and in the assembly of the DREAM complex subunits during the unperturbed cell cycle.

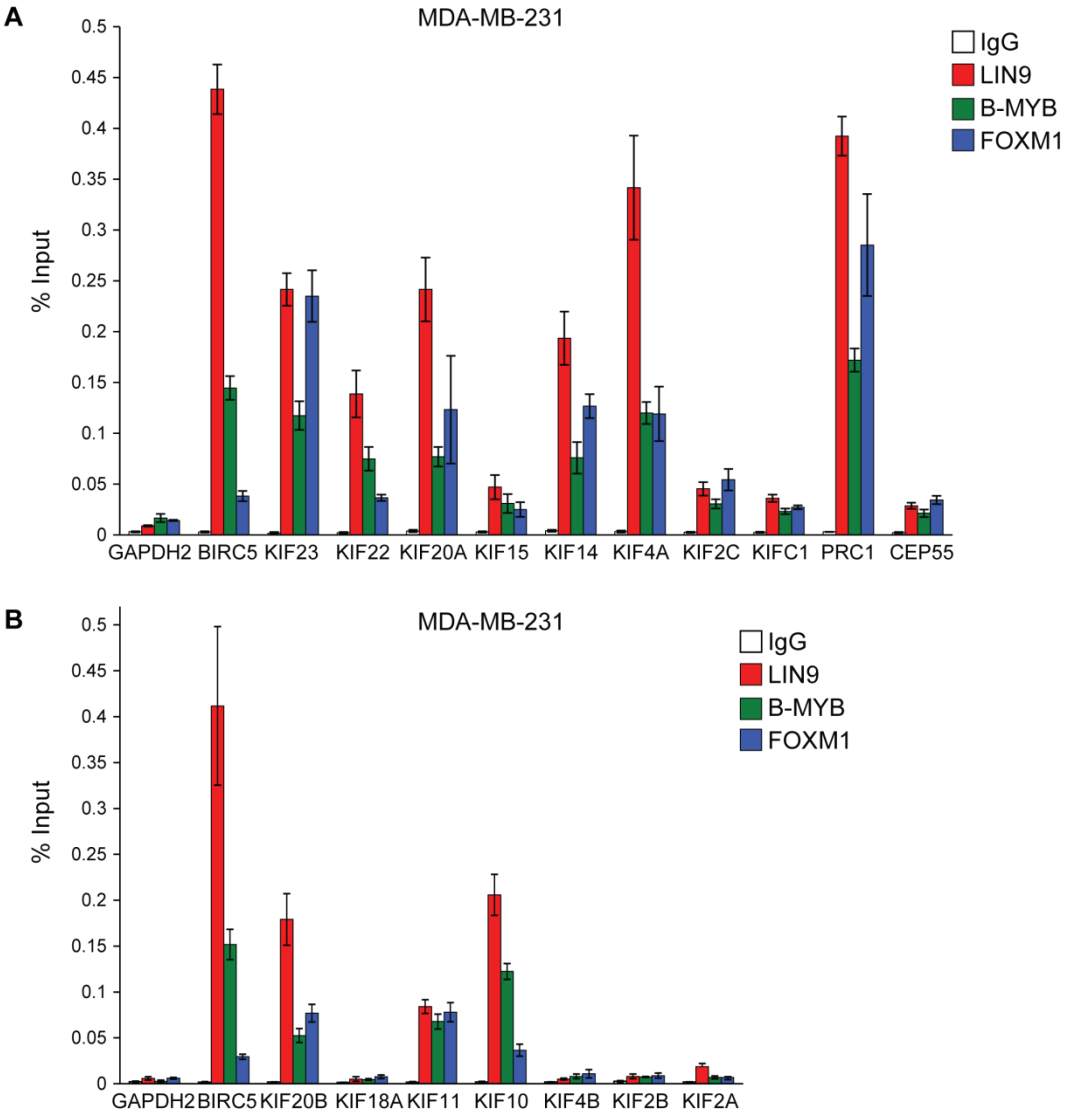

Figure 26: The DREAM complex binds to the promoter of mitotic kinesins, PRC1, and CEP55 in MDA-MB-231 cells.
(**A**-**B**) In the MDA-MB-231 breast cancer cell line chromatin was immunoprecipitated using antibodies directed against LIN9, B-MYB, and FOXM1. Unspecific IgG was used as control. ChIP-qPCR analysis was performed using mitotic kinesin, *PRC1,* and *CEP55* promoter-specific primer with *GAPDH2* and *BIRC5* promoter-specific primer as respective negative and positive control. The ChIP-qPCR analysis shows enrichment of DREAM subunits for multiple mitotic kinesin promoters and for *PRC1*, *CEP55,* and *BIRC5* promoter normalized to 1% input. The error bars of the representative experiment were calculated of triplicates according to 4.2.2.3.

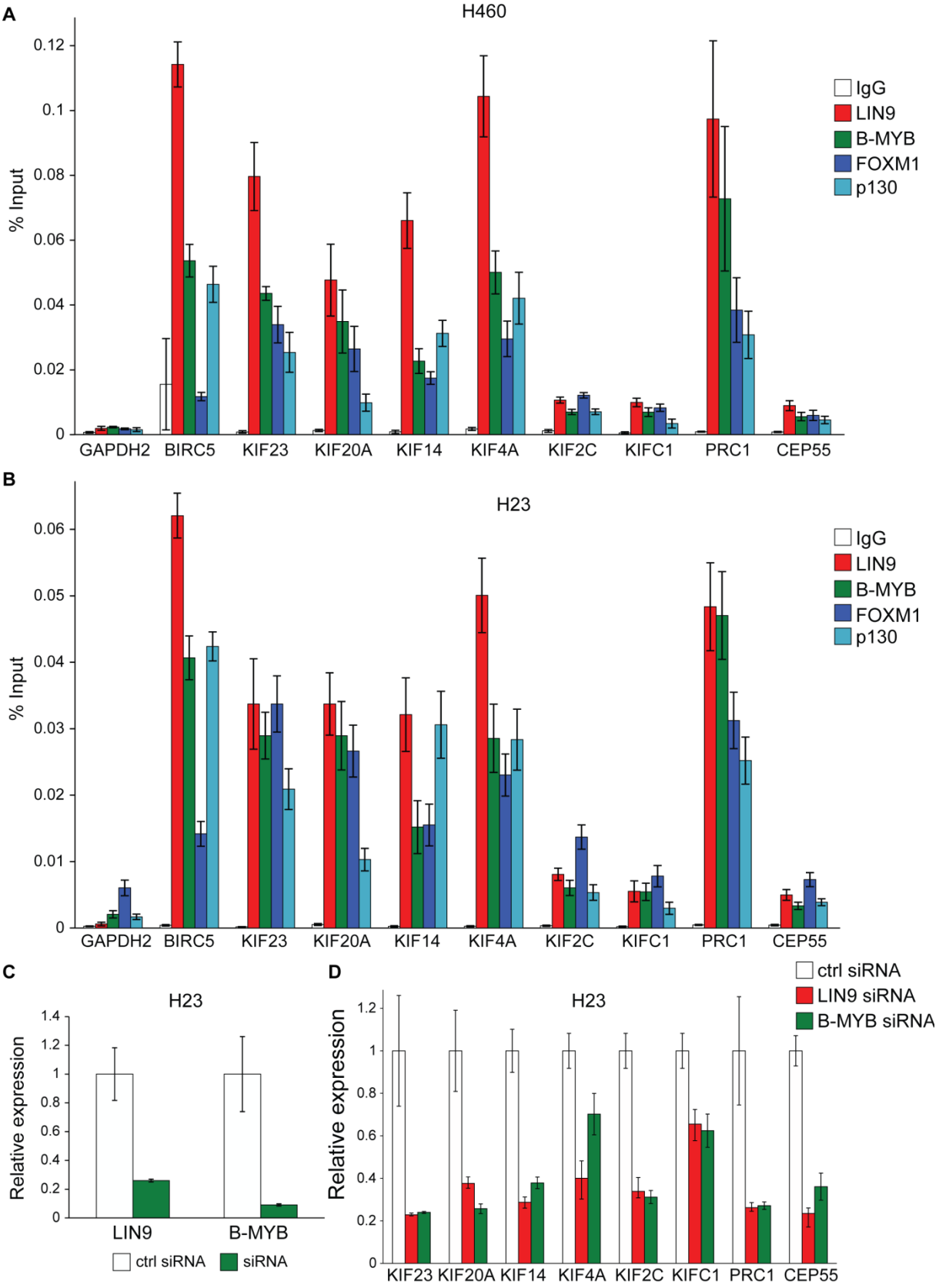
A
H460
% Input
0.12
0.1
0.08
0.06
0.04
0.02
0
IgG
LIN9
B-MYB
FOXM1
p130
GAPDH2
BIRC5
KIF23
KIF20A
KIF14
KIF4A
KIF2C
KIFC1
PRC1
CEP55
B
H23
% Input
0.06
0.05
0.04
0.03
0.02
0.01
0
IgG
LIN9
B-MYB
FOXM1
p130
GAPDH2
BIRC5
KIF23
KIF20A
KIF14
KIF4A
KIF2C
KIFC1
PRC1
CEP55
C
H23
Relative expression
1.4
1.2
1
0.8
0.6
0.4
0.2
0
LIN9
B-MYB
ctrl siRNA
siRNA
D
H23
Relative expression
1.2
1
0.8
0.6
0.4
0.2
0
ctrl siRNA
LIN9 siRNA
B-MYB siRNA
KIF23
KIF20A
KIF14
KIF4A
KIF2C
KIFC1
PRC1
CEP55

Figure 27: The DREAM complex binds to the promoter of mitotic kinesins and cytokinesis MAPs in lung cancer cell lines and has an influence on their transcriptional activity.
(**A**-**B**) In the lung cancer cell lines H460 and H23 chromatin was immunoprecipitated using antibodies directed against LIN9, p130, B-MYB and FOXM1. Nonspecific IgG was used as control. ChIP-qPCR analysis was performed using mitotic kinesin, *PRC1*, *CEP55,* and *GAS2L3* promoter-specific primer with *GAPDH2* and *BIRC5* promoter-specific primer as respective negative and positive control. The ChIP-qPCR analysis shows enrichment in H460 (**A**) and H23 (**B**) cells for the mitotic kinesins, *PRC1*, *CEP55*, *GAS2L3,* and *BIRC5* promoter normalized to 1% input. (**C**) Gene expression analysis was performed after depletion of DREAM complex subunits by RNAi for 48 h in H23 cells. RNA was isolated and depletion of DREAM complex subunits was verified by RT-qPCR (**C1**). Mitotic kinesin, *PRC1*, *CEP55,* and *GAS2L3* gene expression was analyzed by RT-qPCR (**C2**). The housekeeping gene *GAPDH* was used for normalization. The error bars of the representative experiment were calculated of triplicates according to 4.2.2.3.The result of *GAS2L3* is shown in Figure 10.

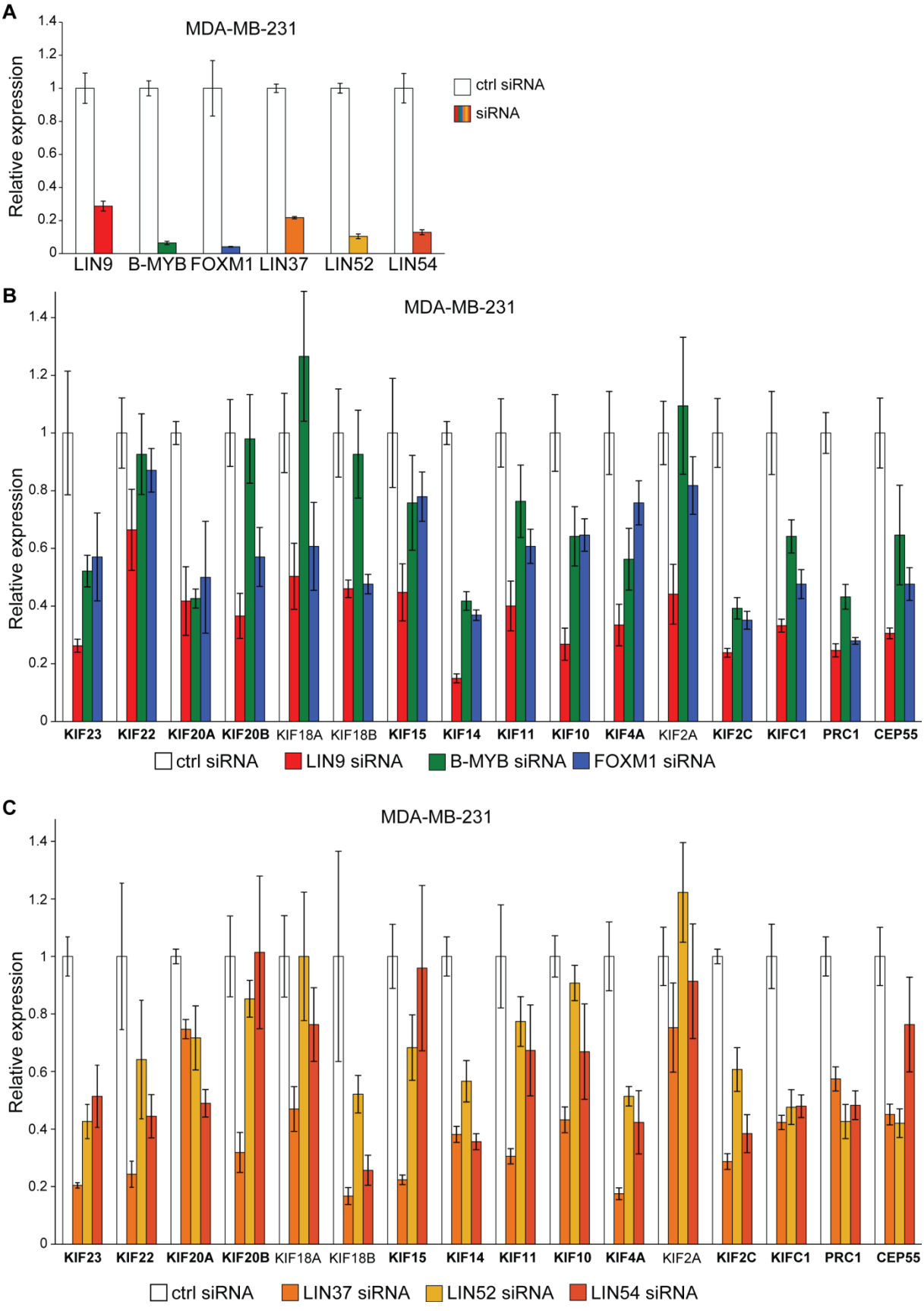
A
MDA-MB-231
Relative expression
ctrl siRNA
siRNA
LIN9
B-MYB
FOXM1
LIN37
LIN52
LIN54
B
MDA-MB-231
Relative expression
KIF23
KIF22
KIF20A
KIF20B
KIF18A
KIF18B
KIF15
KIF14
KIF11
KIF10
KIF4A
KIF2A
KIF2C
KIFC1
PRC1
CEP55
ctrl siRNA
LIN9 siRNA
B-MYB siRNA
FOXM1 siRNA
C
MDA-MB-231
Relative expression
ctrl siRNA
LIN37 siRNA
LIN52 siRNA
LIN54 siRNA

Figure 28: Depletion of DREAM complex subunits lead to down-regulation of mitotic kinesins, PRC1, and CEP55 in MDA-MB-231 cells.
Gene expression analysis was performed in two independent experiments after depletion of DREAM complex subunits by RNAi for 48 h in MDA-MB-231 breast cancer cells. RNA was isolated and depletion of DREAM complex subunits was verified by RT-qPCR (**A1**, **B1**). Mitotic kinesin, *PRC1,* and *CEP55* gene expression was analyzed by RT-qPCR (**A2**, **B2**). The housekeeping gene *GAPDH* was used for normalization. The error bars of the representative experiment were calculated of triplicates according to 4.2.2.3. Genes in bold print indicate DREAM complex promoter binding analyzed in Figure 26.

5.6 Mitotic kinesins are often coordinately up-regulated in human breast and lung cancer cell lines without necessarily correlating with B-MYB up-regulation and p53 status.

In order to investigate the impact of p53 depletion on B-MYB and mitotic kinesin expression in a more unbiased way, I stably infected the immortalized primary BJ-ET skin fibroblast cell line with a retrovirus containing a vector with a shRNA directed against p53 or an empty vector. Then I compared the effects on cell cycle progression and on B-MYB, KIF4A, and KIF20A level before and after DNA damage (Figure 29 A, B, C). To verify p53 depletion, DNA damage was induced by the chemotherapeutic drug doxorubicin and activation of the downstream target gene p21 was analyzed by immunoblotting (Figure 29 C). p21 was only induced in BJ-ET fibroblasts containing the empty vector but not in cells containing the shRNA directed against p53 indicating an efficient disruption of the p53 response by the shRNA. In parallel, I observed that B-MYB and KIF4A level were strongly reduced in control cells, whereas B-MYB and KIF4A level accumulated after DNA damage in p53-depleted cells (Figure 29 C). This observation is in line with ChIP results demonstrating that the DREAM complex does not switch to its repressive form in p53-negative cells (Mannefeld et al., 2009). In this context, the same effect was described for the mitotic kinesin KIF23 (Fischer et al., 2013).
In conclusion, loss of p53 leads to a different response of B-MYB and mitotic kinesin protein levels after induction of DNA damage.
Cell cycle distribution analyzed by FACS demonstrated a reduced fraction of cells in G1 and a higher fraction of G2/M cells in p53 depleted cells (Figure 29A). B-MYB, KIF4A and KIF20A protein levels were increased in p53 depleted cells (Figure 29 B). These results demonstrate that p53 depletion affects B-MYB and mitotic kinesin level and influences the cell cycle.

Single mitotic kinesins were reported to be de-regulated and often up-regulated in several types of cancer (Rath and Kozielski, 2012). Whether mitotic kinesins, cytokinesis MAPs, and B-MYB are rather coordinately up-regulated in tumours is not investigated in detail. To address the question, I analyzed a panel of breast cancer cell lines (MCF7, T-47D, BT-20, BT-549, Hs 578T, MDA-MB-468, and MDA-MB-231) by immunoblotting and comparison of the levels of B-MYB, PRC1, and 6 mitotic kinesins (KIF23, KIF20A, KIF14, KIF4A, KIF2C, and KIFC1) using MCF 10A mammary gland epithelial cells as non-transformed control cell line (Figure 30). B-MYB, KIF23, KIF20A, KIF4A, KIFC1, and PRC1 levels were elevated in all breast cancer cell lines compared to the control cell line. KIF14 levels were elevated in all cancer cell lines except for Hs 578T cells and KIF2C level were elevated in all cancer cell lines except for MCF7, T 47D and Hs 578T cells. Interestingly, although MCF7 was the only cancer cell line in the panel with a p53 wt status, B-MYB, PRC1, and the mitotic kinesin levels of KIF23, KIF20A, KIF14A, KIF4A, and KIFC1 were also elevated similar to the cancer cell lines with p53 mutation.

Next, a similar analysis using a panel of lung cancer cell lines (H226, A549, H460, H522, HOP-92, HOP-62, H358, and H441) was performed (Figure 30). WI-38 lung fibroblasts served as a non-transformed control cell line (Figure 31). All lung cancer cell lines exhibited elevated B-MYB and KIF23 levels in contrast to the control cell line. KIF20A, KIF14, KIF4A, KIF2C, and PRC1 levels were elevated in the lung cancer cell lines with p53 mutation, whereas in the p53 wt tumour cell lines (A549 and H460) protein levels were comparable to WI-38 lung fibroblasts. KIFC1 levels were only elevated in p53 mutated lung cancer cell lines except for H226 cells.

In summary, all analyzed cancer cell lines showed elevated B-MYB levels compared to the control cell lines. High B-MYB levels did not correlate with the p53 status of the cell lines. In almost all cancer cell lines mitotic kinesins and PRC1 protein levels were elevated, except for A549 and H460 cells. Thus, with few exceptions, mitotic kinesins are coordinately up-regulated in cancer cell lines but this up-regulation does not necessarily correlate with the p53 status.

In order to investigate whether mRNA expression levels of *B-MYB*, mitotic kinesins, *PRC1,* and *CEP55* are also up-regulated in cancer cell lines, I analyzed samples of WI-38 (p53 wt), H460 (p53 wt) and H23 (p53 mut) cells. BY FACS, I showed that the cell lines had a similar distribution for the different cell cycle stages, demonstrating that the observations are unlikely to be influenced by the cell cycle (Figure 32 A). The

gene expression analysis by RT-qPCR of *B-MYB*, mitotic kinesins, *PRC1*, and *CEP55* revealed that the analyzed genes were moderately increased in H460 cells and strongly increased in H23 cells compared to the control cell line (Figure 32 B). This result is in line with the elevated protein levels (Figure 31), indicating a coordinated up-regulation of mitotic kinesins and cytokinesis MAPs on the transcriptional level in cancer cells.

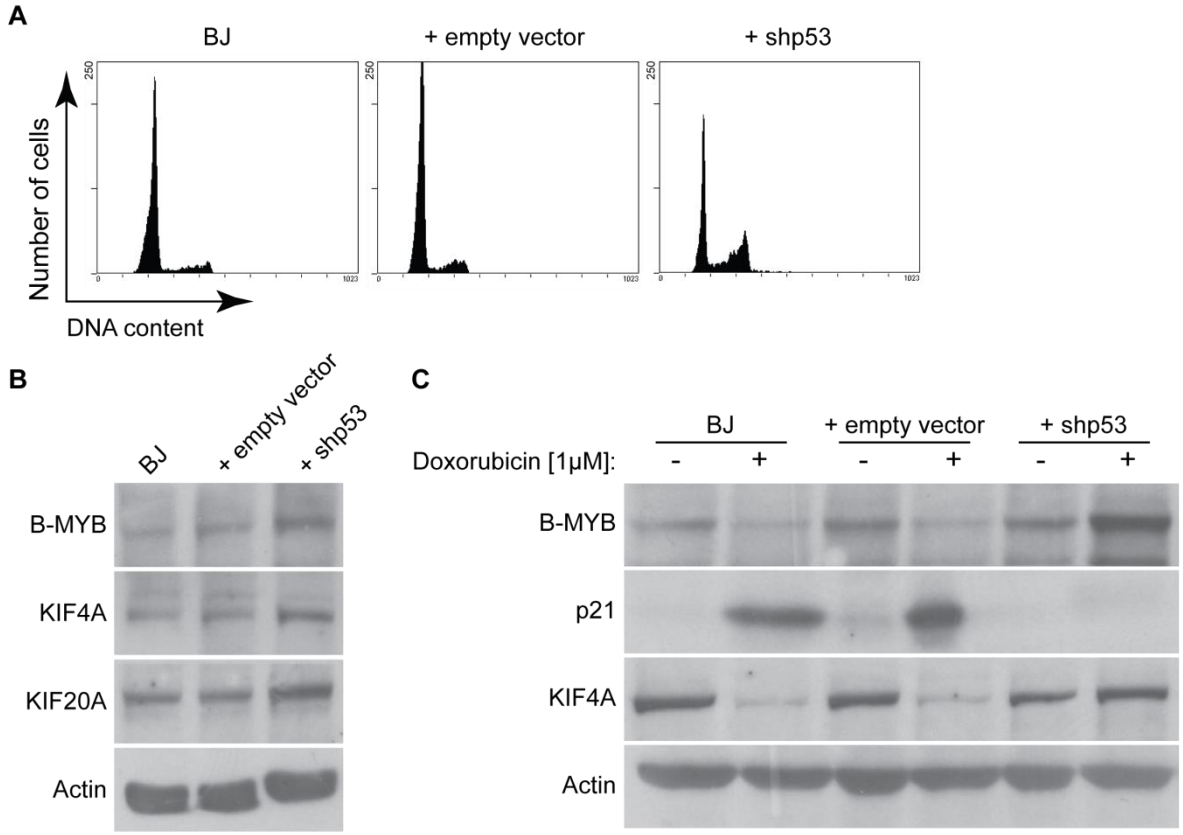

Figure 29: Depletion of p53 and DNA damage affects B-MYB and mitotic kinesin levels in BJ skin fibroblasts.
BJ-ET skin fibroblasts were stably infected by a shRNA directed against p53 and were analyzed for changes in the cell cycle profile by FACS with propidium iodide (**A**) and in parallel for B-MYB and mitotic kinesin levels by immunoblotting (**B**). (**C**) BJ skin fibroblasts were treated with 1 µM of doxorubicin for 1 h. 24 h later the BJ-ET cells were analyzed for B-MYB and KIF4A expression by immunoblotting.

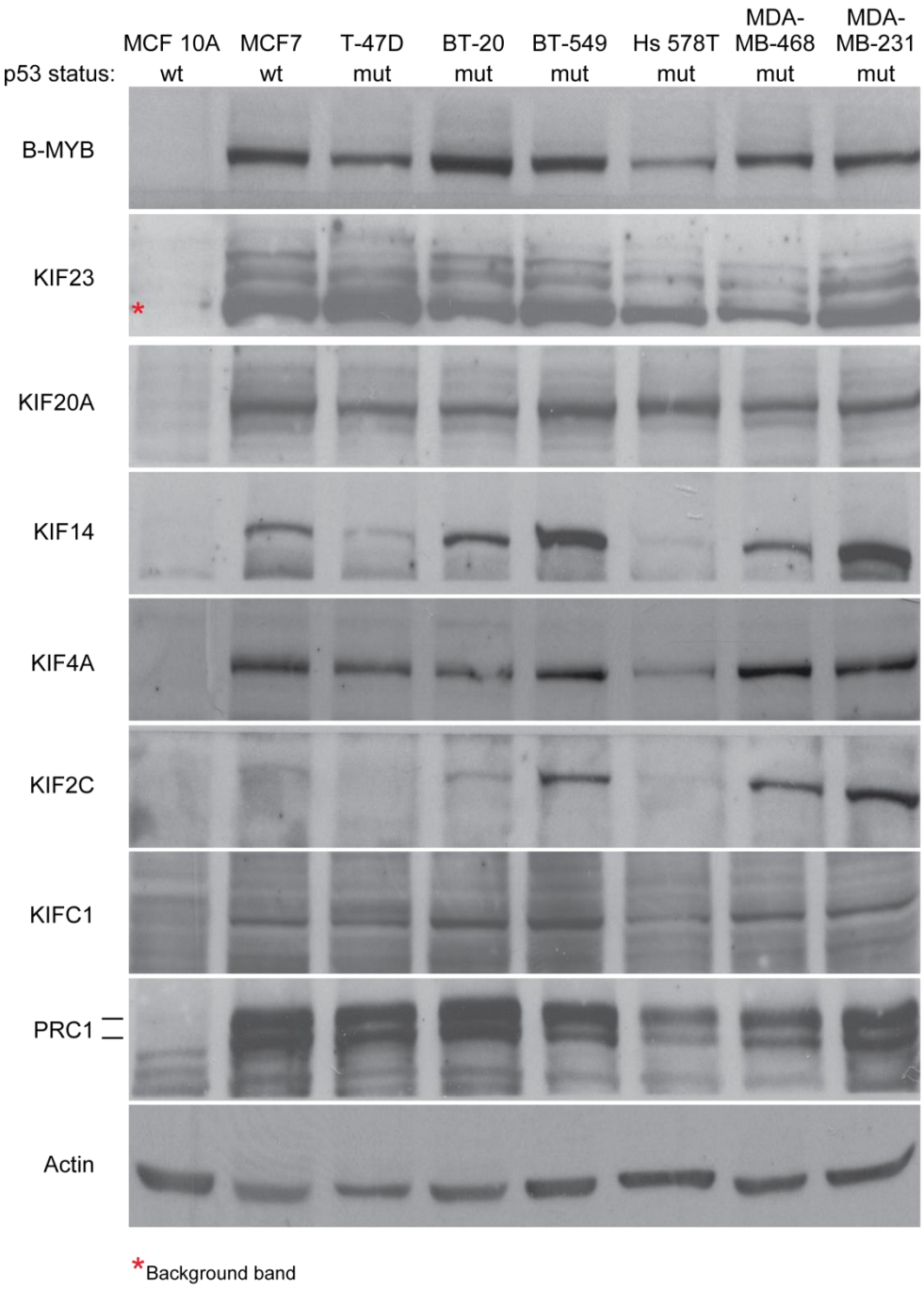

Figure 30: Mitotic kinesins, PRC1, and B-MYB are frequently up-regulated in a panel of breast cancer cell lines.
A panel of breast cancer cell lines was cultured for 48 h, lysed and immunoblotted. Actin was used as loading control and is representative for different immunoblots from the same lysates. MCF 10A mammary gland epithelial cells were used as non-transformed control cell line.

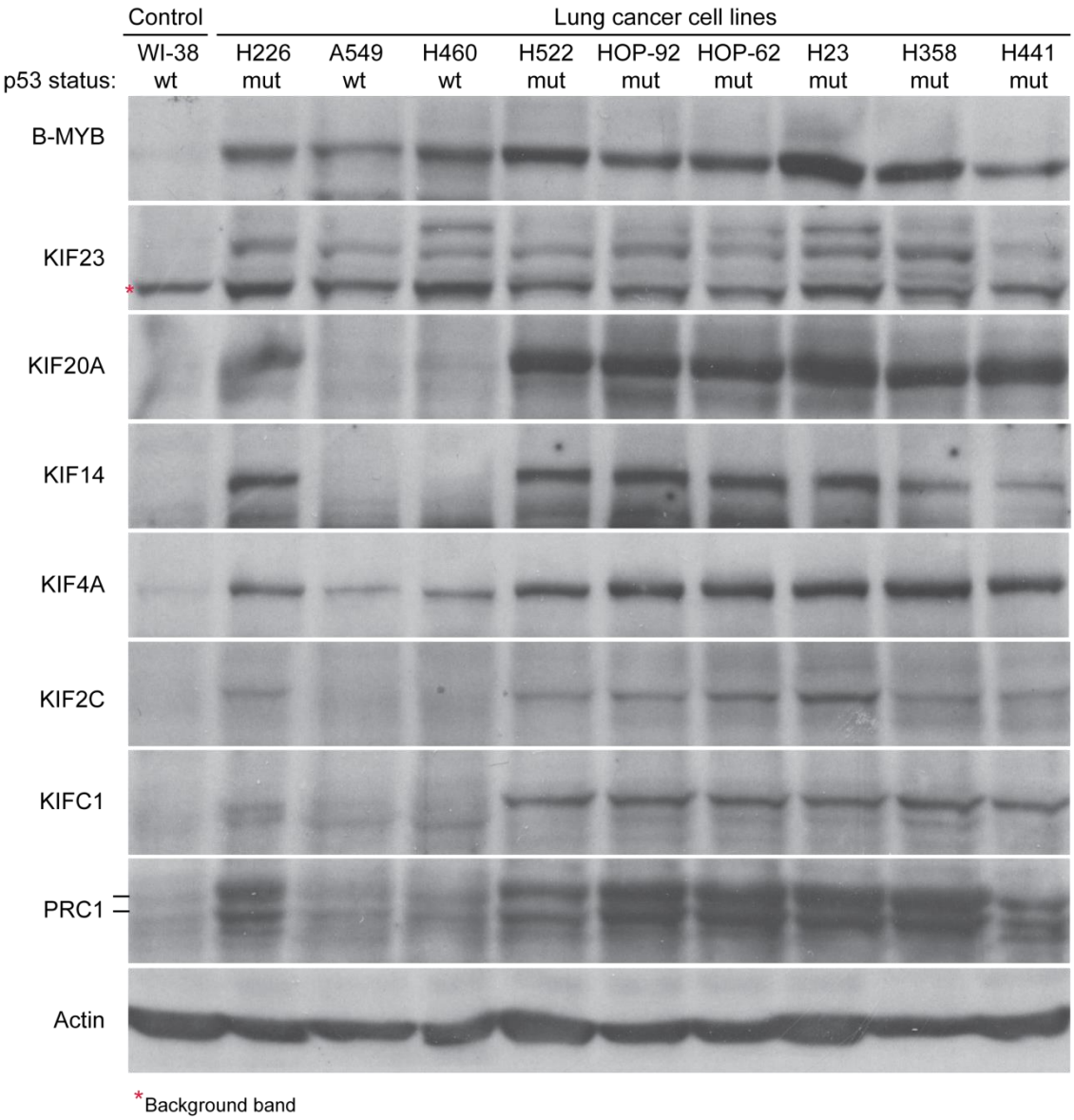

Figure 31: Mitotic kinesins, PRC1, and B-MYB are frequently up-regulated in a panel of lung cancer cell lines.
A lung cancer panel was cultured for 48 h, lysed and immunoblotted. Actin was used as loading control and is representative for different immunoblots from the same lysates. WI-38 lung fibroblasts were used as non-transformed control cell line.

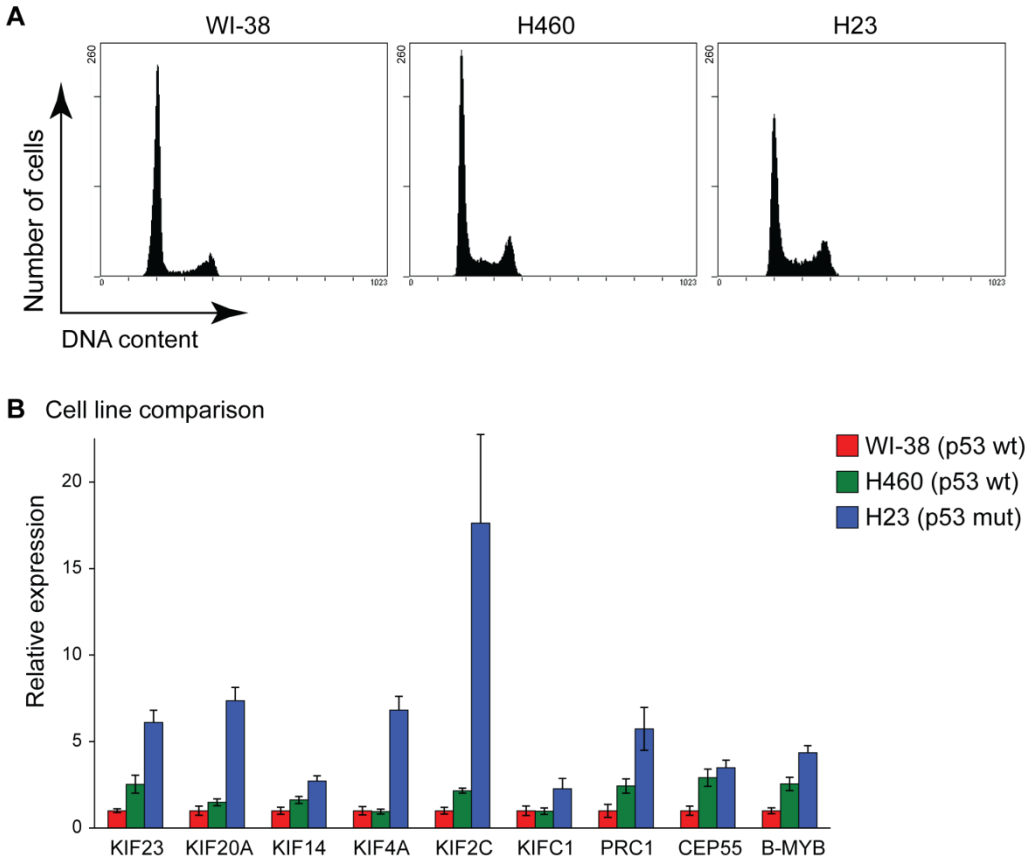

Figure 32: Transcriptional up-regulation of mitotic kinesins, *PRC1*, *CEP55*, and *B-MYB* can correlate with elevated protein level in lung cancer cell lines.
The p53 wild type (wt) lung cancer cell line H460 and the p53 mutant (mut) lung cancer cell line H23 were cultured for 48 h in parallel to the protein sample of Figure 31. (**A**) FACS analysis was performed using propidium iodide to compare cell cycle profiles. (**B**) The RNA was isolated and gene expression was analyzed by RT-qPCR using the ribosomal *RPS14* gene for expression normalization. WI-38 lung fibroblasts were used as non-transformed control cell line. The error bars of the representative experiment were calculated of triplicates according to 4.2.2.3.

5.7 A system to evaluate mitotic kinesins and cytokinesis genes as anti-cancer targets

Anti-mitotic drugs are getting more and more into focus as possible cancer therapeutics (Chan et al., 2012; J.kallio, 2013; Janssen and Medema, 2011). These drugs can inhibit cell proliferation by preventing correct chromosome segregation in mitosis and interfere with cytokinesis. The majority of the available inhibitors induce a prolonged mitotic arrest through activation of the spindle assembly checkpoint (SAC) or they induce multipolar spindles. Both effects can finally trigger mitotic cell death. The current drugs often attack microtubule filaments and thereby show side effects, such as neuropathy. Furthermore, cancer cells can evade mitotic cell death and

subsequently develop resistance against the drugs. Thus, there is a need to identify new mitotic targets. Proteins involved in cytokinesis are possible novel anti-cancer targets and have not been extensively studied yet.

In order to begin to investigate this idea, I focused on mitotic kinesins involved in cytokinesis. The kinesin-specific motor domains are attractive drug targets and as demonstrated mitotic kinesins are often up-regulated in cancer cell lines (see 5.6), indicating cancer related functions and a potential weak point in cancer cells.

To investigate the dependence of cancer cells on mitotic kinesins and two selected MAPs involved in cytokinesis, I used a lentiviral-based system to transduce inducible shRNAs, which deplete protein levels by RNA interference, into the breast cancer cell line MDA-MB-231 (Meerbrey et al., 2011).

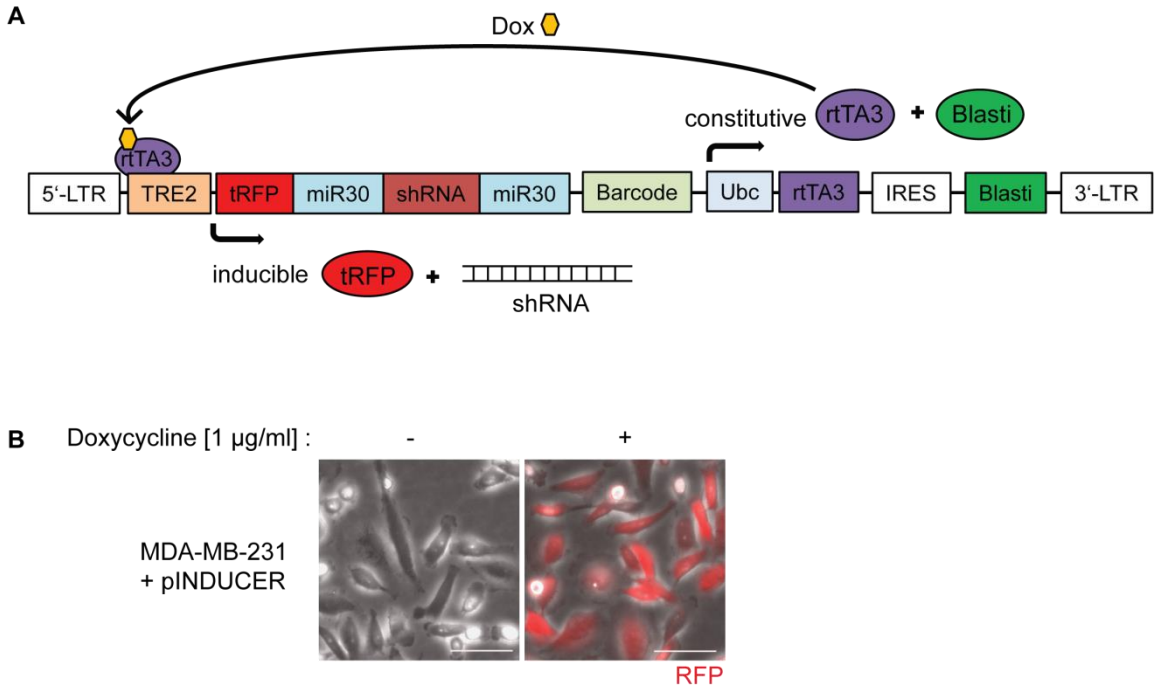

Figure 33: The lentiviral pINDUCER system.
The lentiviral-based pINDUCER system comprises a series of vector backbones designed for stable integration of inducible mIR30-based shRNAs or genes of interest with the intention to control their expression in a time- and dose-dependent manner *in vivo* and *in vitro* (Meerbrey et al., 2011). The pINDUCER10 vector used in this study is illustrated here. (**A**) The vector backbone is equipped with a selection cassette against the antibiotic blasticidin to ensure stable integration (puromycin was replaced by blasticidin in our laboratory). In addition, a reverse tetracycline transactivator (rtTA3) is permanently expressed which can bind to a tetracycline response element (TRE2) upon addition of tetracycline derivates to induce the expression of shRNAs of interest together with the turbo red fluorescent protein (tRFP). (**B**) Subsequently, integration and expression level can be monitored under the microscope and by other methods.
(A) Modified picture from Meerbrey et al. (2011)

Descriptive analysis of single mitotic kinesins, microarray analysis in the Oncomine cancer database and my own experiments (Figure 30) suggest high mRNA and protein levels in MDA-MB-231 breast cancer cells, making the cell line a good test candidate (Shimo et al., 2007; Singel et al., 2013).

First, several shRNAs against the mitotic kinesins KIF23, KIF20A, KIF14, KIF4A, KIF2C, KIFC1, and the two MAPs involved in cytokinesis PRC1 and CEP55 were designed according to Dow et al. (2012) and cloned into the lentiviral pINDUCER vector. Lentiviral supernatants were used to transduce MDA-MB-231 cells by pINDUCER-shRNAs and the cells were subsequently selected for lentiviral integration by blasticidin. The shRNA knockdown efficiency was tested 48 h after induction by 1 µg/ml of doxycycline by immunoblotting.

I was able to identify a set of shRNAs for each target with an adequate knockdown efficiency depicted in Figure 34 C. A compilation of all tested shRNA sequences and their knockdown efficiency on protein level is shown in Figure 40 and listed in Table 2 in the Appendix. The knockdown validation for the most effective shRNAs is shown in Figure 34 A, B. These shRNAs showed an effective knockdown on protein level. B-MYB levels and the levels of the other mitotic kinesins served as controls. The levels of these proteins were similar to each other, suggesting no off-target effects on other mitotic kinesins and no indirect effects due to alterations in the cell cycle.

In addition to MDA-MB-231 cells, lung cancer cell lines (H460, H23) stably transduced by pINDUCER-shRNAs for the inducible knockdown of mitotic kinesins and cytokinesis MAPs were generated. Induction of the shRNAs for 48 h led to an effective knockdown of every target protein (Figure 35 A, B).

Subsequently, I tested whether the shRNAs directed against KIF23 and PRC1 can induce cytokinesis failure in the three cancer cell lines. I analyzed the cell lines 72 h after treatment with or without 1 µg/ml of doxycycline for development of bi- and multi-nucleated cells (Figure 36 A). In every cell line a population of multinucleated cells emerged. This effect was quantified in Figure 36 B, demonstrating that depletion of KIF23 and PRC1 mediated by the shRNAs interferes with proper cytokinesis.

In order to explore the therapeutic potential of the 6 mitotic kinesins, PRC1, and CEP55 depletion in breast and lung cancer cells, MDA-MB-231 cells transduced by pINDUCER-shRNAs were seeded in low density and treated for 10 days with or without 1 µg/ml of doxycycline (Figure 37). Crystal violet staining revealed that cell proliferation was strongly impaired by shRNAs compared to the empty vector control

and untreated cells. The strongest proliferation effects were visible in cells with KIF23 or PRC1 depletion.

Similarly, H23 and H460 cells also showed an impaired proliferation after mitotic kinesin, PRC1, and CEP55 depletion compared to the empty vector control and the untreated cells (Figure 38 A1, B1). The effects were quantified in Figure 38 A2, B2. The strongest impairment was visible after KIF23, PRC1, and CEP55 depletion.

In summary, a lentiviral-based vector system which allows the effective down-regulation of mitotic kinesins and cytokinesis MAPs was established. The initial analysis indicated that mitotic kinesins and the MAPs PRC1 and CEP55 are promising candidates as mitotic anti-cancer targets in breast and lung cancer cells.

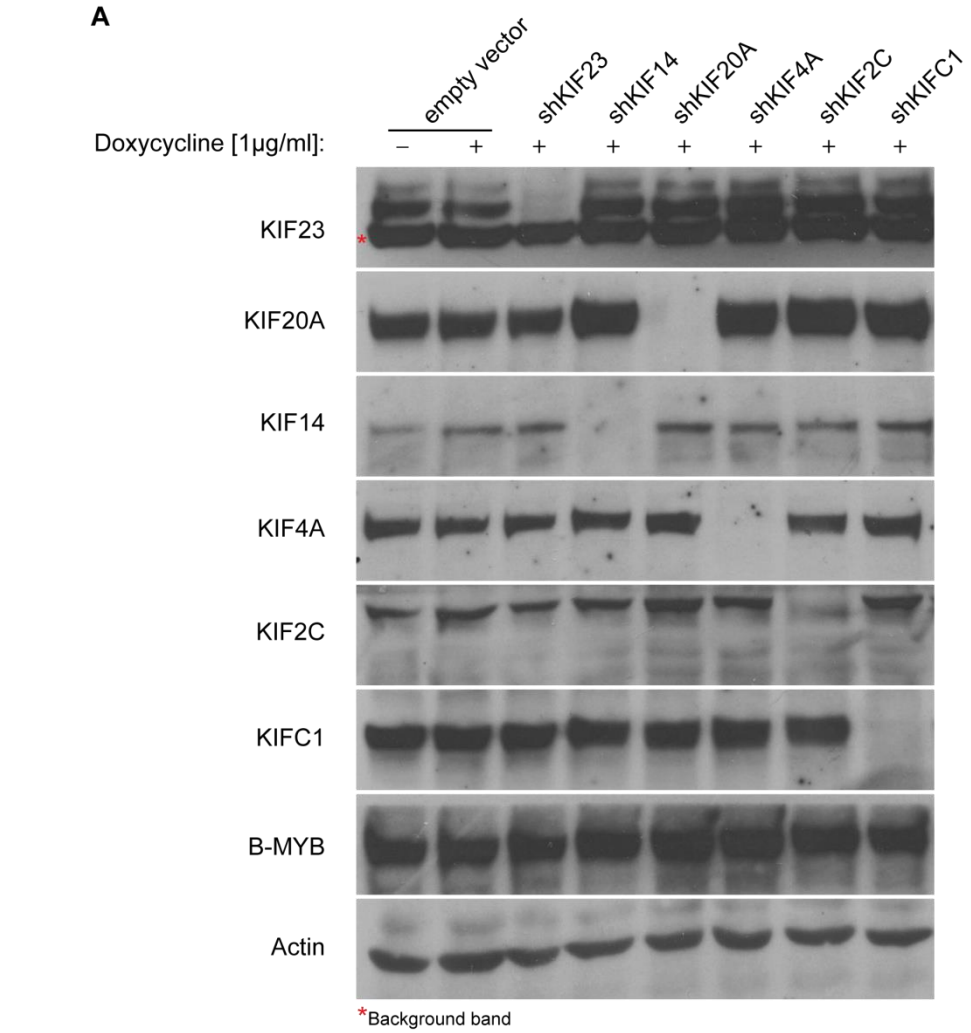

C

Gene	Number of shRNAs
KIF23	2
KIF20A	7
KIF14	3
KIF4A	5
KIF2C	1
KIFC1	3
PRC1	3
CEP55	10

Figure 34: Mitotic kinesin, PRC1, and CEP55 knockdown validation in the breast cancer cell line MDA-MB-231.
MDA-MB-231 cells stably transduced by inducible pINDUCER-shRNAs against mitotic kinesins, PRC1, and CEP55 were treated for 48 h with or without 1 µg/ml of doxycycline to induce shRNA mediated protein depletion. (**A**-**B**) The cells were lysed and mitotic kinesin, PRC1, and CEP55 depletion was validated by immunoblotting using the empty vector as control and B-MYB as cell cycle control (**C**) Summary of validated shRNAs. (The sequences are provided in Table 2 in the Appendix).

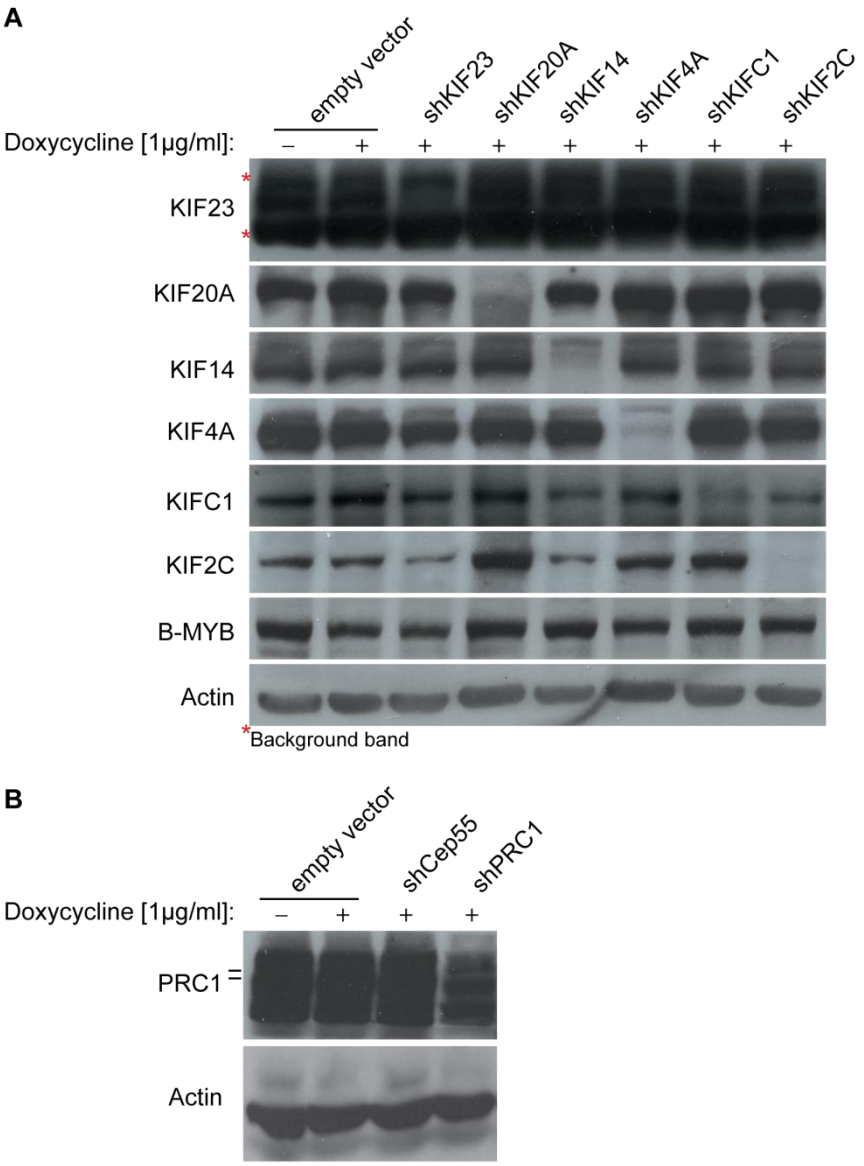

Figure 35: Mitotic kinesin and PRC1 knockdown validation in the lung cancer cell line H23.
H23 cells stably transduced by inducible pINDUCER-shRNAs against mitotic kinesins, PRC1, and CEP55 were treated for 48 h with or without 1 µg/ml of doxycycline to induce shRNA mediated protein depletion. (**A**-**B**) H23 cells were lysed and mitotic kinesin and PRC1 depletion was validated by immunoblotting using the empty vector as control and B-MYB as cell cycle control.

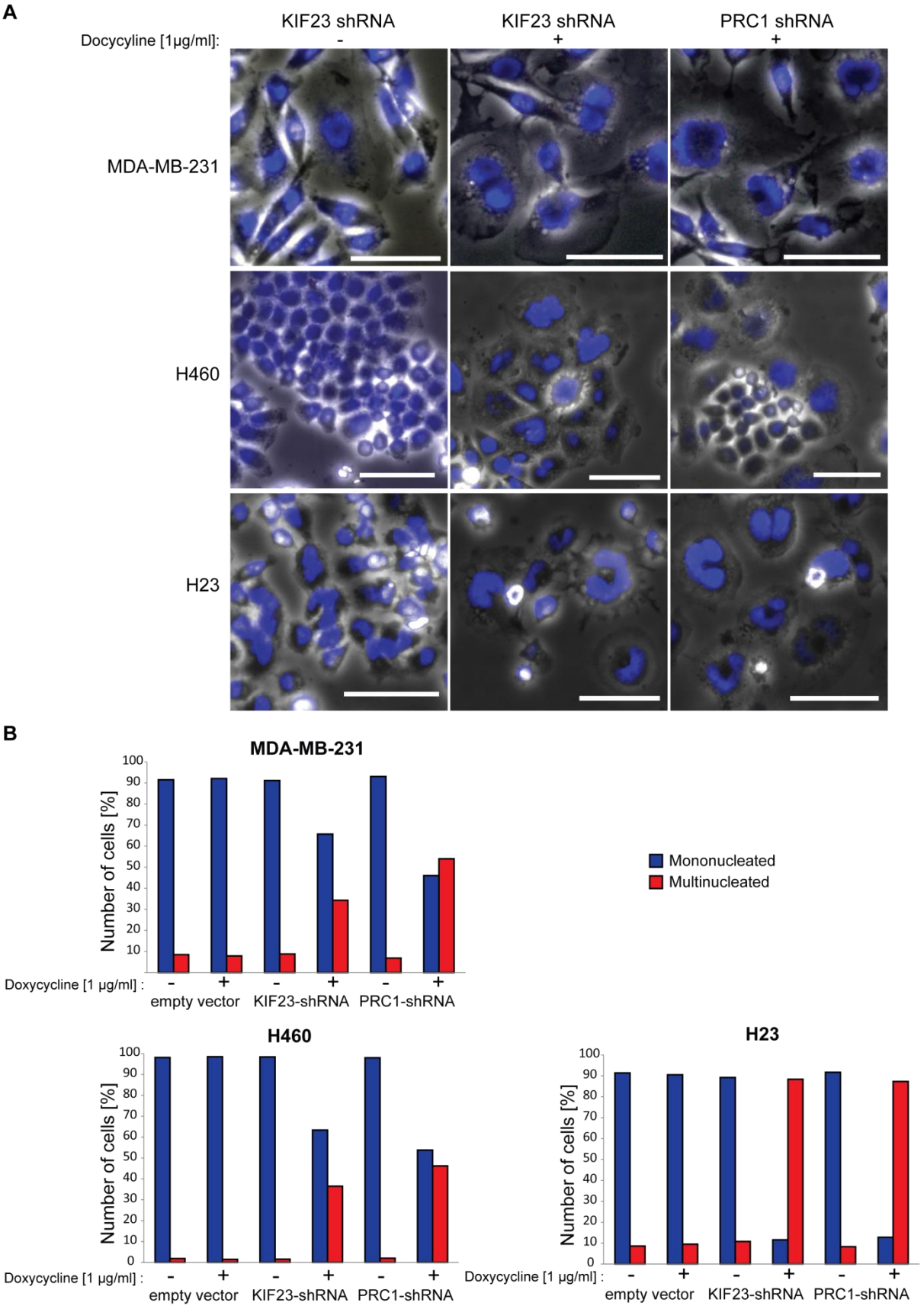
A
KIF23 shRNA
KIF23 shRNA
PRC1 shRNA
Docycyline [1µg/ml]:
-
+
+
MDA-MB-231
H460
H23
B
MDA-MB-231
Number of cells [%]
Mononucleated
Multinucleated
Doxycycline [1 µg/ml] :
empty vector
KIF23-shRNA
PRC1-shRNA
H460
H23

Figure 36: KIF23 and PRC1 depletion leads to cytokinesis failure in breast and lung cancer cell lines.
The breast cancer cell line MDA-MB-231 and the two lung cancer cell lines H460 and H23 were all stably transduced by the empty pINUCER vector or inducible pINDUCER-shRNAs against KIF23 and PRC1. The cell lines were treated with or without 1 µg/ml of doxycycline for 72 h to induce shRNA mediated protein depletion. Subsequently, the cells were fixed in PFA and stained with Hoechst 33342. (**A**) The cell lines were observed for bi- and multi-nucleated cells by a combination of phase contrast and immunofluorescence (blue) microscopy. Scale bars: 75 µm. (**B**) The effect was quantified (n>300 cells).

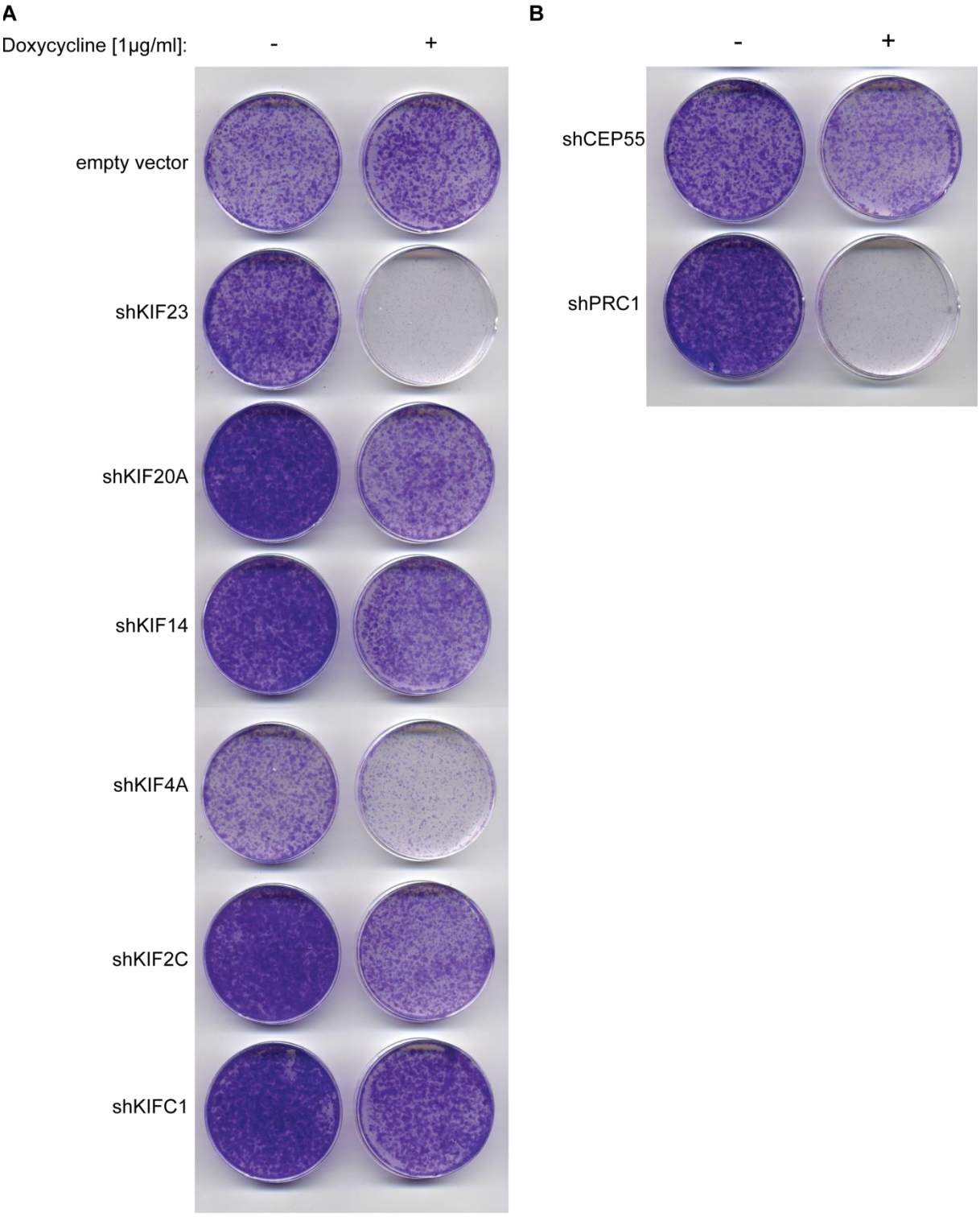

Figure 37: Mitotic kinesin, PRC1, and CEP55 depletion impairs proliferation of the breast cancer cell line MDA-MB-231.
MDA-MB-231 breast cancer cells stably transduced by inducible pINDUCER-shRNAs against mitotic kinesins, PRC1, and CEP55 were seeded in low density and treated for 10 days with 1 µg/ml of doxycycline to induce shRNA mediated protein depletion. The cells were fixed in PFA and stained with crystal violet.

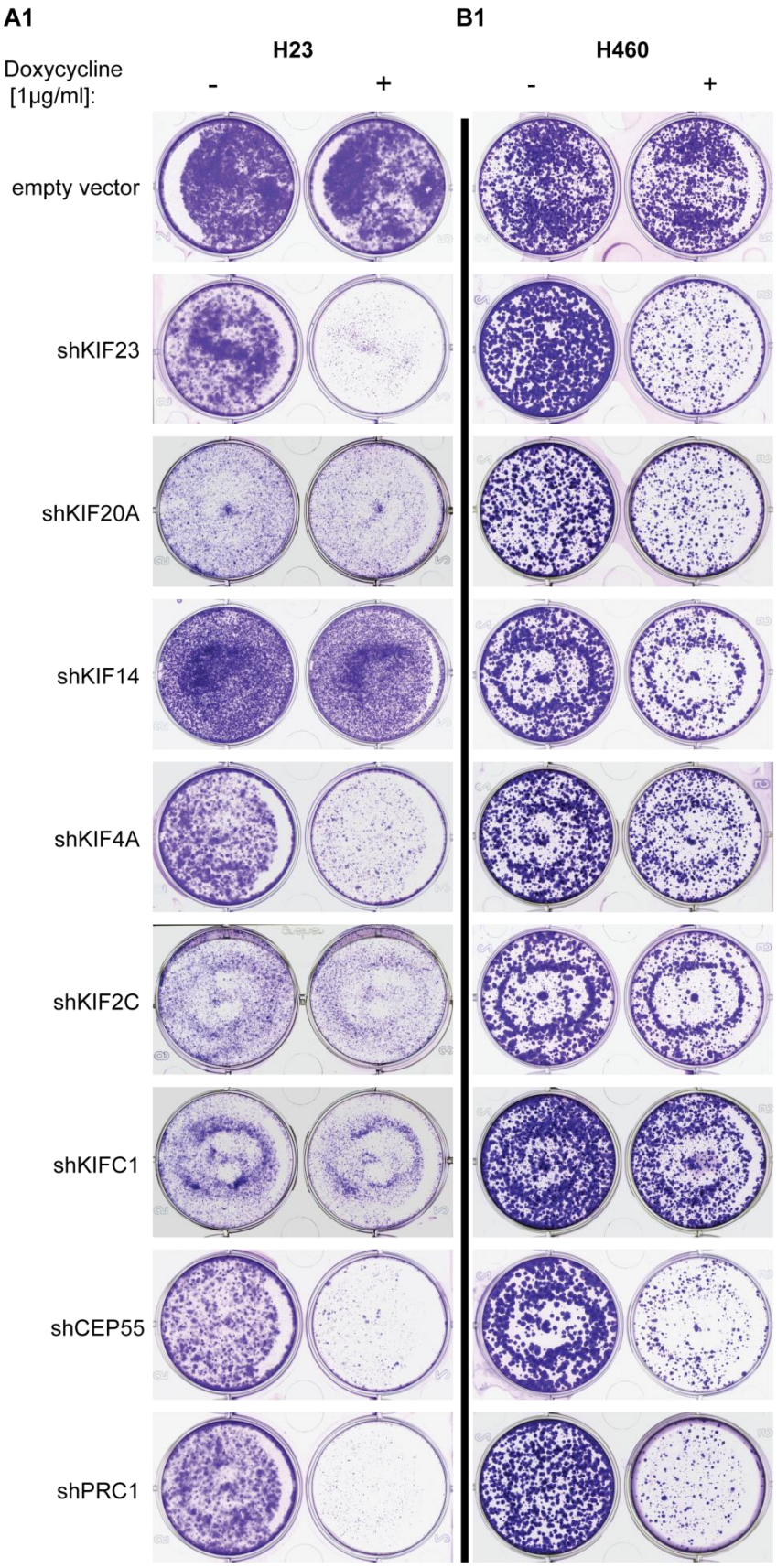
A1
B1
H23
H460
Doxycycline [1µg/ml]:
-
+
-
+
empty vector
shKIF23
shKIF20A
shKIF14
shKIF4A
shKIF2C
shKIFC1
shCEP55
shPRC1

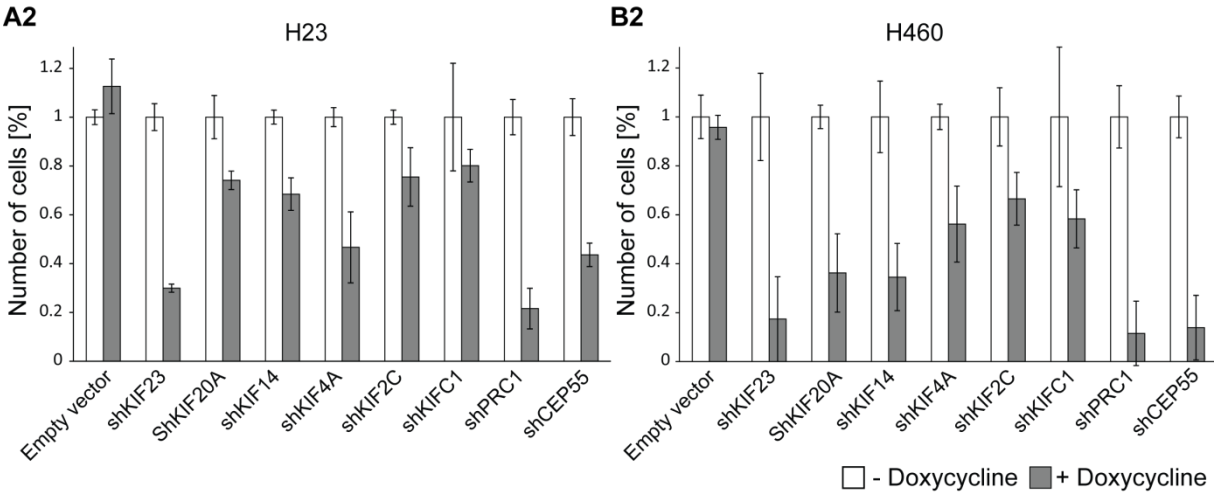

Figure 38: Mitotic kinesin, PRC1, and CEP55 depletion impairs proliferation of the lung cancer cell lines H23 and H460.
(**A**-**B**)The lung cancer cell lines H23 and H460 stably transduced by inducible pINDUCER-shRNAs against mitotic kinesins, PRC1 and CEP55 were seeded as triplicates in low density and treated for 7 days without doxycycline (white) or with 1 µg/ml of doxycycline (grey) to induce shRNA mediated protein depletion. The cells were fixed in PFA and stained with crystal violet. The graphic shows example wells of the triplicates (**A1**, **B1**). Cell proliferation was analyzed by photometric quantification of the eluted crystal violet (**A2, B2**). The error bars represent the normalized standard deviations of triplicates.

6 DISCUSSION

In the first part of the study I characterized the microtubule and F-actin cross-linking protein GAS2L3, its regulation by the DREAM complex and its involvement in mitosis and cytokinesis. I report that the repressive and the activating form of DREAM binds to the *GAS2L3* promoter. I demonstrate that GAS2L3 is required for cytokinesis. Furthermore, I provide evidence for the localization of GAS2L3 in mitosis at the mitotic spindle and in cytokinesis at the midbody. Finally, I demonstrate that the GAR domain of GAS2L3 is crucial for the localization of GAS2L3 to the constriction zone in the abscission process.

On the cellular level, GAS2L3 depletion by RNAi leads to an increase of multinucleated cells and cells with multi-lobed nuclei (Wolter et al., 2012). This phenotype is a typical of cells failing to perform proper cytokinesis. Time-lapse video microscopy showed that this phenotype is caused by abnormal contractions of the cell cortex and oscillations of the mitotic spindle and chromosomes in late anaphase. It starts precisely when the cleavage furrow starts to ingress. Then the entire mitotic spindle and the dividing chromosomes are rocking / oscillating back and forth between the evolving daughter cells. This continued until the cleavage furrow collapsed and finally regressed leading to multi-nucleated cells and multi-lobed nuclei. I also observed a strong correlation between the rocking spindle phenotype and increased membrane blebbing with huge blebs of the polar cortex. These blebs contained abnormal localized RhoA and myosin IIA.

Interestingly, the rocking spindle phenotype after GAS2L3 depletion is similar to phenotypes that were observed after depletion of other proteins involved in cytokinesis. For example, depletion of the cleavage furrow scaffold protein anillin, the actin polymerizing Formin mDia2, the cell cortex stabilizing protein Mip1, and the mitotic kinesins MCAK and HSET results in similar phenotypes (Cai et al., 2010; Mattison et al., 2011; Piekny and Glotzer, 2008; Rankin and Wordeman, 2010; Watanabe et al., 2008; Zhao and Fang, 2005a).

Thus, multiple mechanisms can be responsible for the rocking spindle phenotype. The two RhoA-pathway effector proteins anillin and mDia2 anchor the contractile ring to the cleavage furrow assuring spatial contractility at the equatorial cortex during

cleavage furrow ingression (Piekny and Glotzer, 2008; Watanabe et al., 2008; Watanabe et al., 2010; Zhao and Fang, 2005a). Mip1 is important for cell cortex stability by influencing the actin cytoskeleton (Mattison et al., 2011). The depolymerizing activity of the kinesin MCAK is important for the regulation of astral microtubule stability. Therefore, loss of MCAK activity leads to hyperstabilized astral microtubules (Rankin and Wordeman, 2010). The kinesin HSET participates in the organization of the spindle midzone thereby contributes to its stability (Cai et al., 2010). All reports have in common that the spindle rocking phenotype is accompanied by increased instability of the polar cortex leading to membrane blebbing.

An interesting candidate for further investigations is the actin-crosslinking protein α-actinin-1 which was identified by our group as a possible GAS2L3-binding partner (Fackler, 2014). The protein α-actinin-1 not only localizes to the spindle midzone but also to the cleavage furrow (Fujiwara et al., 1978). Furthermore, it participates in cleavage furrow positioning by influencing the integrity of the midzone spindle (Srinivas and Murata-Hori, 2012) and by actin remodeling of the cortical network (Mukhina et al., 2007).

The importance of the actin-rich polar cortex for cytokinesis is not well understood and the proteins involved in polar blebbing are largely unknown and under current investigation (Charras et al., 2006; Charras et al., 2008; Green et al., 2012; Salbreux et al., 2012; Sedzinski et al., 2011).

Therefore, it will be interesting to analyze how the downstream factors of GAS2L3, RhoA and myosin IIA influence the actin-rich polar cortex and the blebs.

This study shows for the first time the subcellular localization of GAS2L3. I found that GAS2L3 localizes along the complete mitotic spindle from prophase to telophase. After establishment of the midzone spindle GAS2L3 accumulates close to the spindle midzone center and localizes to the intercellular bridge adjacent to the midbody.

GAS2L3 accumulation close to the midzone center strongly correlates with the process of cleavage furrow ingression. First, the midzone spindle assembles and participates in the activation of the contractile ring (Glotzer, 2009; Mierzwa and Gerlich, 2014). Then, the subsequent force, generated by the contractile ring, drives the compaction of the midzone spindle. In this process, multiple microtubule motors and MAPs cooperate to assemble the spindle midzone. They are important for

spindle midzone integrity and communicate with the cell cortex and the contractile ring (Glotzer, 2009; Mierzwa and Gerlich, 2014). A crosstalk between microtubule and actin filaments is necessary, involving cytoskeleton cross-linking proteins like anillin, to guide the ingression and anchoring of the contractile ring to the intercellular bridge (Piekny and Maddox, 2010). Interestingly, GAS2L3 is able to bind actin filaments *in vitro* and is shown to co-localize with actin filaments in interphase cells *in vivo* (Stroud et al., 2011; Wolter et al., 2012). This and its midzone localization could be an indication for its involvement in the ingression and anchoring process of the contractile ring.

Closely linked is the open question how GAS2L3 is accumulating adjacent to the midzone center because GAS2L3 harbors no motor domain for directed movement along the midzone microtubules. One possible explanation could be an interaction with the mitotic kinesin-like protein 2 (MKLP2) and the chromosomal passenger complex (CPC). MKLP2 relocates the CPC from the centromere to the central spindle (Gruneberg et al., 2004). Our group showed that GAS2L3 interacts with the CPC *in vitro* (Fackler et al., 2014) but whether GAS2L3 interacts with MKLP2 has not been analyzed.

Interestingly, MKLP2 plays an important in targeting the CPC to the equatorial cortex and for maintenance of cleavage furrow ingression (Kitagawa et al., 2013).

It is not completely understood how the CPC signals from the mitotic spindle to the cell cortex in early cytokinesis. The current debate is whether the CPC travels along stabilized equatorial microtubules, diffuses with soluble factors or travels along actin cables to the cell cortex (Fededa and Gerlich, 2012; Green et al., 2012; Hu et al., 2008; Mierzwa and Gerlich, 2014). The ability of GAS2L3 to bind and cross-link actin and microtubule filaments together with its localization makes it an interesting candidate in this signaling process. GAS2L3 may support the CPC in traveling to the cortex and may assure proper CPC activity. However, the relocation of the CPC throughout mitosis is not affected by GAS2L3 depletion (unpublished data), suggesting a more subtle and dynamic mechanism.

Besides the discussed GAS2L3 localization, I additionally reported localization patterns at the intercellular bridge in late stages of cytokinesis. GAS2L3 co-localizes with spastin and CPC subunits at the constriction zone adjacent to the midbody as well as with the midbody ring and midbody remnants.

In late stages of cytokinesis, establishment of the intercellular bridge and assembly of the midbody lead to the disassembly of the contractile ring (Mierzwa and Gerlich, 2014). In late stages of cytokinesis, establishment of the intercellular bridge and assembly of the midbody lead to the disassembly of the contractile ring (Mierzwa and Gerlich, 2014). Subsequently, the ingressed cleavage furrow is mechanically anchored by, e.g., the midbody ring protein MKLP1 and other mechanisms involving MKLP1. These events lead to the relocation of a large number of proteins involved in cytokinesis and prepare the cell for abscission(Hu et al., 2012a). Interestingly, the pool of GAS2L3 at the mibody forms a ring-like structure and co-localizes with the midbody ring surrounding the midbody bulge. This localization persists into post abscission stages when the midbody remnant is engulfed into a cell (Crowell et al., 2014). Whether this pool of GAS2L3 is involved in the anchorage of the contractile ring or has some unknown function at the midbody has to be determined in the future.

In this study, I additionally confirmed that GAS2L3 co-localizes with the CPC and the microtubule-severing AAA-ATPase spastin adjacent to the midbody at the constriction zone as reported previously (Pe'er et al., 2013; Wolter et al., 2012). The constriction zone emerges shortly before abscission induced by cortical membrane constriction at the intercellular bridge adjacent to the midbody (Guizetti et al., 2011; Mierzwa and Gerlich, 2014). A major contributor for membrane constriction is the multisubunit ESCRT-III complex (Guizetti et al., 2011; Mierzwa and Gerlich, 2014). This complex is able to form sliding filaments which help to create enough force to constrict the intercellular bridge creating the typical appearance of the constriction zone with thin microtubule filaments. These microtubule filaments are in parallel removed by spastin and the ESCRT-III complex mediates final membrane scission which irreversibly separates the daughter cells. The localization of GAS2L3 strongly suggests an involvement in the process of abscission.

It has been shown that constriction zone microtubules are dispensable for abscission and that the removal of microtubule filaments by spastin is rather a rate limiting process (Guizetti et al., 2011). The fact that GAS2L3 can stabilize and bundle microtubule filaments together with the observation that transient overexpression of GAS2L3 leads to an accumulation of intercellular bridges (Pe'er et al., 2013; Wolter et al., 2012) suggests a role for GAS2L3 in influencing the duration of abscission by influencing constriction zone microtubules.

In the abscission stage of cytokinesis, Aurora B monitors chromosome segregation and therefore functions as negative regulator delaying abscission until any segregation problems are solved (Mathieu et al., 2013; Mierzwa and Gerlich, 2014; Steigemann et al., 2009). This checkpoint works via phosphorylation of CHMP4C, a subunit of the ESCRT-III complex, by Aurora B leading to a temporary re-localization of CHMP4C and thereby inhibiting ESCRT-III function (Carlton et al., 2012). In this context, GAS2L3 might be involved in the checkpoint regulation by influencing Aurora B activity and regulation of constriction zone microtubules by influencing their disintegration timing. GAS2L3 is not a substrate of Aurora B but has a slight influence on the kinase activity and CPC stability (Fackler et al., 2014) suggesting a function for GAS2L3 in maintenance and silencing of the checkpoint. There is also an emerging role for a pool of cyclin B-CDK1 at the intercellular bridge regulating abscission timing and counteracting Aurora B (Mathieu et al., 2013). Because our working group found that GAS2L3 is a substrate of CDK1 *in vitro* (Fackler et al., 2014), it is tempting to speculate whether CDK1 regulates GAS2L3 in the context of abscission.

As mentioned before, our group found that the GAR domain mediates the interaction of GAS2L3 with the CPC *in vitro* (Fackler et al., 2014). The importance of the GAR domain for proper cytokinesis is further highlighted by the fact that the internal deletion of the GAR domain of GAS2L3 is not able to rescue the multinucleated cell and multi-lobed phenotype of GAS2L3-depleted cells (Fackler et al., 2014).

In this study it was revealed that the GAR domain is responsible for targeting GAS2L3 to the constriction zone. A deletion mutant of GAS2L3 lacking the GAR domain was not found at the constriction zone in the immunofluorescense-based localization studies but was rather restricted to the outer part of the intercellular bridge losing its ability to co-localize with the CPC and the constriction zone in cytokinesis. A co-localization of GAS2L3 or the deletion mutant with the CPC earlier in mitosis could not be detected indicating a specific interaction at the intercellular bridge and future constriction zone mediated by the GAR domain.

Surprisingly, I also found that the GAS2L3 GAR domain, when expressed on its own, shows only a midbody ring-specific localization in mitosis and does not co-localize with the CPC. This is in contrast to the *in vitro* analysis where the GAR domain is sufficient to interact with the CPC (Fackler et al., 2014). This indicates that the

interaction between GAS2L3 and the CPC is more complex *in vivo*, probably involving additional domains of GAS2L3 or protein modifications.

To gain a deeper insight into the highly dynamic process of cytokinesis and abscission and the role of GAS2L3 in mitosis and cytokinesis high-resolution and time-lapse microscopy with abscission factors and new identified binding partners will be necessary.
In summary, the first part of this study established GAS2L3 as DREAM target gene. The localization pattern of GAS2L3 in mitosis and cytokinesis are provided. Furthermore, I show that GAS2L3 is important for proper cytokinesis and that the GAR domain is essential for the constriction zone-specific targeting of GAS2L3 in the abscission process.

In the second part of the study, I report that the DREAM complex is a master regulator of mitotic kinesins directing the expression of the majority of human mitotic kinesins in the cell division program. Furthermore, I show that in human breast and lung cancer cell lines, mitotic kinesins are up-regulated in a coordinated fashion. Finally, I report that depletion of mitotic kinesins and cytokinesis MAPs impairs proliferation in cancer cell lines.

So far, the DREAM complex was only known to regulate a few mitotic kinesins and it was not clear whether the complex regulates their repression, activation or both (Müller et al., 2014).
This study, however, demonstrates for the first time by ChIP and RNAi experiments, that DREAM regulates the expression of 12 out of 14 kinesins with mitotic functions. Interestingly, DREAM does not bind to the promoters of KIF18A and KIF2A but has influence on their expression.
The ChIP experiments indicate that both the repressive and the activating form of the complex binds to mitotic kinesin promoters suggesting that DREAM is involved in both the repression and activation of mitotic kinesins.
Similar results were obtained for three selected MAPs involved in cytokinesis (PRC1, CEP55, and GAS2L3) suggesting a central role for DREAM in the regulation of mitotic spindle-associated proteins in mitosis.

The binucleation and malformed nuclei phenotype of Lin9-knockout MEFs (Reichert et al., 2010a) is consistent with observations after RNAi mediated depletion of mitotic kinesins. Depletion of mitotic kinesins often leads to chromosome misalignment, followed by chromosome segregation errors or cytokinesis failures (Zhu et al., 2005).
Thus, given the similarity of phenotypes, it is tempting to speculate that the mitotic defects upon Lin9 deletion of are caused by partial down-regulation of mitotic kinesins and MAPs leading to a synergistic effect and finally ending in mitotic catastrophe.
Interestingly, similar cytokinesis failure were observed in *Myb*-null ovarian follicle cells and in wing disc epithelia of *D*. *melanogaster* supporting the idea that reduced G2/M expression of cytokinesis genes are phenotype-determining (DeBruhl et al., 2013).

Multiple reports provide evidence for the up-regulation of selected mitotic kinesins in several types of cancer. The up-regulation is often linked to tumourigenesis and resistance of tumours and cancer cell lines (Table 1) (Chandrasekaran et al., 2015; Liu et al., 2013; Rath and Kozielski, 2012; Yu and Feng, 2010).
So far, a comprehensive analysis of mitotic kinesin expression in cancer cell lines is missing.
My comparative expression analyses in breast and lung cancer cell line panels show that multiple mitotic kinesins are up-regulated in contrast to the non-transformed control cell lines. Increased mitotic mRNA and protein level were observed. These results suggest that cancer cells have mitotic kinesins up-regulated as coordinated cluster in their cell division program.
Whether the up-regulation reflects only a faster doubling time with a higher mitotic index in cancer cells has to be determined for the individual cell lines in the future, e.g., by comparison of synchronized mitotic cells.
The necessity for the up-regulation of multiple mitotic kinesins instead of a single one is plausible as mitotic kinesins are often force generators and as an unbalanced activity of opposing kinesins can interfere with cell division. For example, it was demonstrated that unbalanced activity of KIF11, KIF15, and the motor protein dynein interferes with bipolar spindle assembly and chromosome segregation (vanHeesbeen et al., 2013).

Interestingly, a similar type of coordinated up-regulation in tumours was observed for kinetochore proteins *in silico* (Thiru et al., 2014). Kinetochore proteins often compete with each other at kinetochores and the expression de-regulation of only a single kinetochore protein would therefore be of disadvantage for proper chromosome attachment and segregation.

The physiological relevance for the coordinated up-regulation of mitotic kinesins and kinetochore proteins in evolved tumours is unknown.

Given that cancer cells are often highly aneuploid (Gordon et al., 2012), it is tempting to speculate that a higher number of chromosomes requires higher levels of mitotic kinesins and kinetochore proteins to assure proper chromosome-microtubule attachment, spindle integrity, chromosome segregation and cytokinesis. This idea does not exclude a potential role of single mitotic kinesin de-regulation in the early stages of tumourigenesis by promoting, e.g., chromosomal instability.

Furthermore, it did not escape my notice that B-MYB was also frequently up-regulated in the investigated breast and lung cancer cell lines in contrast to the non-transformed controls. Up-regulation of B-MYB in p53 mutated tumour cells might be of consequence for G2/M gene expression in these cells:

The finding that formation of the repressive DREAM complex and repression of its target genes is promoted by p53 after DNA damage (Mannefeld et al., 2009) suggests that inactivation of the p53 pathway in tumour cells could result in expression of mitotic kinesins by DREAM/B-MYB. Consistent with this notion, at least four mitotic kinesins are regulated by p53 in human cell lines: For example, KIF2C was shown to be regulated in a p53-dependent manner after DNA damage in breast cancer cells (Shimo et al., 2008) and KIF23 expression is regulated in an p53-p21-DREAM-dependent manner (Fischer et al., 2013). Furthermore, I observed an increased expression of B-MYB, KIF4A, and KIF20A upon RNAi-mediated depletion of p53 in BJ skin fibroblasts. Finally, re-activation of p53 in a mouse lung cancer cell line leads to the down-regulation of B-MYB and of at least 6 mitotic kinesins (Kifc1, Kif2c, Kif4, Kif14, Kif20a, and KIF23) (Fabian Iltzsche, unpublished data). Together, these data suggests a regulation of many mitotic kinesins by the p53-p21-DREAM axis.

Moreover, it will be interesting to see whether K-RAS plays a role in DREAM composition and target gene expression because oncogenic activity of K-RAS in cancer uncouples the cell cycle from mitogenic signals and leads to increased cyclin

D expression which in consequence has an influence on G1/S transition, e.g., by regulation of the pocket protein family and cell cycle timing (Coleman et al., 2004; Foster et al., 2010). It is tempting to speculate that a compromised G1/S transition alters DREAM composition and leads to a de-regulation of G2/M target genes with consequences for proper transition through G2/M.
Whether B-MYB up-regulation has an impact on DREAM composition, the expression of DREAM target genes, e.g., mitotic kinesins, the implication for tumourigenesis and the resulting therapeutic potential remain to be investigated.

More progress has been achieved in the description of single mitotic kinesins and their role in cancer cells. Emerging evidence demonstrates that mitotic kinesins, often up-regulated, can acquire new functions in cancer cells besides their usual function in mitosis. The next section describes selected examples of mitotic kinesins and their cancer-specific functions:
Current estimation suggest that ~37% of all human tumours underwent at least one whole genome-duplication in their evolution (Dewhurst et al., 2014; Zack et al., 2013). Failure in mitosis and cytokinesis are thought to be the most common events in this process and in consequence are often accompanied by centrosome amplification in these cells. Cancer cells need to cluster the amplified centrosomes to evade cytokinesis failure caused by multipolar spindles.
KIFC1 is shown to be essential for mitotic centrosome clustering whereas most of the somatic cells seem not to be affected by KIFC1 depletion or inhibition (Kleylein-Sohn et al., 2012; Kwon et al., 2008; Watts et al., 2013; Wu et al., 2013).
KIF2C up-regulation is proposed to mediate docetaxel drug resistance of cancer cells by its microtubule depolymerizing activity (Ganguly et al., 2011).
Furthermore, the kinesin-13 family members KIF2A and KIF2C can be regulated by the Ras-ERK1/2 signaling pathway influencing the capability for cell migration in K-Ras^{G12V} transformed human bronchial epithelial cells (HBECs) (Zaganjor et al., 2013). More recently, it was shown that overexpression of KIF2A and KIF2C in HBECs and HeLa cells enhances extracellular signal-regulated kinase 1 and 2 (ERK1/2) activity providing a potential cancer-dependent positive feedback loop for this pathway (Zaganjor et al., 2014).
KIF14 is shown to influence protein kinase B (PKB/Akt) phosphorylation (Singel et al., 2014) whereas the cytokinesis MAP CEP55 is shown to influence phosphoinositide

3-kinase (Pl3k) stability and activity (Chen et al., 2007; Chen et al., 2009; Jeffery et al., 2015).

The Ras-ERK1/2 and the Ras-Pl3K /Akt signaling pathways are frequently mutated and activated in tumours with impact on, e.g., cell proliferation, cell survival, transcription, and migration (Altomare and Testa, 2005; Downward, 2003; Hanahan and Weinberg, 2011; Hennessy et al., 2005; Neuzillet et al., 2014).

Indirect evidence which suggest a special role of mitotic kinesins and MAPs in cancer cells comes from investigations of the tubulin cytoskeleton. In a variety of cancers an altered stability of microtubules, expression of tubulin isotypes and post-translational modification were observed (Parker et al., 2014). These changes of the tubulin cytoskeleton together with MAPs are shown to influence the response of cancer cells to cellular stress pathways mediating their chemotherapeutic drug resistance and survival. It is also reported that tubulin isotypes and post-translational modifications can have a direct influence on kinesins (Sirajuddin et al., 2014). Tubulin modifications can influence the binding capacity and motility of these motor proteins. The insight of the consequences for cancer cells just emerge and further investigation is needed to establish an integrative model which explains mitotic kinesin and MAPs action in cancer cells.

At the moment, an important class of successfully used anti-mitotic cancer drugs target the tubulin cytoskeleton like *Vinca* alkaloids, taxanes and Epothilions by stabilizing microtubules thereby interfering with proper cell division (Chan et al., 2012; J.kallio, 2013; Janssen and Medema, 2011; Jordan and Wilson, 2004). This approach is not mitosis-specific and the used drugs are risk factors for peripheral neuropathy (Argyriou et al., 2014). The neurotoxic side effects allow only a discontinuous treatment which reduces chemotherapy effectiveness. Furthermore, cancer cells are known to develop resistances against these drugs which create the need for new anti-cancer drugs which target the tubulin cytoskeleton and reduce the neurotoxicity.

In this context, it was recently reported that paclitaxel targets FOXM1 to regulate KIF20A expression which contributes to paclitaxel resistance in breast cancer cells (Khongkow et al., 2015). Due to this observation and the other mentioned reports which link different mitotic kinesins to paclitaxel resistance, it is tempting to speculate whether a paclitaxel-DREAM-mitotic kinesin axis exists which mediates the

resistance to paclitaxel and transfers the observations from single genes to a systemic level.

Prominent candidates as therapeutic targets are the family of mitotic kinesins and mitotic MAPs which are specifically expressed in G2/M of somatic cells (Rath and Kozielski, 2012) and degraded by the APC/C in the end of mitosis (Singh et al., 2014). Their unique abilities to interact with the tubulin cytoskeleton and to mediate proper cell division propose mitotic kinesins and MAPs as anti-mitotic and proliferation-specific anti-cancer targets to replace or support existing drugs. Additionally, the cancer-specific functions of mitotic kinesins and MAPs may render cancer cells dependent on them and open a therapeutic window.

Careful characterization of these proteins will be necessary because some mitotic kinesins are also reported to play a role in postmitotic neurons. Kif2a and Kif4 are, e.g., important for mice brain development (Hirokawa and Tanaka, 2015) as well as Eg5/Kif11 (Ferhat et al., 1998). The mitotic kinesins Kif15 and Kif23/Mklp1 are shown to regulate microtubule pattern in axons and dendrites in the rat (Lin et al., 2012).

Recently, it was also reported that the centralspindlin (MKLP1/CYK-4) complex regulates Rho signaling together with α-catenin in interphase cells at cell-cell junctions, named zonula adherens (Ratheesh et al., 2012).

Although our knowledge of mitotic kinesin function in the brain and in other systems is still rudimentary, first inhibitors against mitotic kinesins were designed and tested in clinical trials, e.g., KSP/EG5/KIF11 and CENP-E/KIF10 (Rath and Kozielski, 2012). Inhibitors of the mitotic kinesin spindle protein KSP/EG5/KIF11 are used as mitosis-specific drugs to selectively attack cells undergoing cell division (Song et al., 2013; Tao et al., 2005; Tao et al., 2007). KSP is important for the establishment of a bipolar spindle. Depletion or inhibition of KSP leads to monopolar spindles. Induction of monopolar spindles triggers the spindle assembly checkpoint (SAC) (Musacchio, 2011; Musacchio and Salmon, 2007). The forced constant activation of the checkpoint leads to cell type specific responses like apoptosis, mitotic catastrophe, and mitotic slippage (Gascoigne and Taylor, 2009; Topham and Taylor, 2013). KSP inhibitors showed strong anti-proliferative effects *in vitro* and are used in Phase I and II clinical trials for mono and combinational therapy (Rath and Kozielski, 2012).

Despite the great *in vitro* activity of KSP inhibitors, the compounds struggle to be effective *in vivo* used for mono therapy (Janssen and Medema, 2011; Song et al., 2013). It is reported that mutations in KSP occur to render cancer cells resistant to

the inhibitors. Moreover, overexpression of the redundant motor protein KIF15 helps cancer cells to overcome the mitotic-arrest induced by KSP inhibitors. Finally, KSP inhibitors show cell type-specific effects *in vitro* making it more difficult to predict their action *in vivo* (Shi et al., 2008).

The ineffectiveness of KSP inhibitors in clinical trials revealed that our knowledge of the function and interaction of mitotic kinesins and MAPs must be further extended to exploit their therapeutic potential.

To begin to investigate mitotic kinesin function and to test the therapeutic usefulness of mitotic kinesins, I established a lentiviral-based inducible shRNA system to effectively deplete selected mitotic kinesins and two cytokinesis MAPs after induction with doxycycline. Depletion of these mitotic kinesins resulted in cytokinesis failure and impaired proliferation in multiple cancer cell lines. The strongest anti-proliferative effects were achieved after depletion of KIF23 and PRC1, two master regulators of cytokinesis (Glotzer, 2009). PRC1 and KIF23 are both essential proteins for cytokinesis and their depletion affects all stages of cytokinesis. Most important, PRC1 is a key protein in spindle midzone assembly and KIF23, as part of the centralspindlin complex, mediates proper midzone formation and cleavage furrow activation. Depletion of the two proteins strongly interferes with starting events in cytokinesis and affects the localization and function of multiple proteins which leads to mitotic catastrophe and binucleated cells (see 3.4). Therefore, it is not surprising that depletion of PRC1 and KIF23 equally affected p53 wt and p53 mutated cancer cell proliferation. Only the response to failed cytokinesis was dependent on the p53 status:

In H460 cells (p53 wt) most of the cells stopped cell cycling after bi-nucleation whereas the H23 (p53 mut) and MDA-MB-231 (p53 mut) cells could complete multiple rounds of failed cytokinesis with the surviving cells finally ending as polyploid giant cancer cells containing multiple nuclei (data not shown). This is in line with reports that cell cycle arrest in G1 phase after cytokinesis failure is dependent on p53 (Andreassen et al., 2001; Ganem and Pellman, 2012; Ganem et al., 2007; Kuffer et al., 2013; Lanni and Jacks, 1998).

These results provide a basis for future investigations. The lentiviral-based inducible shRNA system will allow the dose-dependent down-regulation of mitotic kinesins to physiological levels in cancer cell lines. Furthermore, it will help to discover new

mitotic kinesin functions at kinesin levels where the prominent cytokinesis phenotype is suppressed.

This approach will help to investigate the reason for the up-regulation of mitotic kinesins and MAPs and will likewise provide important insights for cancer treatment strategies.

Furthermore, this system will be useful to conduct complementary experiments with inhibitors against mitotic kinesins and other anti-mitotic and anti-cancer drugs to find synergistic effects. Additionally, this inducible system is applicable to *in vivo* studies in mice. Lentiviral transduced inducible shRNAs against mitotic kinesins can be used to investigate their effect on tumourigenesis and on evolved tumours in a variety of tumour mouse models as well as mimic cyclic treatment conditions.

7 REFERENCES

Alberts, B., Johnson, A., Lewis, J., Raff, M., Roberts, K. and Walter, P. (2008). *Molecular Biology of the Cell*. 5th ed. New York: Garland Science, Taylor & Francis Group.

Altomare, D. a and Testa, J. R. (2005). Perturbations of the AKT signaling pathway in human cancer. *Oncogene* **24**, 7455–7464.

Andreassen, P. R., Lohez, O. D., Lacroix, F. B. and Margolis, R. L. (2001). Tetraploid state induces p53-dependent arrest of nontransformed mammalian cells in G1. *Mol. Biol. Cell* **12**, 1315–1328.

Argyriou, A. a., Kyritsis, A. P., Makatsoris, T. and Kalofonos, H. P. (2014). Chemotherapy-induced peripheral neuropathy in adults: A comprehensive update of the literature. *Cancer Manag. Res.* **6**, 135–147.

Asghar, U., Witkiewicz, A. K., Turner, N. C. and Knudsen, E. S. (2015). The history and future of targeting cyclin-dependent kinases in cancer therapy. *Nat. Publ. Gr.* **14**, 130–146.

Barr, F. a and Gruneberg, U. (2007). Cytokinesis: placing and making the final cut. *Cell* **131**, 847–60.

Bassi, Z. I., Audusseau, M., Giovanna, M., Callaini, G., Paolo, P. and Avino, D. (2013). Citron kinase controls a molecular network required for midbody formation in cytokinesis.

Bastos, R. N. and Barr, F. a (2010). Plk1 negatively regulates Cep55 recruitment to the midbody to ensure orderly abscission. *J. Cell Biol.* **191**, 751–60.

Bastos, R. N., Penate, X., Bates, M., Hammond, D. and Barr, F. a (2012). CYK4 inhibits Rac1-dependent PAK1 and ARHGEF7 effector pathways during cytokinesis. *J. Cell Biol.* **198**, 865–80.

Bastos, R. N., Cundell, M. J. and Barr, F. a (2014). Kif4A and PP2A-B56 form a spatially restricted feedback loop opposing Aurora B at the anaphase central spindle. **207**,.

Bertoli, C., Skotheim, J. M. and de Bruin, R. a M. (2013). Control of cell cycle transcription during G1 and S phases. *Nat. Rev. Mol. Cell Biol.* **14**, 518–28.

Bradford, M. M. (1976). A rapid and sensitive method for the quantitation of microgram quantities of protein utilizing the principle of protein-dye binding. *Anal. Biochem.* **72**, 248–254.

Brancolini, C., Bottega, S. and Schneider, C. (1992). Gas2, a growth arrest-specific protein, is a component of the microfilament network system. *J. Cell Biol.* **117**, 1251–1261.

Cai, S., Weaver, L. N., Ems-McClung, S. C. and Walczak, C. E. (2010). Proper organization of microtubule minus ends is needed for midzone stability and cytokinesis. *Curr. Biol.* **20**, 880–5.

Canman, J. C., Lewelly, L., Kimberley Laband, Smerdon, S. J., Desai, A., Bowerman, B. and Oegma, K. (2008). Inhibition of Rac by the GAP Activity of Centralspindlin Is Essential for Cytokinesis. *Science (80-.).* **322**, 1543–1546.

Carlton, J. G. and Martin-Serrano, J. (2007). Parallels between cytokinesis and retroviral budding: a role for the ESCRT machinery. *Science* **316**, 1908–1912.

Carlton, J. G., Agromayor, M. and Martin-Serrano, J. (2008). Differential requirements for Alix and ESCRT-III in cytokinesis and HIV-1 release. *Proc. Natl. Acad. Sci. U. S. A.* **105**, 10541–10546.

Carlton, J. G., Caballe, A., Agromayor, M., Kloc, M. and Serrano, J. M. (2012). ESCRT-III Governs the Aurora B-Mediated Abscission Checkpoint Through CHMP4C. *Science (80-.).* **336**, 10–12.

Carmena, M., Wheelock, M., Funabiki, H. and Earnshaw, W. C. (2012). The chromosomal passenger complex (CPC): from easy rider to the godfather of mitosis. *Nat. Rev. Mol. Cell Biol.* **13**, 789–803.

Carter, S., Eklund, A., Kohane, I., Harris, L. and Szallasi, Z. (2006). A signature of chromosomal instability inferred from gene expression profiles predicts clinical outcome in multiple human cancers. *Nat. Genet.* **38**, 1043–1048.

Chan, K.-S., Koh, C.-G. and Li, H.-Y. (2012). Mitosis-targeted anti-cancer therapies: where they stand. *Cell Death Dis.* **3**, e411.

Chandrasekaran, G., Tátrai, P. and Gergely, F. (2015). Hitting the brakes: targeting microtubule motors in cancer. *Br. J. Cancer* 1–6.

Charras, G. T., Hu, C. K., Coughlin, M. and Mitchison, T. J. (2006). Reassembly of contractile actin cortex in cell blebs. *J. Cell Biol.* **175**, 477–490.

Charras, G. T., Coughlin, M., Mitchison, T. J. and Mahadevan, L. (2008). Life and times of a cellular bleb. *Biophys. J.* **94**, 1836–1853.

Chen, C.-H., Lu, P.-J., Chen, Y.-C., Fu, S.-L., Wu, K.-J., Tsou, a-P., Lee, Y.-C. G., Lin, T.-C. E., Hsu, S.-L., Lin, W.-J., et al. (2007). FLJ10540-elicited cell transformation is through the activation of PI3-kinase/AKT pathway. *Oncogene* **26**, 4272–83.

Chen, C. H., Lai, J. M., Chou, T. Y., Chen, C. Y., Su, L. J., Lee, Y. C., Cheng, T. S., Hong, Y. R., Chou, C. K., Whang-Peng, J., et al. (2009). VEGFA upregulates

FLJ10540 and modulates migration and invasion of lung cancer via PI3K/AKT pathway. *PLoS One* **4**, e5052.

Chen, X., Muller, G. a., Quaas, M., Fischer, M., Han, N., Stutchbury, B., Sharrocks, a. D. and Engeland, K. (2012). The forkhead transcription factor FOXM1 controls cell cycle-dependent gene expression through an atypical chromatin binding mechanism. *Mol. Cell. Biol.* **33**, 227–236.

Coleman, M. L., Marshall, C. J. and Olson, M. F. (2004). RAS and RHO GTPases in G1-phase cell-cycle regulation. *Nat. Rev. Mol. Cell Biol.* **5**, 355–366.

Connell, J. W., Lindon, C., Luzio, J. P. and Reid, E. (2009). Spastin couples microtubule severing to membrane traffic in completion of cytokinesis and secretion. *Traffic* **10**, 42–56.

Cross, R. a. and McAinsh, A. (2014). Prime movers: the mechanochemistry of mitotic kinesins. *Nat. Rev. Mol. Cell Biol.* **15**, 257–271.

Crowell, E. F., Gaffuri, a.-L., Gayraud-Morel, B., Tajbakhsh, S. and Echard, a. (2014). Engulfment of the midbody remnant after cytokinesis in mammalian cells. *J. Cell Sci.* **127**, 3840–3851.

Cundell, M. J., Bastos, R., Zhang, T., Holder, J., Gruneberg, U., Novak, B. and Barr, F. a. (2013). The BEG (PP2A-B55/ENSA/Greatwall) Pathway Ensures Cytokinesis follows Chromosome Separation. *Mol. Cell* **52**, 393–405.

David O Morgan (2007). *The Cell Cycle-Principles of Control*. London: Oxford University Press.

DeBruhl, H., Wen, H. and Lipsick, J. S. (2013). The complex containing Drosophila Myb and RB/E2F2 regulates cytokinesis in a histone H2Av-dependent manner. *Mol. Cell. Biol.* **33**, 1809–18.

Dewhurst, S. M., Mcgranahan, N. and Burrell, R. a (2014). Tolerance of Whole-Genome Doubling Propagates Chromosomal Instability and Accelerates Cancer Genome Evolution Tolerance of Whole- Genome Doubling Propagates Chromosomal Instability and Accelerates Cancer Genome Evolution. 175–185.

Di Fiore, R., D'Anneo, A., Tesoriere, G. and Vento, R. (2013). RB1 in cancer: Different mechanisms of RB1 inactivation and alterations of pRb pathway in tumorigenesis. *J. Cell. Physiol.* **228**, 1676–1687.

Douglas, M. E., Davies, T., Joseph, N. and Mishima, M. (2010). Aurora B and 14-3-3 coordinately regulate clustering of centralspindlin during cytokinesis. *Curr. Biol.* **20**, 927–33.

Dow, L. E., Premsrirut, P. K., Zuber, J., Fellmann, C., McJunkin, K., Miething, C., Park, Y., Dickins, R. a, Hannon, G. J. and Lowe, S. W. (2012). A pipeline for the generation of shRNA transgenic mice. *Nat. Protoc.* **7**, 374–93.

Downward, J. (2003). Targeting RAS signalling pathways in cancer therapy. *Nat. Rev. Cancer* **3**, 11–22.

Elia, N., Sougrat, R., Spurlin, T. a, Hurley, J. H. and Lippincott-Schwartz, J. (2011). Dynamics of endosomal sorting complex required for transport (ESCRT) machinery during cytokinesis and its role in abscission. *Proc. Natl. Acad. Sci. U. S. A.* **108**, 4846–4851.

Esterlechner, J., Reichert, N., Iltzsche, F., Krause, M., Finkernagel, F. and Gaubatz, S. (2013). LIN9, a Subunit of the DREAM Complex, Regulates Mitotic Gene Expression and Proliferation of Embryonic Stem Cells. *PLoS One* **8**,.

Fackler, M. (2014). Biochemical characterization of GAS2L3 , a target gene of the DREAM complex.

Fackler, M., Wolter, P. and Gaubatz, S. (2014). The GAR domain of GAS2L3 mediates binding to the chromosomal passenger complex and is required for localization of GAS2L3 to the constriction zone during abscission. *FEBS J.* **281**, 2123–2135.

Fededa, J. P. and Gerlich, D. W. (2012). Molecular control of animal cell cytokinesis. *Nat. Cell Biol.* **14**, 440–447.

Ferhat, L., Cook, C., Chauviere, M., Harper, M., Kress, M., Lyons, G. E. and Baas, P. W. (1998). Expression of the mitotic motor protein Eg5 in postmitotic neurons: implications for neuronal development. *J. Neurosci.* **18**, 7822–7835.

Filhol, O., Ciais, D., Lajaunie, C., Charbonnier, P., Foveau, N., Vert, J. P. and Vandenbrouck, Y. (2012). DSIR: Assessing the Design of Highly Potent siRNA by Testing a Set of Cancer-Relevant Target Genes. *PLoS One* **7**, 1–11.

Fischer, M. and Decaprio, J. A. (2015). Does Arabidopsis thaliana DREAM of cell cycle control ? 1–3.

Fischer, M., Grundke, I., Sohr, S., Quaas, M., Hoffmann, S., Knörck, A., Gumhold, C. and Rother, K. (2013). p53 and Cell Cycle Dependent Transcription of kinesin family member 23 (KIF23) Is Controlled Via a CHR Promoter Element Bound by DREAM and MMB Complexes. *PLoS One* **8**, e63187.

Foster, D. a, Yellen, P., Xu, L. and Saqcena, M. (2010). Regulation of G1 Cell Cycle Progression: Distinguishing the Restriction Point from a Nutrient-Sensing Cell Growth Checkpoint(s). *Genes Cancer* **1**, 1124–1131.

Fujiwara, K., Porter, M. E. and Pollard, T. D. (1978). FURROW DURING These observations prompted us to investigate Cells and Staining Preparation o f Fluorescein Labeled Antibodies Biochemical Methods Downloaded from jcb . rupress . org on July 2 , 2010 Purification o f Alpha- Actinin Antibodies Characterizat. *October* **79**,.

Ganem, N. J. and Pellman, D. (2012). Linking abnormal mitosis to the acquisition of DNA damage. *J. Cell Biol.* **199**, 871–881.

Ganem, N. J., Storchova, Z. and Pellman, D. (2007). Tetraploidy, aneuploidy and cancer. *Curr. Opin. Genet. Dev.* **17**, 157–162.

Ganguly, A., Yang, H., Pedroza, M., Bhattacharya, R. and Cabral, F. (2011). Mitotic centromere-associated kinesin (MCAK) mediates paclitaxel resistance. *J. Biol. Chem.* **286**, 36378–84.

Gao, Y.-F., Li, T., Chang, Y., Wang, Y.-B., Zhang, W.-N., Li, W.-H., He, K., Mu, R., Zhen, C., Man, J.-H., et al. (2011). Cdk1-phosphorylated CUEDC2 promotes spindle checkpoint inactivation and chromosomal instability. *Nat. Cell Biol.* **13**, 924–33.

Gascoigne, K. E. and Taylor, S. S. (2009). How do anti-mitotic drugs kill cancer cells? *J. Cell Sci.* **122**, 2579–2585.

Georlette, D., Ahn, S., MacAlpine, D. M., Cheung, E., Lewis, P. W., Beall, E. L., Bell, S. P., Speed, T., Manak, J. R. and Botchan, M. R. (2007). Genomic profiling and expression studies reveal both positive and negative activities for the Drosophila Myb MuvB/dREAM complex in proliferating cells. *Genes Dev.* **21**, 2880–2896.

Glotzer, M. (2005). The molecular requirements for cytokinesis. *Science* **307**, 1735–9.

Glotzer, M. (2009). The 3Ms of central spindle assembly: microtubules, motors and MAPs. *Nat. Rev. Mol. Cell Biol.* **10**, 9–20.

Gordon, D. J., Resio, B. and Pellman, D. (2012). Causes and consequences of aneuploidy in cancer. *Nat. Rev. Genet.* **13**, 189–203.

Goriounov, D., Leung, C. L. and Liem, R. K. H. (2003). Protein products of human Gas2-related genes on chromosomes 17 and 22 (hGAR17 and hGAR22) associate with both microfilaments and microtubules. *J. Cell Sci.* **116**, 1045–1058.

Green, R. a, Paluch, E. and Oegema, K. (2012). Cytokinesis in animal cells. *Annu. Rev. Cell Dev. Biol.* **28**, 29–58.

Gruneberg, U., Neef, R., Honda, R., Nigg, E. a and Barr, F. a (2004). Relocation of Aurora B from centromeres to the central spindle at the metaphase to anaphase transition requires MKlp2. *J. Cell Biol.* **166**, 167–72.

Gruneberg, U., Neef, R., Li, X., Chan, E. H. Y., Chalamalasetty, R. B., Nigg, E. a and Barr, F. a (2006). KIF14 and citron kinase act together to promote efficient cytokinesis. *J. Cell Biol.* **172**, 363–72.

Guizetti, J., Schermelleh, L., Mäntler, J., Maar, S., Poser, I., Leonhardt, H., Müller-Reichert, T. and Gerlich, D. W. (2011). Cortical constriction during

abscission involves helices of ESCRT-III-dependent filaments. *Science* **331**, 1616–20.

Guse, A., Mishima, M. and Glotzer, M. (2005). Phosphorylation of ZEN-4/MKLP1 by aurora B regulates completion of cytokinesis. *Curr. Biol.* **15**, 778–86.

Hanahan, D. and Weinberg, R. a. (2011). Hallmarks of cancer: The next generation. *Cell* **144**, 646–674.

Harrison, M. M., Ceol, C. J., Lu, X. and Horvitz, H. R. (2006). Some C. elegans class B synthetic multivulva proteins encode a conserved LIN-35 Rb-containing complex distinct from a NuRD-like complex. *Proc. Natl. Acad. Sci. U. S. A.* **103**, 16782–16787.

Heald, R., Tournebize, R., Blank, T., Sandaltzopoulos, R., Becker, P., Hyman, a and Karsenti, E. (1996). Self-organization of microtubules into bipolar spindles around artificial chromosomes in Xenopus egg extracts. *Nature* **382**, 420–425.

Hennessy, B. T., Smith, D. L., Ram, P. T., Lu, Y. and Mills, G. B. (2005). Exploiting the PI3K/AKT pathway for cancer drug discovery. *Nat. Rev. Drug Discov.* **4**, 988–1004.

Hirokawa, N. and Tanaka, Y. (2015). Kinesin superfamily proteins (KIFs): Various functions and their relevance for important phenomena in life and diseases. *Exp. Cell Res.* **334**, 16–25.

Hirokawa, N., Noda, Y., Tanaka, Y. and Niwa, S. (2009). Kinesin superfamily motor proteins and intracellular transport. *Nat. Rev. Mol. Cell Biol.* **10**, 682–696.

Hu, C. K., Coughlin, M., Field, C. M. and Mitchison, T. J. (2008). Cell polarization during monopolar cytokinesis. *J. Cell Biol.* **181**, 195–202.

Hu, C.-K., Coughlin, M. and Mitchison, T. J. (2012a). Midbody assembly and its regulation during cytokinesis. *Mol. Biol. Cell* **23**, 1024–34.

Hu, C.-K., Ozlü, N., Coughlin, M., Steen, J. J. and Mitchison, T. J. (2012b). Plk1 negatively regulates PRC1 to prevent premature midzone formation before cytokinesis. *Mol. Biol. Cell* **23**, 2702–11.

Hümmer, S. and Mayer, T. U. (2009). Cdk1 Negatively Regulates Midzone Localization of the Mitotic Kinesin Mklp2 and the Chromosomal Passenger Complex. *Curr. Biol.* **19**, 607–612.

Hutterer, A., Glotzer, M. and Mishima, M. (2009). Clustering of centralspindlin is essential for its accumulation to the central spindle and the midbody. *Curr. Biol.* **19**, 2043–9.

J.kallio, A.-L. S. M. (2013). Mitosis as an anti-cancer target. *Chromosoma* **30**, 431–449.

Janssen, A. and Medema, R. H. (2011). Mitosis as an anti-cancer target. *Oncogene* **30**, 2799–2809.

Jeffery, J., Sinha, D., Srihari, S., Kalimutho, M. and Khanna, K. K. (2015). Beyond cytokinesis: the emerging roles of CEP55 in tumorigenesis. *Oncogene* 1–8.

Jiang, W., Jimenez, G., Wells, N. J., Hope, T. J., Wahl, G. M., Hunter, T., Fukunaga, R. and Jolla, L. (1998). PRC1 : A Human Mitotic Spindle – Associated CDK Substrate Protein Required for Cytokinesis. **2**, 877–885.

Jordan, M. A. and Wilson, L. (2004). Microtubules as a target for anticancer drugs. *Nat. Rev.* **4**,.

Kapoor, T. M., Mayer, T. U., Coughlin, M. L. and Mitchison, T. J. (2000). Probing spindle assembly mechanisms with monastrol, a small molecule inhibitor of the mitotic kinesin, Eg5. *J. Cell Biol.* **150**, 975–988.

Khongkow, P., Gomes, a R., Gong, C., Man, E. P. S., Tsang, J. W.-H., Zhao, F., Monteiro, L. J., Coombes, R. C., Medema, R. H., Khoo, U. S., et al. (2015). Paclitaxel targets FOXM1 to regulate KIF20A in mitotic catastrophe and breast cancer paclitaxel resistance. *Oncogene* 1–13.

Kitagawa, M., Fung, S. Y. S., Onishi, N., Saya, H. and Lee, S. H. (2013). Targeting Aurora B to the equatorial cortex by MKlp2 is required for cytokinesis. *PLoS One* **8**, e64826.

Kittler, R., Pelletier, L., Heninger, A.-K., Slabicki, M., Theis, M., Miroslaw, L., Poser, I., Lawo, S., Grabner, H., Kozak, K., et al. (2007). Genome-scale RNAi profiling of cell division in human tissue culture cells. *Nat. Cell Biol.* **9**, 1401–1412.

Kleylein-Sohn, J., Pöllinger, B., Ohmer, M., Hofmann, F., Nigg, E. a, Hemmings, B. a and Wartmann, M. (2012). Acentrosomal spindle organization renders cancer cells dependent on the kinesin HSET. *J. Cell Sci.* **125**, 5391–402.

Knight, a S., Notaridou, M. and Watson, R. J. (2009). A Lin-9 complex is recruited by B-Myb to activate transcription of G2/M genes in undifferentiated embryonal carcinoma cells. *Oncogene* **28**, 1737–1747.

Kobayashi, K., Suzuki, T., Iwata, E., Nakamichi, N., Suzuki, T., Chen, P., Ohtani, M., Ishida, T., Hosoya, H., Müller, S., et al. (2015). Transcriptional repression by MYB 3 R proteins regulates plant organ growth. 1–16.

Koo, C. Y., Muir, K. W. and Lam, E. W. F. (2012). FOXM1: From cancer initiation to progression and treatment. *Biochim. Biophys. Acta - Gene Regul. Mech.* **1819**, 28–37.

Korenjak, M., Taylor-Harding, B., Binné, U. K., Satterlee, J. S., Stevaux, O., Aasland, R., White-Cooper, H., Dyson, N. and Brehm, A. (2004). Native E2F/RBF complexes contain Myb-interacting proteins and repress transcription of developmentally controlled E2F target genes. *Cell* **119**, 181–193.

Kotak, S. and Gönczy, P. (2013). Mechanisms of spindle positioning: Cortical force generators in the limelight. *Curr. Opin. Cell Biol.* **25**, 741–748.

Kotak, S., Busso, C. and Gönczy, P. (2012). Cortical dynein is critical for proper spindle positioning in human cells. *J. Cell Biol.* **199**, 97–110.

Kremling, H. (2010). Role of new target genes of the human LINC / DREAM Complex in cell cycle and cytokinesis Diploma thesis.

Kuffer, C., Kuznetsova, A. Y. and Storchová, Z. (2013). Abnormal mitosis triggers p53-dependent cell cycle arrest in human tetraploid cells. *Chromosoma* **122**, 305–18.

Kurasawa, Y., Earnshaw, W. C., Mochizuki, Y., Dohmae, N. and Todokoro, K. (2004). Essential roles of KIF4 and its binding partner PRC1 in organized central spindle midzone formation. *EMBO J.* **23**, 3237–48.

Kwon, M., Godinho, S. a, Chandhok, N. S., Ganem, N. J., Azioune, A., Thery, M. and Pellman, D. (2008). Mechanisms to suppress multipolar divisions in cancer cells with extra centrosomes. *Genes Dev.* **22**, 2189–203.

Laemmli, U. K. (1970). Cleavage of structural proteins during the assembly of the head of bacteriophage T4. *Nature* **227**, 680–685.

Lanni, J. S. and Jacks, T. (1998). Characterization of the p53-dependent postmitotic checkpoint following spindle disruption. *Mol. Cell. Biol.* **18**, 1055–1064.

Lawrence, C. J., Dawe, R. K., Christie, K. R., Cleveland, D. W., Dawson, S. C., Endow, S. a., Goldstein, L. S. B., Goodson, H. V., Hirokawa, N., Howard, J., et al. (2004). A standardized kinesin nomenclature. *J. Cell Biol.* **167**, 19–22.

Lee, H. H., Elia, N., Ghirlando, R., Lippincott-Schwartz, J. and Hurley, J. H. (2008). Midbody Targeting of the ESCRT Machinery by a Noncanonical. 576–580.

Lee, K. Y., Davies, T. and Mishima, M. (2012). Cytokinesis microtubule organisers at a glance. *J. Cell Sci.* **125**, 3495–3500.

Lewis, P. W., Beall, E. L., Fleischer, T. C., Georlette, D., Link, A. J. and Botchan, M. R. (2004). Identification of a Drosophila Myb – E2F2 / RBF transcriptional repressor complex. 2929–2940.

Lin, S., Liu, M., Mozgova, O. I., Yu, W. and Baas, P. W. (2012). Mitotic motors coregulate microtubule patterns in axons and dendrites. *J. Neurosci.* **32**, 14033–49.

Litovchick, L., Sadasivam, S., Florens, L., Zhu, X., Swanson, S. K., Velmurugan, S., Chen, R., Washburn, M. P., Liu, X. S. and DeCaprio, J. a. (2007). Evolutionarily Conserved Multisubunit RBL2/p130 and E2F4 Protein Complex Represses Human Cell Cycle-Dependent Genes in Quiescence. *Mol. Cell* **26**, 539–551.

Litovchick, L., Florens, L. a., Swanson, S. K., Washburn, M. P. and Decaprio, J. a. (2011). DYRK1A protein kinase promotes quiescence and senescence through DREAM complex assembly. *Genes Dev.* **25**, 801–813.

Liu, X., Gong, H. and Huang, K. (2013). Oncogenic role of kinesin proteins and targeting kinesin therapy. *Cancer Sci.* **104**, 651–6.

Loria, A., Longhini, K. M. and Glotzer, M. (2012). The RhoGAP domain of CYK-4 Has an essential role in RhoA activation. *Curr. Biol.* **22**, 213–219.

Makyio, H., Ohgi, M., Takei, T., Takahashi, S., Takatsu, H., Katoh, Y., Hanai, A., Ueda, T., Kanaho, Y., Xie, Y., et al. (2012). Structural basis for Arf6-MKLP1 complex formation on the Flemming body responsible for cytokinesis. *EMBO J.* **31**, 2590–603.

Mannefeld, M., Klassen, E. and Gaubatz, S. (2009). B-MYB is required for recovery from the DNA damage-induced G2 checkpoint in p53 mutant cells. *Cancer Res.* **69**, 4073–4080.

Martinez-Garay, I., Rustom, A., Gerdes, H.-H. and Kutsche, K. (2006). The novel centrosomal associated protein CEP55 is present in the spindle midzone and the midbody. *Genomics* **87**, 243–53.

Mathieu, J., Cauvin, C., Moch, C., Radford, S., Sampaio, P., Perdigoto, C. N., Schweisguth, F., Bardin, A. J., Sunkel, C. E., McKim, K., et al. (2013). Aurora B and Cyclin B have opposite effects on the timing of cytokinesis abscission in drosophila germ cells and in vertebrate somatic cells. *Dev. Cell* **26**, 250–265.

Matsumura, F. (2005). Regulation of myosin II during cytokinesis in higher eukaryotes. *Trends Cell Biol.* **15**, 371–377.

Mattison, C. P., Stumpff, J., Wordeman, L. and Winey, M. (2011). Mip1 associates with both the Mps1 kinase and actin, and is required for cell cortex stability and anaphase spindle positioning. *Cell Cycle* **10**, 783–793.

Matuliene, J. and Kuriyama, R. (2002). Kinesin-like Protein CHO1 Is Required for the Formation of Midbody Matrix and the Completion of Cytokinesis in Mammalian Cells. **13**, 1832–1845.

Meerbrey, K. L., Hu, G., Kessler, J. D., Roarty, K., Li, M. Z., Fang, J. E., Herschkowitz, J. I., Burrows, A. E., Ciccia, A., Sun, T., et al. (2011). The pINDUCER lentiviral toolkit for inducible RNA interference in vitro and in vivo. *Proc. Natl. Acad. Sci. U. S. A.* **108**, 3665–3670.

Mierzwa, B. and Gerlich, D. W. (2014). Cytokinetic Abscission: Molecular Mechanisms and Temporal Control. *Dev. Cell* **31**, 525–538.

Mishima, M., Kaitna, S. and Glotzer, M. (2002). Central Spindle Assembly and Cytokinesis Require a Kinesin-like Protein/RhoGAP Complex with Microtubule Bundling Activity. *Dev. Cell* **2**, 41–54.

Mishima, M., Pavicic, V. and Gru, U. (2004). Cell cycle regulation of central spindle assembly. *Nature* **430**, 0–5.

Mollinari, C., Kleman, J.-P., Jiang, W., Schoehn, G., Hunter, T. and Margolis, R. L. (2002). PRC1 is a microtubule binding and bundling protein essential to maintain the mitotic spindle midzone. *J. Cell Biol.* **157**, 1175–86.

Morita, E., Sandrin, V., Chung, H.-Y., Morham, S. G., Gygi, S. P., Rodesch, C. K. and Sundquist, W. I. (2007). Human ESCRT and ALIX proteins interact with proteins of the midbody and function in cytokinesis. *EMBO J.* **26**, 4215–27.

Mukhina, S., Wang, Y. L. and Murata-Hori, M. (2007). ??-Actinin Is Required for Tightly Regulated Remodeling of the Actin Cortical Network during Cytokinesis. *Dev. Cell* **13**, 554–565.

Müller, G. a, Wintsche, A., Stangner, K., Prohaska, S. J., Stadler, P. F. and Engeland, K. (2014). The CHR site: definition and genome-wide identification of a cell cycle transcriptional element. *Nucleic Acids Res.* **42**, 1–20.

Musacchio, A. (2011). Spindle assembly checkpoint: the third decade. *Philos. Trans. R. Soc. Lond. B. Biol. Sci.* **366**, 3595–604.

Musacchio, A. and Hardwick, K. G. (2002). The spindle checkpoint: structural insights into dynamic signalling. *Nat. Rev. Mol. Cell Biol.* **3**, 731–741.

Musacchio, A. and Salmon, E. D. (2007). The spindle-assembly checkpoint in space and time. *Nat. Rev. Mol. Cell Biol.* **8**, 379–93.

Neef, R., Preisinger, C., Sutcliffe, J., Kopajtich, R., Nigg, E. a., Mayer, T. U. and Barr, F. a. (2003). Phosphorylation of mitotic kinesin-like protein 2 by polo-like kinase 1 is required for cytokinesis. *J. Cell Biol.* **162**, 863–875.

Neto, H. and Gould, G. W. (2011). The regulation of abscission by multi-protein complexes. *J. Cell Sci.* **124**, 3199–207.

Neuzillet, C., Tijeras-Raballand, A., de Mestier, L., Cros, J., Faivre, S. and Raymond, E. (2014). MEK in cancer and cancer therapy. *Pharmacol. Ther.* **141**, 160–71.

Osterloh, L., von Eyss, B., Schmit, F., Rein, L., Hübner, D., Samans, B., Hauser, S. and Gaubatz, S. (2007). The human synMuv-like protein LIN-9 is required for transcription of G2/M genes and for entry into mitosis. *EMBO J.* **26**, 144–57.

Otegui, M. S., Verbrugghe, K. J. and Skop, A. R. (2005). Midbodies and phragmoplasts: analogous structures involved in cytokinesis. *Trends Cell Biol.* **15**, 404–13.

Parikh, N., Hilsenbeck, S., Creighton, C. J., Dayaram, T., Shuck, R., Shinbrot, E., Xi, L., Gibbs, R., Wheeler, D. and Donehower, L. (2014). Effects of TP53 mutational status on gene expression patterns across 10 human cancer types. *J. Pathol.* **232**, 522–33.

Parker, A. L., Kavallaris, M. and McCarroll, J. a (2014). Microtubules and their role in cellular stress in cancer. *Front. Oncol.* **4**, 153.

Pavicic-kaltenbrunner, V., Mishima, M. and Glotzer, M. (2007). Cooperative Assembly of CYK-4 / MgcRacGAP and ZEN-4 / MKLP1 to Form the Centralspindlin Complex □. **18**, 4992–5003.

Pe'er, T., Lahmi, R., Sharaby, Y., Chorni, E., Noach, M., Vecsler, M., Zlotorynski, E., Steen, H., Steen, J. a. and Tzur, A. (2013). Gas2l3, a Novel Constriction Site-Associated Protein Whose Regulation Is Mediated by the APC/CCdh1 Complex. *PLoS One* **8**, e57532.

Piekny, A. J. and Glotzer, M. (2008). Anillin Is a Scaffold Protein That Links RhoA, Actin, and Myosin during Cytokinesis. *Curr. Biol.* **18**, 30–36.

Piekny, A. J. and Maddox, A. S. (2010). The myriad roles of Anillin during cytokinesis. *Semin. Cell Dev. Biol.* **21**, 881–891.

Pilkinton, M., Sandoval, R. and Colamonici, O. R. (2007). Mammalian Mip/LIN-9 interacts with either the p107, p130/E2F4 repressor complex or B-Myb in a cell cycle-phase-dependent context distinct from the Drosophila dREAM complex. *Oncogene* **26**, 7535–7543.

Pines, M. K., Housden, B. E., Bernard, F., Bray, S. J. and Röper, K. (2010). The cytolinker Pigs is a direct target and a negative regulator of Notch signalling. *Development* **137**, 913–22.

Pohl, C. and Jentsch, S. (2008). Final stages of cytokinesis and midbody ring formation are controlled by BRUCE. *Cell* **132**, 832–45.

Ramsay, R. G. and Gonda, T. J. (2008). MYB function in normal and cancer cells. *Nat. Rev. Cancer* **8**, 523–534.

Rankin, K. E. and Wordeman, L. (2010). Long astral microtubules uncouple mitotic spindles from the cytokinetic furrow. *J. Cell Biol.* **190**, 35–43.

Raschellà, G., Cesi, V., Amendola, R., Negroni, A., Tanno, B., Altavista, P., Tonini, G. P., De Bernardi, B. and Calabretta, B. (1999). Expression of B-myb in neuroblastoma tumors is a poor prognostic factor independent from MYCN amplification. *Cancer Res.* **59**, 3365–3368.

Rath, O. and Kozielski, F. (2012). Kinesins and cancer. *Nat. Rev. Cancer* **12**, 527–39.

Ratheesh, A., Gomez, G. a., Priya, R., Verma, S., Kovacs, E. M., Jiang, K., Brown, N. H., Akhmanova, A., Stehbens, S. J. and Yap, A. S. (2012). Centralspindlin and α-catenin regulate Rho signalling at the epithelial zonula adherens. *Nat. Cell Biol.* **14**, 818–828.

Reichert, N., Wurster, S., Ulrich, T., Schmitt, K., Hauser, S., Probst, L., Götz, R., Ceteci, F., Moll, R., Rapp, U., et al. (2010a). Lin9, a subunit of the mammalian

DREAM complex, is essential for embryonic development, for survival of adult mice, and for tumor suppression. *Mol. Cell. Biol.* **30**, 2896–2908.

Reichert, N., Wurster, S., Ulrich, T., Schmitt, K., Hauser, S., Probst, L., Götz, R., Ceteci, F., Moll, R., Rapp, U., et al. (2010b). Lin9, a subunit of the mammalian DREAM complex, is essential for embryonic development, for survival of adult mice, and for tumor suppression. *Mol. Cell. Biol.* **30**, 2896–908.

Sadasivam, S. and DeCaprio, J. a (2013). The DREAM complex: master coordinator of cell cycle-dependent gene expression. *Nat. Rev. Cancer* **13**, 585–95.

Sadasivam, S., Duan, S. and DeCaprio, J. a. (2012). The MuvB complex sequentially recruits B-Myb and FoxM1 to promote mitotic gene expression. *Genes Dev.* **26**, 474–489.

Safran, M., Chalifa-Caspi, V., Shmueli, O., Olender, T., Lapidot, M., Rosen, N., Shmoish, M., Peter, Y., Glusman, G., Feldmesser, E., et al. (2003). Human gene-centric databases at the Weizmann Institute of science: GeneCards, UDB, CroW 21 and HORDE. *Nucleic Acids Res.* **31**, 142–146.

Salbreux, G., Charras, G. and Paluch, E. (2012). Actin cortex mechanics and cellular morphogenesis. *Trends Cell Biol.* **22**, 536–45.

Schmit, F., Korenjak, M., Mannefeld, M., Schmitt, K., Franke, C., Eyss, B. Von, Gagrica, S., Hanel, F., Brehm, A. and Gaubatz, S. (2007). LINC, a Human Complex That is Related to pRB-Containing Complexes in Invertebrates Regulates the Expression of G2/M Genes. *Cell Cycle* **6**, 1903–1913.

Schmitt, K. (2010). Identification and Characterization of GAS2L3 as a Novel Mitotic Regulator in Human Cells.

Schneider, C., King, R. M. and Philipson, L. (1988). Genes specifically expressed at growth arrest of mammalian cells. *Cell* **54**, 787–793.

Sedzinski, J., Biro, M., Oswald, A., Tinevez, J.-Y., Salbreux, G. and Paluch, E. (2011). Polar actomyosin contractility destabilizes the position of the cytokinetic furrow. *Nature* **476**, 462–6.

Severson, A. F., Baillie, D. L. and Bowerman, B. (2002). A Formin Homology protein and a profilin are required for cytokinesis and Arp2/3-independent assembly of cortical microfilaments in C. elegans. *Curr. Biol.* **12**, 2066–2075.

Shi, J., Orth, J. D. and Mitchison, T. (2008). Cell type variation in responses to antimitotic drugs that target microtubules and kinesin-5. *Cancer Res.* **68**, 3269–3276.

Shimo, A., Nishidate, T., Ohta, T., Fukuda, M., Nakamura, Y. and Katagiri, T. (2007). Elevated expression of protein regulator of cytokinesis 1, involved in the growth of breast cancer cells. *Cancer Sci.* **98**, 174–181.

Shimo, A., Tanikawa, C., Nishidate, T., Lin, M. L., Matsuda, K., Park, J. H., Ueki, T., Ohta, T., Hirata, K., Fukuda, M., et al. (2008). Involvement of kinesin family member 2C/mitotic centromere-associated kinesin overexpression in mammary carcinogenesis. *Cancer Sci.* **99**, 62–70.

Singel, S. M., Cornelius, C., Batten, K., Fasciani, G., Wright, W. E., Lum, L. and Shay, J. W. (2013). A targeted RNAi screen of the breast cancer genome identifies KIF14 and TLN1 as genes that modulate docetaxel chemosensitivity in triple-negative breast cancer. *Clin. Cancer Res.* **19**, 2061–2070.

Singel, S. M., Cornelius, C., Zaganjor, E., Batten, K., Sarode, V. R., Buckley, D. L., Peng, Y., John, G. B., Li, H. C., Sadeghi, N., et al. (2014). KIF14 promotes AKT phosphorylation and contributes to chemoresistance in triple-negative breast cancer. *Neoplasia (United States)* **16**, 247–256.

Singh, S. a., Winter, D., Kirchner, M., Chauhan, R., Ahmed, S., Ozlu, N., Tzur, A., Steen, J. a. and Steen, H. (2014). Co-regulation proteomics reveals substrates and mechanisms of APC/C-dependent degradation. *EMBO J.* **33**, 385–399.

Sirajuddin, M., Rice, L. M. and Vale, R. D. (2014). Regulation of microtubule motors by tubulin isotypes and post-translational modifications. *Nat. Cell Biol.* **16**, 335–44.

Song, H., Zhou, S., Wang, R. and Li, S. (2013). Kinesin spindle protein (KSP) inhibitors in combination with chemotherapeutic agents for cancer therapy. *ChemMedChem* **8**, 1736–49.

Srinivas, V. and Murata-Hori, M. (2012). Proper positioning of the cleavage furrow requires -actinin to regulate the specification of different populations of microtubules. *J. Cell Sci.* 4713–4719.

Steigemann, P. and Gerlich, D. W. (2009). Cytokinetic abscission: cellular dynamics at the midbody. *Trends Cell Biol.* **19**, 606–16.

Steigemann, P., Wurzenberger, C., Schmitz, M. H. a, Held, M., Guizetti, J., Maar, S. and Gerlich, D. W. (2009). Aurora B-mediated abscission checkpoint protects against tetraploidization. *Cell* **136**, 473–84.

Stroud, M. J., Kammerer, R. a. and Ballestrem, C. (2011). Characterization of G2L3 (GAS2-like 3), a new microtubule- and actin-binding protein related to spectraplakins. *J. Biol. Chem.* **286**, 24987–24995.

Stroud, M. J., Nazgiewicz, A., McKenzie, E. a, Wang, Y., Kammerer, R. a and Ballestrem, C. (2014). GAS2-like proteins mediate communication between microtubules and actin through interactions with end-binding proteins. *J. Cell Sci.* **127**, 2672–82.

Su, K. C., Takaki, T. and Petronczki, M. (2011). Targeting of the RhoGEF Ect2 to the Equatorial Membrane Controls Cleavage Furrow Formation during Cytokinesis. *Dev. Cell* **21**, 1104–1115.

Sun, D., Leung, C. L. and Liem, R. K. H. (2000). Characterization of the microtubule binding domain of microtubule actin crosslinking factor (MACF): identification of a novel group of microtubule associated proteins.

Suozzi, K. C., Wu, X. and Fuchs, E. (2012). Spectraplakins: Master orchestrators of cytoskeletal dynamics. *J. Cell Biol.* **197**, 465–475.

Swanton, C., Nicke, B., Schuett, M., Eklund, A. C., Ng, C., Li, Q., Hardcastle, T., Lee, A., Roy, R., East, P., et al. (2009). Chromosomal instability determines taxane response. *Proc. Natl. Acad. Sci. U. S. A.* **106**, 8671–8676.

Tao, W., South, V. J., Zhang, Y., Davide, J. P., Farrell, L., Kohl, N. E., Sepp-Lorenzino, L. and Lobell, R. B. (2005). Induction of apoptosis by an inhibitor of the mitotic kinesin KSP requires both activation of the spindle assembly checkpoint and mitotic slippage. *Cancer Cell* **8**, 49–59.

Tao, W., South, V. J., Diehl, R. E., Davide, J. P., Sepp-Lorenzino, L., Fraley, M. E., Arrington, K. L. and Lobell, R. B. (2007). An inhibitor of the kinesin spindle protein activates the intrinsic apoptotic pathway independently of p53 and de novo protein synthesis. *Mol. Cell. Biol.* **27**, 689–698.

Tao, D., Pan, Y., Lu, H., Zheng, S., Lin, H., Fang, H. and Cao, F. (2014). B-myb is a gene implicated in cell cycle and proliferation of breast cancer. **7**, 5819–5827.

Thiru, P., Kern, D. M., McKinley, K. L., Monda, J. K., Rago, F., Su, K.-C., Tsinman, T., Yarar, D., Bell, G. W. and Cheeseman, I. M. (2014). Kinetochore genes are coordinately up-regulated in human tumors as part of a FoxM1-related cell division program. *Mol. Biol. Cell* **25**, 1983–94.

Topham, C. H. and Taylor, S. S. (2013). Mitosis and apoptosis: How is the balance set? *Curr. Opin. Cell Biol.* **25**, 780–785.

Uehara, R. and Goshima, G. (2010). Functional central spindle assembly requires de novo microtubule generation in the interchromosomal region during anaphase. *J. Cell Biol.* **191**, 259–67.

Uehara, R., Tsukada, Y., Kamasaki, T., Poser, I., Yoda, K., Gerlich, D. W. and Goshima, G. (2013). Aurora B and Kif2A control microtubule length for assembly of a functional central spindle during anaphase. *J. Cell Biol.* **202**, 623–36.

Van Der Horst, A. and Lens, S. M. a (2014). Cell division: Control of the chromosomal passenger complex in time and space. *Chromosoma* **123**, 25–42.

vanHeesbeen, R. H. P., Tanenbaum, M. and Medema, R. (2013). Balanced Activity of Three Mitotic Motors Is Required for Bipolar Spindle Assembly and Chromosome Segregation. *Cell Rep.*

Verhey, K. J. and Hammond, J. W. (2009). Traffic control: regulation of kinesin motors. *Nat. Rev. Mol. Cell Biol.* **10**, 765–777.

Vicente, J. J. and Wordeman, L. (2015). Mitosis, microtubule dynamics and the evolution of kinesins. *Exp. Cell Res.* **334**, 61–69.

Walczak, C. E. and Shaw, S. L. (2010). A MAP for bundling microtubules. *Cell* **142**, 364–7.

Watanabe, S., Yoshikazu Ando, Yasuda, S., Hosoya, H., Naoki Watanabe, Toshimasa Ishizaki and Shuh Narumiya (2008). mDia2 Induces the Actin Scaffold for the Contractile Ring and Stabilizes Its Position during Cytokinesis in NIH 3T3 Cells. *Mol. Biol. Cell* **19**, 2328–2338.

Watanabe, S., Okawa, K., Miki, T., Sakamato, S., Morinaga, T., Segawa, K., Arakawa, T., Kinoshita, M., Ishizaki, T. and Marumiya, S. (2010). Rho and Anillin-dependent Control of mDia2 Localization and Function in Cytokinesis. *Mol. Biol. Cell* **21**, 3193–3204.

Watts, C. a., Richards, F. M., Bender, A., Bond, P. J., Korb, O., Kern, O., Riddick, M., Owen, P., Myers, R. M., Raff, J., et al. (2013). Design, synthesis, and biological evaluation of an allosteric inhibitor of HSET that targets cancer cells with supernumerary centrosomes. *Chem. Biol.* **20**, 1399–1410.

Welburn, J. P. I. (2013). The molecular basis for kinesin functional specificity during mitosis. *Cytoskeleton* **70**, 476–493.

Wolfe, B. a, Takaki, T., Petronczki, M. and Glotzer, M. (2009). Polo-like kinase 1 directs assembly of the HsCyk-4 RhoGAP/Ect2 RhoGEF complex to initiate cleavage furrow formation. *PLoS Biol.* **7**, e1000110.

Wolter, P. (2011). GAS2L3, a novel target of the DREAM/LIN-complex, is important for progression through mitosis and maintenance of chromosomal stability.

Wolter, P., Schmitt, K., Fackler, M., Kremling, H., Probst, L., Hauser, S., Gruss, O. J. and Gaubatz, S. (2012). GAS2L3, a target gene of the DREAM complex, is required for proper cytokinesis and genomic stability. *J. Cell Sci.* **125**, 2393–2406.

Wu, J., Mikule, K., Wang, W., Su, N., Petteruti, P., Gharahdaghi, F., Code, E., Zhu, X., Jacques, K., Lai, Z., et al. (2013). Discovery and mechanistic study of a small molecule inhibitor for motor protein KIFC1. *ACS Chem. Biol.* **8**, 2201–8.

Yang, D., Rismanchi, N., Renvoisé, B., Lippincott-Schwartz, J., Blackstone, C. and Hurley, J. H. (2008). Structural basis for midbody targeting of spastin by the ESCRT-III protein CHMP1B. *Nat. Struct. Mol. Biol.* **15**, 1278–1286.

Yount, A. L., Zong, H. and Walczak, C. E. (2015). Regulatory mechanisms that control mitotic kinesins. *Exp. Cell Res.* 1–8.

Yu, Y. and Feng, Y. M. (2010). The role of kinesin family proteins in tumorigenesis and progression. *Cancer* **116**, 5150–5160.

Yüce, O., Piekny, A. and Glotzer, M. (2005). An ECT2-centralspindlin complex regulates the localization and function of RhoA. *J. Cell Biol.* **170**, 571–82.

Zack, T. I., Schumacher, S. E., Carter, S. L., Cherniack, A. D., Saksena, G., Tabak, B., Lawrence, M. S., Zhang, C.-Z., Wala, J., Mermel, C. H., et al. (2013). Pan-cancer patterns of somatic copy number alteration. *Nat. Genet.* **45**, 1134–1140.

Zaganjor, E., Osborne, J. K., Weil, L. M., Diaz-Martinez, L. a, Gonzales, J. X., Singel, S. M., Larsen, J. E., Girard, L., Minna, J. D. and Cobb, M. H. (2013). Ras regulates kinesin 13 family members to control cell migration pathways in transformed human bronchial epithelial cells. *Oncogene* **33**, 1–10.

Zaganjor, E., Weil, L. M., Gonzales, J. X., Minna, J. D. and Cobb, M. H. (2014). Ras transformation uncouples the kinesin-coordinated cellular nutrient response. *Proc. Natl. Acad. Sci. U. S. A.* **111**, 10568–73.

Zhao, W. M. and Fang, G. (2005a). Anillin is a substrate of anaphase-promoting complex/cyclosome (APC/C) that controls spatial contractility of myosin during late cytokinesis. *J. Biol. Chem.* **280**, 33516–33524.

Zhao, W. and Fang, G. (2005b). MgcRacGAP controls the assembly of the contractile ring and the initiation of cytokinesis. *Proc. Natl. Acad. Sci. U. S. A.* **102**, 13158–63.

Zhao, W., Seki, A. and Fang, G. (2006). Cep55 , a Microtubule-bundling Protein , Associates with Centralspindlin to Control the Midbody Integrity and Cell Abscission during Cytokinesis □. **17**, 3881–3896.

Zhu, C. and Jiang, W. (2005). Cell cycle-dependent translocation of PRC1 on the spindle by Kif4 is essential for midzone formation and cytokinesis. *Proc. Natl. Acad. Sci. U. S. A.* **102**, 343–8.

Zhu, C., Zhao, J., Bibikova, M., Leverson, J. D., Bossy-wetzel, E., Fan, J., Abraham, R. T., Jiang, W., Jolla, L., Diego, S., et al. (2005). Functional Analysis of Human Microtubule-based Motor Proteins , the Kinesins and Dyneins, in Mitosis / Cytokinesis Using RNA Interference. *Mol. Biol. Cell* **16**, 3187–3199.

Zhu, C., Lau, E., Schwarzenbacher, R., Bossy-wetzel, E. and Jiang, W. (2006). Spatiotemporal control of spindle midzone formation by PRC1 in human cells. *Proc. Natl. Acad. Sci.* **103**, 6196–6201.

8 APPENDIX

8.1 EGFP-GAS2L3 localization in mitosis

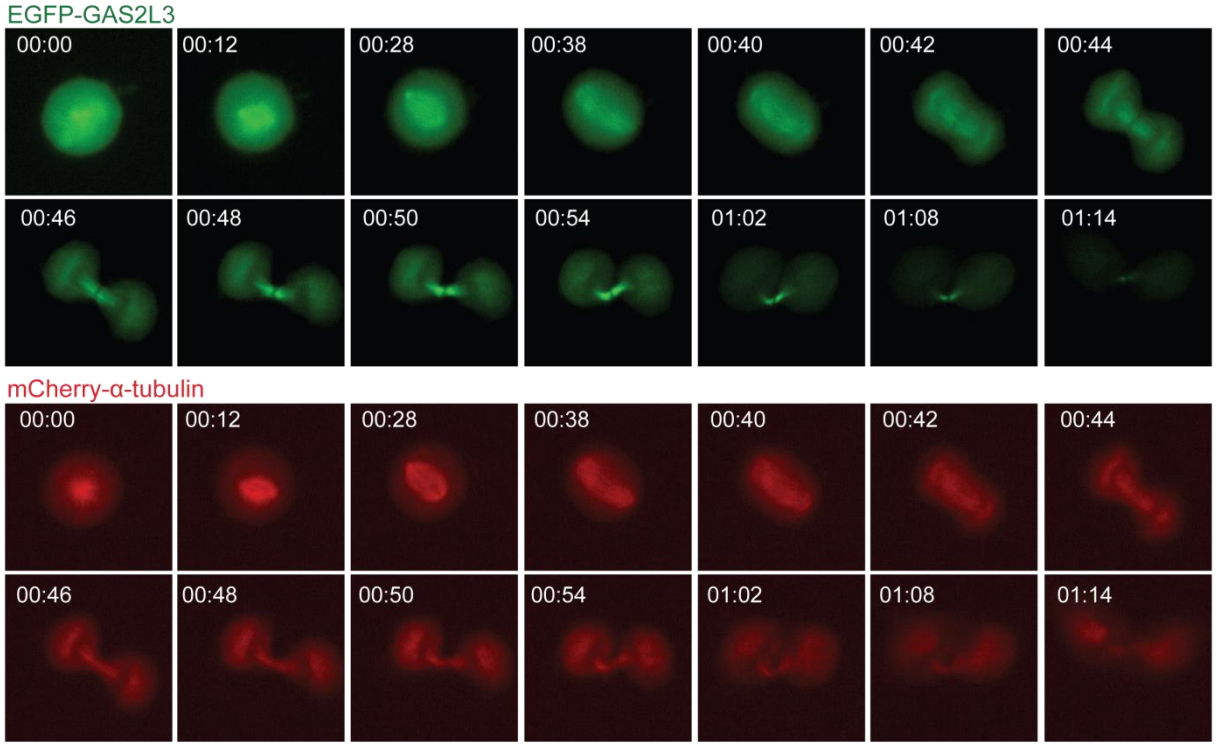

Figure 39: Individual channels of the transient overexpression of EGFP-GAS2L3 in Figure 14. HeLa cells stably expressing mCherry-α-tubulin were transiently transfected with EGFP-GAS2L3 and time-lapse movies were recorded. GAS2L3 localization at different mitotic stages was analyzed by immunofluorescence. Selected frames from the individual channel are presented here.

8.2 Screen for functional pINDUCER-shRNAs

All the tested shRNA sequences and their knockdown efficiencies on protein level are shown in Figure 40 and listed in Table 2.

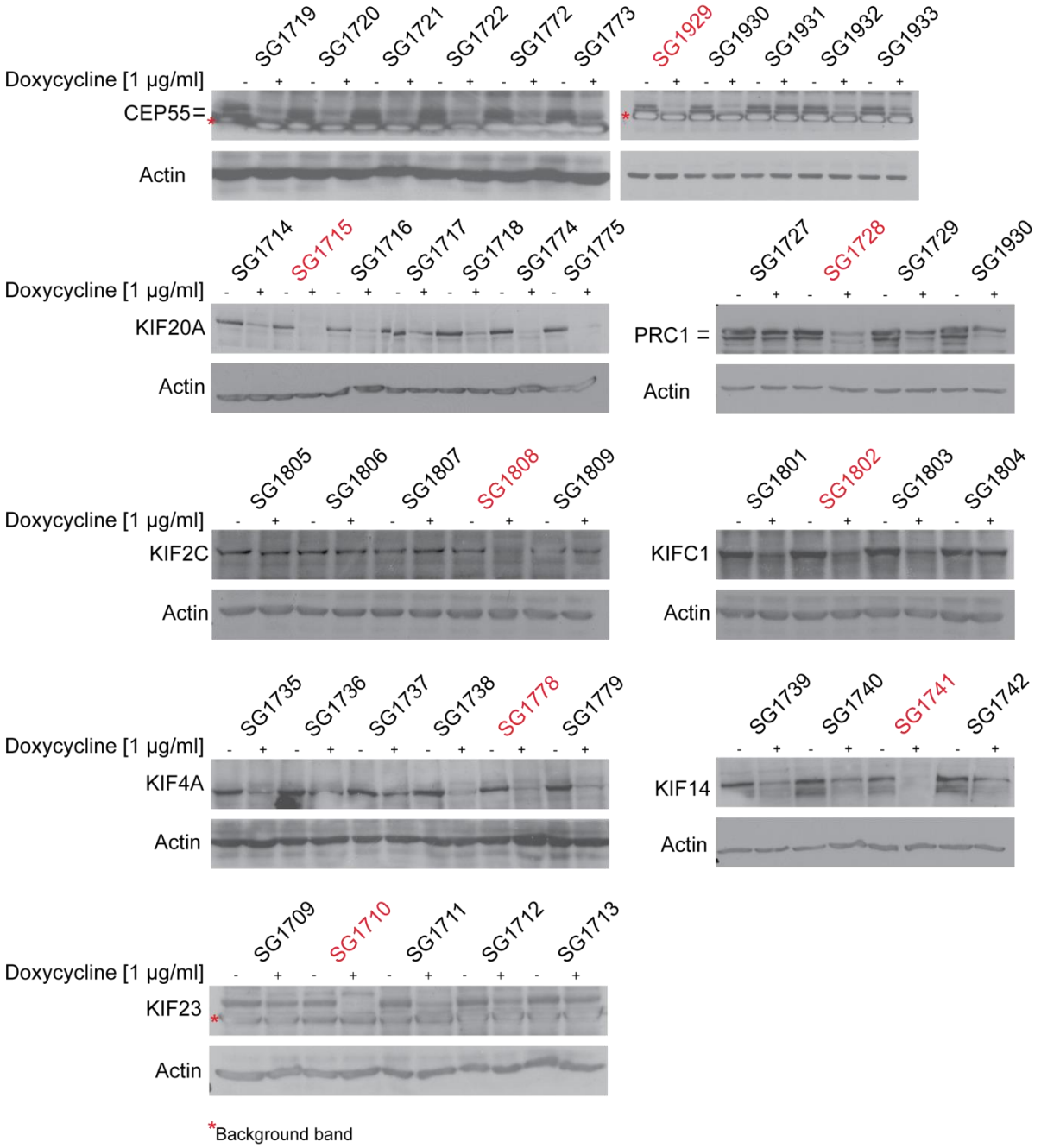

Figure 40: Screen for miR30-based inducible shRNAs.
MDA-MB-231 cells stably transduced by inducible pINDUCER-shRNAs against mitotic kinesins, PRC1, and CEP55 were treated for 48 h with or without 1 µg/ml doxycycline to induce shRNA mediated protein depletion. The cells were lysed and mitotic kinesin, PRC1, and CEP55 depletion was validated by immunoblotting. The SG numbers are the Lab ID for the 97-Oligos. The corresponding sequences are provided in Table 2. The numbers in red indicate the most efficient shRNA sequences which were used in the thesis.

Table 2: List of the miR30-based shRNA sequences used in Figure 40.

Oligo ID:	Gene KIFC1
SG1801	TGCTGTTGACAGTGAGCGcagcaagctacgtagagatctaTAGTGAAGCCACAGATGTAtagatctctacgtagcttgctaTGCCTACTGCCTCGGA
SG1802	TGCTGTTGACAGTGAGCGatagtgctaagatgctcatgttTAGTGAAGCCACAGATGTAaacatgagcatcttagcactacTGCCTACTGCCTCGGA
SG1803	TGCTGTTGACAGTGAGCGaaaggtgaaccagtgtgttattTAGTGAAGCCACAGATGTAaataacacactggttcaccttcTGCCTACTGCCTCGGA
SG1804	TGCTGTTGACAGTGAGCGaagcctgagaagaaacggacaaTAGTGAAGCCACAGATGTAttgtccgtttcttctcaggctcTGCCTACTGCCTCGGA
Oligo ID:	**Gene KIF2C**
SG1805	TGCTGTTGACAGTGAGCGaacagaatatgtgtctgtgttaTAGTGAAGCCACAGATGTAtaacacagacacatattctgtgTGCCTACTGCCTCGGA
SG1806	TGCTGTTGACAGTGAGCGacagacaaataagcagcaagaaTAGTGAAGCCACAGATGTAttcttgctgcttatttgtctgcTGCCTACTGCCTCGGA
SG1807	TGCTGTTGACAGTGAGCGaaagaaagaaattgatgtgattTAGTGAAGCCACAGATGTAaatcacatcaatttctttcttgTGCCTACTGCCTCGGA
SG1808	TGCTGTTGACAGTGAGCGccccacgcgtgcttccaaattaTAGTGAAGCCACAGATGTAtaatttggaagcacgcgtgggaTGCCTACTGCCTCGGA
SG1809	TGCTGTTGACAGTGAGCGcgacattcttcgagatctacaaTAGTGAAGCCACAGATGTAttgtagatctcgaagaatgtcaTGCCTACTGCCTCGGA
Oligo ID:	**Gene KIF4A**
SG1735	TGCTGTTGACAGTGAGCGccaggaagaagtcttcaatacaTAGTGAAGCCACAGATGTAtgtattgaagacttcttcctgtTGCCTACTGCCTCGGA
SG1736	TGCTGTTGACAGTGAGCGcaaggtgtatttaaaggatataTAGTGAAGCCACAGATGTAtatatcctttaaatacaccttTGCCTACTGCCTCGGA
SG1737	TGCTGTTGACAGTGAGCGcaaggtgtatttaaaggatataTAGTGAAGCCACAGATGTAtatatcctttaaatacaccttTGCCTACTGCCTCGGA
SG1738	TGCTGTTGACAGTGAGCGatcgctggatcagaaagacagaTAGTGAAGCCACAGATGTAtctgtcttctgatccagcgagTGCCTACTGCCTCGGA
SG1778	TGCTGTTGACAGTGAGCGcgccgagatagagacagagttaTAGTGAAGCCACAGATGTAtaactctgtctctatctcggcaTGCCTACTGCCTCGGA
SG1779	TGCTGTTGACAGTGAGCGccggagtcagaagattctattaTAGTGAAGCCACAGATGTAtaatagaatcttctgactccgaTGCCTACTGCCTCGGA
Oligo ID:	**Gene KIF14**
SG1739	TGCTGTTGACAGTGAGCGacaggtaaagtcagagacataaTAGTGAAGCCACAGATGTAttatgtctctgactttacctgcTGCCTACTGCCTCGGA
SG1740	TGCTGTTGACAGTGAGCGccagactgaagttgttagatcaTAGTGAAGCCACAGATGTAtgatctaacaacttcagtctgaTGCCTACTGCCTCGGA
SG1741	TGCTGTTGACAGTGAGCGccagagcaagttggatatcaaaTAGTGAAGCCACAGATGTAtttgatatccaacttgctctgaTGCCTACTGCCTCGGA
SG1742	TGCTGTTGACAGTGAGCGaccgacttaagctgcatttgaaTAGTGAAGCCACAGATGTAttcaaatgcagcttaagtcggcTGCCTACTGCCTCGGA
Oligo ID:	**Gene KIF20A**
SG1714	TGCTGTTGACAGTGAGCGatccgatgacgatgtcgtagttTAGTGAAGCCACAGATGTAaactacgacatcgtcatcggacTGCCTACTGCCTCGGA
SG1715	TGCTGTTGACAGTGAGCGcacgcaagaacctgctatcagaTAGTGAAGCCACAGATGTAtctgatagcaggttcttgcgtaTGCCTACTGCCTCGGA
SG1716	TGCTGTTGACAGTGAGCGatatggagaaggtgaaagtataTAGTGAAGCCACAGATGTAtatactttcaccttctccatacTGCCTACTGCCTCGGA
SG1717	TGCTGTTGACAGTGAGCGcaactgtgaaggagatggtaaaTAGTGAAGCCACAGATGTAtttaccatctccttcacagttaTGCCTACTGCCTCGGA
SG1718	TGCTGTTGACAGTGAGCGaaggcatccttcttcaacctaaTAGTGAAGCCACAGATGTAttaggttgaagaaggatgcctgTGCCTACTGCCTCGGA
SG1774	TGCTGTTGACAGTGAGCGccaggaggttaaagctaaattaTAGTGAAGCCACAGATGTAtaatttagctttaacctcctgaTGCCTACTGCCTCGGA
SG1775	TGCTGTTGACAGTGAGCGaaaggaacatagtcttcaggtaTAGTGAAGCCACAGATGTAtacctgaagactatgttccttgTGCCTACTGCCTCGGA
Oligo ID:	**Gene KIF23**
SG1709	TGCTGTTGACAGTGAGCGctagaagtgatcaataatacaaTAGTGAAGCCACAGATGTAttgtattattgatcacttctatTGCCTACTGCCTCGGA
SG1710	TGCTGTTGACAGTGAGCGcccagagtttgcagatatgataTAGTGAAGCCACAGATGTAtatcatatctgcaaactctggaTGCCTACTGCCTCGGA
SG1711	TGCTGTTGACAGTGAGCGaagggctacagactcaaccgaaTAGTGAAGCCACAGATGTAttcggttgagtctgtagccctcTGCCTACTGCCTCGGA
SG1712	TGCTGTTGACAGTGAGCGccaaccgaaatggagactataaTAGTGAAGCCACAGATGTAttatagtctccatttcggttgaTGCCTACTGCCTCGGA
SG1713	TGCTGTTGACAGTGAGCGaaagagtgttgcatagaagtgaTAGTGAAGCCACAGATGTAtcacttctatgcaacactcttgTGCCTACTGCCTCGGA
Oligo ID:	**Gene PRC1**
SG1727	TGCTGTTGACAGTGAGCGatccatagtatgtctgcagaaaTAGTGAAGCCACAGATGTAtttctgcagacatactatggacTGCCTACTGCCTCGGA
SG1728	TGCTGTTGACAGTGAGCGcgacgaccatcttgcaactagaTAGTGAAGCCACAGATGTAtctagttgcaagatggtcgtctTGCCTACTGCCTCGGA
SG1729	TGCTGTTGACAGTGAGCGccagatcatactgtgtatggaaTAGTGAAGCCACAGATGTAttccatacacagtatgatctgtTGCCTACTGCCTCGGA
SG1730	TGCTGTTGACAGTGAGCGccagatccaaatcgatttacaaTAGTGAAGCCACAGATGTAttgtaaatcgatttggatctgaTGCCTACTGCCTCGGA
Oligo ID:	**Gene CEP55**
SG1719	TGCTGTTGACAGTGAGCGaaaggagaagaatgcttatcaaTAGTGAAGCCACAGATGTAttgataagcattcttctccttcTGCCTACTGCCTCGGA
SG1720	TGCTGTTGACAGTGAGCGcaagggagaaattgcacacttaTAGTGAAGCCACAGATGTAtaagtgtgcaatttctccctttTGCCTACTGCCTCGGA
SG1721	TGCTGTTGACAGTGAGCGctccagaagtaccaaagatttaTAGTGAAGCCACAGATGTAtaaatctttggtacttctggaaTGCCTACTGCCTCGGA
SG1722	TGCTGTTGACAGTGAGCGcagggagaaattgcacacttaaTAGTGAAGCCACAGATGTAttaagtgtgcaattttctcccttTGCCTACTGCCTCGGA
SG1772	TGCTGTTGACAGTGAGCGccagctggaagagacaacgagaTAGTGAAGCCACAGATGTAtctcgttgtctcttccagctgtTGCCTACTGCCTCGGA
SG1773	TGCTGTTGACAGTGAGCGctcagaaggttatcttcaagaaTAGTGAAGCCACAGATGTAttcttgaagataaccttctgatTGCCTACTGCCTCGGA
SG1810	TGCTGTTGACAGTGAGCGaaagcagaaatgttacaacgatTAGTGAAGCCACAGATGTAatcgttgtaacatttctgcttcTGCCTACTGCCTCGGA
SG1811	TGCTGTTGACAGTGAGCGaagctgttgtattcacaaagaaTAGTGAAGCCACAGATGTAttctttgtgaatacaacagctgTGCCTACTGCCTCGGA
SG1812	TGCTGTTGACAGTGAGCGaacagagaaggacaaagaaataTAGTGAAGCCACAGATGTAtatttctttgtccttctctgtgTGCCTACTGCCTCGGA
SG1813	TGCTGTTGACAGTGAGCGcagcagcaagaagaacaaacaaTAGTGAAGCCACAGATGTAttgtttgttcttcttgctgcttTGCCTACTGCCTCGGA
SG1814	TGCTGTTGACAGTGAGCGcgaggttgaacgacaaaccataTAGTGAAGCCACAGATGTAtatggtttgtcgttcaacctcaTGCCTACTGCCTCGGA
SG1929	TGCTGTTGACAGTGAGCGccagatgcaggcatgtactttaTAGTGAAGCCACAGATGTAtaaagtacatgcctgcatctgtTGCCTACTGCCTCGGA
SG1930	TGCTGTTGACAGTGAGCGcaaggagggagcaggtgttgaaTAGTGAAGCCACAGATGTAttcaacacctgctccctcctttTGCCTACTGCCTCGGA
SG1931	TGCTGTTGACAGTGAGCGcaagctgactgataaagagagaTAGTGAAGCCACAGATGTAtctctcttatcagtcagctttTGCCTACTGCCTCGGA
SG1932	TGCTGTTGACAGTGAGCGaaaagccttatctgaagagaaaTAGTGAAGCCACAGATGTAtttctcttcagataaggctttcTGCCTACTGCCTCGGA
SG1933	TGCTGTTGACAGTGAGCGctcgaagcctagtaactccaaaTAGTGAAGCCACAGATGTAtttggagttactaggcttcgatTGCCTACTGCCTCGGA

8.3 List of figures

8.4 List of tables

8.5 Abbreviations

aa	Amino acid
APC/C	Anaphase-promoting complex/cyclosome
ADP	Adenosine diphosphate
APS	Ammonium persulfate
ATP	Adenosine triphosphate
bp	Base pairs
BSA	Bovine serum albumin
$CaCl_2$	Calcium chloride
Ca_3COOH	Acetic acid
CH	Calponin homology
CIN	Chromosomal instability
ChIP	Chromatin immunoprecipitation
CO_2	Carbon dioxide
CPC	Chromosomal passenger complex
DEPC	Diethylpyrocarbonate
DMEM	Dulbecco modified Eagle's minimal essential medium
DMSO	Dimethyl sulfoxide

DNA	Deoxyribonucleic acid
DTT	Dithiothreitol
dREAM	*Drosophila* Rbf, E2f2 and Mip complex
DREAM	DP, RB-like, E2F and MuvB complex
DRM	Dp, Rb and MuvB complex
EDTA	Ethylenediaminetetraacetic acid
EGFP	Enhanced green fluorescent protein
ESB	Electrophoresis sample buffer
ECL solution	Enhanced chemiluminisence solution
ESC	Embryonic stem cells
FACS	Fluoresence-activated cell sorting by flow cytometry
FCS	Fetal calve serum
G1	Gap1 phase
G2	Gap2 phase
GAP	GTPase activating protein
GAR	Gas2-related
GEF	Guanine-nucleotide exchange factor
ddH_2O	Distilled deionized water
H_2O_2	Hydrogren peroxide
HBS	HEPES buffer solution
HRP	Horseradish peroxidase
IgG	Immunglobulin G
KCH_3COO	Potassium acetate
KH_2PO_4	Potassium dihydrogen phosphate
KIF	Kinesin family
LAS 3.7	Leica Application Suite 3.7
LiCl	Lithium chloride
M phase	Mitotic phase
MAP	Microtubule-associated protein
MCC	Mitotic checkpoint complex
MTOC	Microtubule organizing center
Myb-MuvB	MMB
NaCl	Sodium chloride
Na_2PO_4	Disodium phosphate

Na_2HPO_4	Disodium phosphate
NEB	Nuclear envelope break down
NSCLC	Non-small cell lung cancer
NTP	Nucleoside triphosphate
PBS	Phosphate buffered saline
Pen-Strep	Penicillin-Streptomycin
PFA	Paraformaldehyde
PI	Propidium iodide
PIC	Protease inhibitor cocktail
qPCR	Quantitative real-time polymerase chain reaction
PMSF	Phenylmethylsulfonyl fluoride
Rb	Retinoblastoma
RNA	Ribonucleic acid
RNAi	RNA interference
RFP	Red fluorescent protein
RPMI	Roswell Park Memorial Institute medium
RT	Room temperature
RT-PCR	Reverse transcription polymerase chain reaction
S phase	Synthesis phase
SAC	Spindle assembly checkpoint
SDS	Sodium dodecyle sulfate
TBS	Tris buffered saline
TCA	Trichloracetic acid
TEMED	Tetramethylethylenediamine
Wt	Wild type

8.6 Curriculum vitae

PATRICK WOLTER

Born on 17th of April 1984 in Bad Mergentheim, Germany

EDUCATION

Since 04/2011	**PhD student** Julius-Maximilians-University Würzburg, Theoder Boveri Institute, Department of Physiological Chemistry I, laboratory of Prof. Dr. Stefan Gaubatz Topic: "Characterization of the mitotic localization and function of the novel DREAM target GAS2L3." & "Mitotic kinesins are regulated by the DREAM complex, often up-regulated in cancer cells, and are potential targets for anti-cancer therapy."
03/2011	**Dipl. Biol. univ.** (grade: 1.0)
04/2010 – 02/2011	**Diploma thesis** Julius-Maximilians-University Würzburg, Theodor Boveri Institute, Department of Physiological Chemistry I, laboratory of Prof. Dr. Stefan Gaubatz Topic: "GAS2L3, a novel target of the DREAM/LIN-complex, is important for progression through mitosis and maintenance of chromosomal stability."
10/2005 – 04/2010	**Studies in Biology** Julius-Maximilians-University Würzburg, Faculty of Biology Main subjects: Cell and Developmental biology, Genetics, and Biochemistry
10/2004 – 10/2005	**Studies in Nanostructural Engineering** Julius-Maximilians-University Würzburg, Faculty of Physics
2003 – 2004	**Voluntary social year** at German Red Cross ambulance service
1994 – 2003	**Grammar school and German Abitur** at Deutschorden-Gymnasium, Bad Mergentheim

Würzburg, August 2015

8.7 Publication list

PUBLICATIONS

Wolter, P.*, Schmitt, K.*, Fackler, M.*, Kremling, H., Probst, L., Hauser, S., Gruss, O. J., and Gaubatz, S. (2012). **GAS2L3, a novel target gene of the DREAM complex, is required for proper cytokinesis and genomic stability.** *J Cell Sci.* 125:2393-406

Fackler, M.*, **Wolter, P.***, and Gaubatz, S. (2014): **The GAR domain of GAS2L3 mediates binding to the chromosomal passenger complex and is required for localization of GAS2L3 to the constriction zone during abscission.** FEBS J. 281:2123-2135; DOI: 10.1111/febs.12766

*These authors contributed equally to this work.

CONFERENCE CONTRIBUTIONS

09/2012 Jacques Monod Conference in Roscoff, France
"Cell Division: from single molecule mechanics to multicellular organisms"
Poster:
Wolter, P., Schmitt, K., Fackler, M., Hauser, S., and Gaubatz, S. (2012). GAS2L3 is required for proper cytokinesis and genomic stability.

10/2013 8th International GSLS Symposium. "Scientific Crosstalk" held at RVZ, Würzburg, Germany.
Poster:
Wolter, P., and Gaubatz, S. (2013). Why are cytokinesis regulators and kinesins up-regulated in a variety of cancer.

10/2014 Jacques Monod Conference in Roscoff, France
"Cell cycle: bridging scales in cell division"
Poster:
Wolter, P., Mannefeld, M., and Gaubatz, S. (2014). The human DREAM complex is an important regulator of mitotic kinesins and mediates their upregulation in p53 mutant cancer cells.

8.8 Acknowledgement

First and foremost, I want to thank my supervisor Prof. Dr. Stefan Gaubatz. His guidance, encouragement and friendship allowed me to dive into the fantastic world of basic research and somehow sparked a seemingly irresistible research curiosity in me. The last years in his lab improved my scientific insight and formed me to a scientist for which I am very grateful.

Besides my supervisor, I would like to thank the rest of my thesis committee: Prof. Dr. Georg Krohne and Prof. Dr. Antje Gohla, for their comments and encouragement during our meetings. They were always available when needed.

I want to thank Dr. Marc Fackler for the productive collaboration. His friendly manner and scientific competence made the last years very enjoyable when we shared the same working bench in the lab.

My sincere thanks also goes to the technical assistants Adelgunde Wolpert and Susanne Spahr who always supported my practical research and gave me useful practical as well as bureaucracy relating advice.

I thank all my fellow labmates for the nice time and fun we had together and all the lasting memories. In particular, I want to mention Dr. Geeta Kumari who was responsible for a cheerful atmosphere and provided me with private English lessons while lunch time. I won a new friend in her.

Of course, I want to thank the GSLS and the Transregio17 program for the opportunity to take part at a variety of courses, retreats and conferences.

Finally, I want to thank my parents and my sister who were supporting me my whole life and my girlfriend Dr. Christine Damrau who accepted my love for science and all the resulting consequences and even persuades me to further follow this path.

8.9 Affidavit

Hiermit erkläre ich an Eides statt, die Dissertation mit dem Titel „Charakterisierung der mitotischen Lokalisation und Funktion von GAS2L3, eines kürzlich gefundenen Zielgens des DREAM Komplexes.“ und „Mitotische Kinesine werden vom DREAM Komplex reguliert, sind in Krebszellen häufig hochreguliert und sind potentielle Ziele für die Krebstherapie“ eigenständig, d.h. insbesondere selbständig und ohne Hilfe eines kommerziellen Promotionsberaters, angefertigt und keine anderen als die von mir angegebenen Quellen und Hilfsmittel verwendet zu haben.
Ich erkläre außerdem, dass die Dissertation weder in gleicher noch in ähnlicher Form bereits in einem anderen Prüfungsverfahren vorgelegen hat.

Ort, Datum Unterschrift

I hereby confirm that my thesis entitled “Characterization of the mitotic localization and function of the novel DREAM target GAS2L3.” and “Mitotic kinesins are regulated by the DREAM complex, often up-regulated in cancer cells, and are potential targets for anti-cancer therapy.” is the result of my own work. I did not receive any help or support from commercial consultants. All sources and / or materials applied are listed and specified in the thesis.
Furthermore, I confirm that this thesis has not yet been submitted as part of another examination process neither in identical nor in similar form.

Place, Date Signature